UNIVERSIDADE DE LISBOA
FACULDADE DE CIÊNCIAS
DEPARTAMENTO DE ENGENHARIA GEOGRÁFICA, GEOFÍSICA E ENERGIA

Study and Characterization of the Impacts of Soiling on the Performance of Photovoltaic Systems

Francisco Pile Mendes Pinto

Mestrado Integrado em Engenharia da Energia e do Ambiente

Dissertação orientada por:
Anne Migan (GEEPS)
João Serra (FCUL)

2019

Acknowledgements

I would like to express my gratitude towards my parents for their unconditional love and encouragement, patiently assisting me on the completion of my studies.

I am also profoundly grateful to Anne Migan, without whom this work would not have been possible, and whose tireless support proved instrumental throughout this project.

I would like to acknowledge Vincent Bourdin and Jordi Badossa for their invaluable guidance, criticism, friendship and optimism, as well as for their continuous availability and assistance in any of the numerous challenges I've encountered.

Finally, my sincerest appreciation goes to Elsa Heyd for her companionship, advice, and illuminating views on a number of issues related to the project.

Preface/Motivation

The accumulation of particles on the surface of solar panels is an important factor affecting solar panel production. This phenomenon, commonly referred to as soiling, can amount to a sizeable portion of the system losses. Despite this, perhaps due to its inevitability, soiling losses remain largely overlooked.

It's for this reason that I'm particularly interested in understanding and quantifying soiling related losses, aiming to determine the extent of their impact on photovoltaic systems and their conversion efficiency.

Although several studies have been published on this subject, few analyzed soiling through the correlation between efficiency and rain, a much more accessible method for those without the time or means to more accurately assess soiling losses.

This study is aimed at all those who seek to understand how soiling affects the conversion efficiency of photovoltaic systems, and particularly at those interested on its impact on modules located close to the region of Paris, where this study was performed.

Abstract

Soiling can be one of the major causes of power loss on photovoltaic systems. Despite this, these remain largely ignored. This study analyzed the soiling-induced efficiency degradation of five different solar modules, aiming to characterize and quantify the impact of soiling on the performance of these systems. This was accomplished through the analysis of the module efficiencies over dry periods, during which rain was insufficient to effectively clean the panels. Results showed that all panels registered an efficiency decrease within a ninety percent confidence interval during the longest dry period, with an average power degradation rate of -0.042 %/Day, suggesting a stable trend of soiling induced efficiency degradation. All other periods exhibited non-significant trends, likely due to the high day-to-day efficiency fluctuations which persisted despite the thermal correction of the efficiency values. The accuracy of two thermal models was tested, aiming to obtain the most reliable module temperature records to be employed in the thermal correction procedure. The first, already existent in the literature and based on the panels' NOCT yielded the best results, with an average error of 3.55 ºC. The second, based on the precise modelling of the panels' heat fluxes, proved less practical and reliable, yielding a slightly average error in the order of 3.9 ºC. Finally, the impact of the diffuse radiation on the dispersion of the daily efficiency values was studied, revealing that the latter is proportional to the diffuse ratio. This was achieved through the analysis of the monthly standard deviation for different day types, so as to bypass the effect of seasonal variations. Results suggest that solar panel cleaning can be neglected in the region of Palaiseau, as soiling losses are rendered insignificant due to the combination of moderate panel inclinations and the natural cleaning provided by the high frequency of rainfall events.

Keywords: Soiling, Photovoltaic Losses, Dust Accumulation, PV Performance, Particle Deposition

Resumo

A acumulação de partículas na superfície de painéis solares é um fenómeno transversal a todas as tecnologias fotovoltaicas. Este fenómeno é designado por Soiling, e têm como principal consequência a redução da eficiência fotovoltaica dos painéis.

Esta tese tem como por objetivo a caracterização e quantificação das perdas causadas pelo efeito do soiling em painéis solares. Para tal, serão estudados cinco módulos instalados nos arredores de Paris com o intuito de obter uma taxa de degradação da potência para cada painel.

O impacto do Soiling será estudado através da análise da eficiência dos painéis durante períodos secos, com um foco especial no maior período seco de que existem registos, durante o qual todos os módulos sofreram um decréscimo de eficiência para um intervalo de confiança superior a noventa por cento.

Os painéis encontram-se no Observatório SIRTA [1], orientados a Sul a uma inclinação fixa de vinte e sete graus. Situados em terreno aberto, a cerca de vinte centímetros do solo, os painéis estão inseridos numa área rodeada por extensos relvados, caracterizada por uma fraca intensidade rodoviária.

Para a realização deste estudo, foi disponibilizada uma ampla gama de dados amostrados em intervalos de dez minutos, permitindo uma precisa análise intra-diária da eficiência fotovoltaica. Dados como a temperatura, potência, corrente e tensão dos painéis, irradiância, temperatura ambiente, pluviosidade, velocidade do vento, humidade relativa, entre muitos outros, possibilitaram não só o estudo do impacto do soiling na performance dos painéis, como também várias outras análises acessórias relevantes.

A tese inicia-se por uma abordagem aos principais fatores que afectam a taxa de deposição de partículas nos módulos, assim como os seus variados impactos na eficiência dos painéis. Esta secção visa introduzir o leitor aos conceitos básicos indispensáveis à compreensão da tese, e igualmente fornecer uma contextualização alargada de modo a facilitar a interpretação dos resultados apresentados.

Seguem-se depois os métodos e objetivos, o capítulo central desta tese, o qual explica em detalhe todo o processo que culminou na quantificação do impacto do soiling na performance dos painéis estudados.

Este capítulo encontra-se dividido em aproximadamente três partes. A primeira, relativa ao processamento inicial dos dados, envolve o cálculo da temperatura dos módulos, a sua eficiência de conversão e subsequente correção térmica. Grande parte desta seção é dedicada estimação das temperaturas dos módulos, as quais serão necessárias para preencher eventuais lacunas devido a falhas dos sensores térmicos.

Estas temperaturas serão obtidas através da implementação de dois modelos térmicos capazes de simular a temperatura dos módulos. O primeiro, já existente na literatura, requer apenas a introdução da temperatura ambiente, irradiância, e a temperatura nominal de operação das células solares. Embora este valor seja geralmente fornecido pelo fabricante, este último foi calculado experimentalmente, assegurando que o modelo fosse fornecido com temperaturas nominais de operação de células reais, medidas nas suas verdadeiras condições de operação.

O segundo modelo, baseado na modelação /dos fluxos de calor entre o painel e o ambiente, foi criado de raiz com o intuito de aumentar a precisão das estimativas. A estabilidade e desempenho destes modelos será avaliada, comparando a sua precisão e fiabilidade sob diferentes condições.

De seguida, a eficiência dos painéis será calculada e corrigida para uma temperatura base de vinte e cinco graus Celcius. Esta correção é indispensável à análise da degradação do desempenho dos painéis, uma vez que remove o efeito da temperatura na eficiência, permitindo o cálculo das taxas de degradação

de potência normalizadas. A qualidade desta correção será também estudada de modo a garantir a validade dos resultados.

O segundo passo centra-se no reprocessamento dos valores de eficiência por forma a facilitar a deteção de eventuais perdas, permitindo obter uma taxa de degradação da potência fiável. Para tal, a eficiência diária acumulada dos painéis será calculada, com o objetivo de simplificar a análise através da redução das variações intra-diárias, obtendo uma série mais representativa das variações de eficiência. Nesta fase serão também filtrados valores anormais de eficiência, resultantes de erros de medição ou condições de fraca iluminação, detrimentais ao estudo em curso.

Será ainda feita uma análise da relação entre a dispersão dos valores diários de eficiência e as condições climatéricas, uma vez que estas podem dificultar a análise dos impactos do soiling, afetando a extração e significância estatística das taxas de degradação de eficiência.

O terceiro e último passo consiste na identificação dos períodos secos, ou intervalos durante os quais a chuva não foi suficientemente forte por forma a interferir com a acumulação de partículas nos painéis, e portanto ideais para o cálculo das taxas de degradação da eficiência. Estas serão baseadas no declive da recta resultante de uma regressão linear das eficiências durante estes períodos.

O uso de uma regressão linear na previsão de perdas pelo efeito do soiling é baseado em estudos de natureza semelhante, os quais concluíram que o declínio do desempenho fotovoltaico observado durante períodos secos é aproximadamente linear, decrescendo continuamento durante períodos sem chuva e regressando a níveis normais após um episódio de precipitação [2]. Estes factos sugerem que os efeitos do soiling no desempenho de um Sistema PV podem ser estimados adotando um modelo linear de perdas de eficiência entre eventos significativos de precipitação.

A quantificação destas perdas foi feita para dois tipos de períodos. Inicialmente, apenas períodos durante os quais a precipitação diária não excedeu os cinco milímetros foram estudados. Isto consistiu no cálculo das taxas de degradação da eficiência para estes intervalos. De seguida, este limiar foi fixado num valor mais conservador, assegurando que nenhum processo de limpeza possa ter acontecido, e as taxas de degradação recalculadas.

Uma ênfase especial foi dada ao mais longo período seco de que existem registos, durante o qual todos os painéis registaram uma diminuição inequívoca de eficiência. A taxa de degradação média de potência durante este intervalo foi de -0.042 %/Dia, um valor que se encontra de acordo com vários outros estudos semelhantes [2,3]. Devido à sua incomparável duração, estendendo-se por trinta e sete dias, uma especial atenção foi dada a este intervalo, uma vez que este foi o mais longo período de acumulação ininterrupta de partículas.

Por fim, foi feita uma breve análise estatística das regressões lineares, visando validar os resultados. As regressões lineares foram testadas unidireccionalmente, de modo a determinar a probabilidade de um painel registar um decréscimo de eficiência durante este período. Para tal, foram calculados os intervalos de confiança de cada regressão baseados na distribuição t de student, focando-se exclusivamente no intervalo superior, revelando o revelando o nível de confiança com o qual se pode afirmar que perdas devidas ao efeito do soiling estão presentes em cada painel.

Os resultados indicaram que todos os painéis sofreram uma queda de eficiência para um intervalo de confiança superior a noventa porcento durante este período mais longo, e de noventa e cinco por cento para quatro dos painéis.

Palavras-Chave: Soiling, Perdas Fotovoltaicas, Acumulação de Poeiras, Performance PV, Partículas

Table of Contents

List of Figures and Tables

List of Acronyms

AM	Air Mass Coefficient
BNEF	Bloomberg New Energy Finance
IEC	International Electrotechnical Commission
IPSL	Institut Pierre Simon Laplace
NOCT	Nominal Operating Cell Temperature
PM	Particulate Matter
PV	Photovoltaic
RMSE	Root Mean Squared Error
SIRTA	Site Instrumental de Recherche par Télédétection Atmosphérique
STC	Standard Test Conditions

Chapter 1 – Introduction

Over the past two decades the photovoltaic industry has grown exponentially, evolving from a niche market of small-scale applications to a mainstream electricity source.

Solar prices have been dropping at an astonishing rate, consistently ahead of even the most bullish projections. Just three years ago, the Bloomberg New Energy Finance was forecasting solar dropping from 0.53 €/Watt in 2015 to 0.18 €/Watt in 2050. Today, the price already stands between 0.28-0.31€/Watt, and is expected to fall to around 0.20 €/Watt by the end of 2019.

The plunging costs of this technology are the key to its widespread adoption, catering not only to the renewable enthusiasts but to the average consumer as well. With the price per watt falling rapidly, embracing solar is becoming an increasingly economic decision, and not simply an environmentally conscious one.

As the solar PV market grows increasingly competitive, so does the need for accurate energy forecasting in order for this technology to thrive on an industrial scale. An important aspect of this prediction relates to soiling, as it is essential to understand the impacts of soiling in order to properly assess the system's energy yield.

Soiled solar modules have long been considered a minor nuisance, but with the solar market booming, the proper assessment of soiling losses is becoming increasingly relevant. In recent years, several studies have been conducted by research programs with the goal of assessing the impact of soiling on photovoltaic modules.

On the south of Europe, in Malaga (Spain), a study concluded that the mean daily energy loss along a year caused by dust deposited on the surface of the PV module was around 4.4%, this value increased to 20% during extended periods without rain [4].

Closer to the center of Europe, in Belgium, soiling induced power losses were found to be between 3% and 4%, over a period of just five weeks [5]. In another study, on the island of Crete, yearly power losses were estimated at 5.86% [6]. In the south of Italy, a 6.9% and 1.1% monthly power loss was registered, on plants built on a sandy and a more compact soil, respectively [7].

On the Canary Islands, efficiencies dropped to 20% of their initial values over five months, recovering to their initial values after rainfall [8]. In Kuwait, a notoriously arid climate, soiling losses reached 45.8% over three months without cleaning [9], and in California they amounted to about 7% annually [10].

Other studies report even higher annual yield losses, depending both on system location and the specifications of the analyzed plant.

Despite this, soiling losses are often underestimated, and in part due to the difficulties encountered in their detection. In most cases, the irradiance sensor suffers from the same amount of soil that is covering the PV panels. Consequently, the measured irradiance level decreases, despite the actual irradiance remaining the same. This decrease in the measured irradiance balances out the decrease in the energy production of the panels, allowing for the efficiency to remain constant, and thus effectively hiding the power losses.

But with the increasing number of studies published each year on this subject, the understanding of the impacts of soiling on photovoltaic modules increases, allowing for the development of new techniques and technologies aimed to tackle the persistent problem of dirty module surfaces.

Chapter 2 – Theoretical Background

Over the course of this chapter, there will be an extensive review of the main factors affecting soiling deposition, as well as a brief summary of the key factors related to the impacts of soiling on photovoltaic performance.

2.1. What is Soiling?

Soiling is the phenomenon of dust deposition on the surface of solar panels, resulting in the attenuation of the incoming solar irradiance, and causing a reduction of the modules' conversion efficiency.

This causes PV systems to perform sub-optimally, registering lower efficiencies and generating less power under these conditions. Soiling not only reduces the irradiation on the solar cells, but also the incidence angle of such radiation, further affecting the panel.

These losses can be significantly reduced by a periodical cleansing of the top surface of the solar modules, thus reducing the particle deposition. The ideal time period in-between cleaning depends essentially on the rate of soiling, the type of solar cell technology and the cost of cleaning.

2.2. Causes

There are essentially two interdependent parameters that govern the process of soiling accumulation on solar panels: the local environment and the properties of the soil.

The first defines the rate at which the solar module surface is contaminated, and is directly related to the intensity of the pollution processes and the nature of the prevailing activities. These can be of natural sources, such as pollen, bird droppings and particles brought by the wind, or resultant of human activity, such as combustion products, soot, and rubber dust from nearby road transport.

The second refers to the properties of the soil, which vary with the geographical and atmospheric characteristics of the place, such as with wind, humidity, temperature or pressure, that determine the type, size, weight and shape of the particles.

The physical and chemical properties of such particles are also relevant to determine the effect of soiling on the transmittance of the glass.

There are several other parameters affecting the rate of soiling on a solar panel, such as rainfall, wind speed, orientation, temperature and humidity. These, in conjunction with the environmental characteristics of the location, define the rate of particle deposition on solar modules.

2.3. Atmospheric Parameters Influencing the Rate of Soiling

In this short section, the main atmospheric agents affecting soiling deposition will be covered, providing a summary overview of their impacts.

2.3.1. Rainfall

Rain is an efficient cleaning agent when it occurs frequently and with intensity, as it has the ability to wash away dust particles from a PV module's surface.

Conversely, light rains tend to drop the suspended particles from the atmosphere, forming thin layers that make PV performance worse. This phenomenon is called wet deposition, and occurs when rain traps air pollutants inside the rain drops and transfers them onto the panel's surface.

Among all weather variables, rainfall has the highest cleaning potential, allowing for an energy output recovery of up to 99.5% after the modules are cleaned by rain [11].

In the vast majority of the cases, rainfall has a positive effect on PV systems, increasing the transmission coefficient of the glass cover. This is especially true in dry areas where panels can go for months without natural cleaning.

There are, however, some instances in which rain will increase the soiling related losses. In the case of a severely dusted panel, a small amount of rainfall can turn the dust into mud, further promoting dust adhesion and increased soiling deposition.

Similarly, the rain induced transmittance reduction at the lower portion of the glass is more pronounced than at the upper portion, since sometimes rainfall does not clean the sample completely, causing dust from the upper part of the panel to be resettled on the lower part [12].

Finally, it's worth noting that without proper and regular cleaning, the dust accumulated on the panel's surface may thicken and not be easily dislodged by rain [13]. Although these cases are rare, requiring manual cleaning in order to restore the panels to their original state, sharp declines in performance have been registered.

2.3.2. Wind

Much like rainfall, wind can be a powerful agent governing the soil deposition process. Whereas strong winds can clear the panel effectively, a slow breeze will often result in dust accumulation. Depending on the geographical location of the solar panels, the wind can act as a serious deposition agent.

In a dry deposition process, wind carries particles until they're eventually deposited onto PV panel surfaces. This can happen by several means, the most common of which is sedimentation. The orientation of the panels is also marginally relevant to this process, since the dust deposition rate may increase when the panel is facing the wind.

In addition to that, wind velocity also affects the dust sedimentation and deposition characteristics. Dust coatings created by slow winds are less transparent than those created by high speed winds.

At low wind speeds, long sedimentation times allow dust ripples to become more and more mature, where many individual short ripples merge to form long macro-ripples. As the result, empty spaces

between the ripples disappear. This means that the PV module surface is covered by a continuous dust coating, and the surface's light transmittance is significantly reduced [14].

On the other hand, the removal efficiency of dust by the wind depends on the relative strength of the adhesion forces between surface and particles. Depending on the dust nature, increasing sand accumulation tends to form clusters and upper layers of particles. Under the effect of wind, these clusters will be destroyed but then will resettle on the surface, compared to the single layer particles which will be blown off the surface by the wind. Sand particles tend bounce on the glass surface before settling, hence delaying cluster formation [15].

Finally, the airflow over the panel can have accumulative or dissipative effects at particular places of the module. The air speed and pressure are not constant over the solar panel's surface, and wherever the airspeed is higher, there will be lower pressure, which can result in lesser soil accumulation and vice versa.

2.3.3. Humidity

When the relative humidity is high, the adhesion of particles to surfaces tends to increase. This means that humidity promotes the adhesion of dust particles onto solar panel surfaces, increasing the soiling rate, and resulting in a more rapid formation of clusters.

Similarly, dew formation due to high relative humidity promotes dust settlement on flat surfaces, while dust adhesion to these surfaces is reinforced by evaporation [13,16].

Furthermore, higher humidity levels lead to capillary forces, creating a bonding bridge between the surface and the contaminant, increasing particle adhesion to surfaces. This means that when contaminated water droplets in fog, mist or clouds come into contact with the panel's surface, they're more likely to be deposited.

In a nutshell, the higher the relative humidity in the atmosphere, higher the particle stickiness to the PV panel, and lower the cleansing effect of the wind [17].

2.4. Main Parameters Affecting Soiling Deposition and PV Performance

2.4.1. Deposition Density

There's a very clear correlation between dust accumulation and PV performance. This has to do with the fact that the accumulation of dust reduces the transmittance of the solar panel's glass cover, which in turn reduces the I_{sc} of the system.

As the dust deposition on the glass surface increases, the reduction of the transmission increases at a progressively decreasing rate until its upper limit. When this limit has been reached, the effect of the deposition density on glass transmittance vanishes, remaining constant for higher density levels [18].

Just as the transmissivity of the glass cover, both the I_{sc} and performance decline as the dust deposition density increases. This I_{sc} degradation rate is higher at initial deposition until a certain level, after which it decreases only slightly.

The efficiency degradation associated with the loss of transmittance follows an exponential relation with deposition density. However, panel and dust type can govern the degree of efficiency reduction.

2.4.2. Installation Design

The PV installation design itself has an influence on the dust deposition rate. It has been shown experimentally that for the same tilt angle, orientation does not have a noticeable influence on dust accumulation.

However, dust density deviation may occur at certain orientations due to the predominant wind direction or the source of dust. Similarly, the least accumulation would be found on the samples facing the opposite direction [12].

Particle accumulation tends to reduce as the tilt angle increases [19]. This is because particles tend to roll down the surface due to the effect of gravity. Biryukob proved that the deposition rate is proportional to cosine of the panel tilt for inclinations until 85º. Furthermore, the cleaning effect of rainfall is less effective on less tilted horizontal surfaces [20,21].

Additionally, on tilted glass samples, the transmittance reduction at the lower portion of the glass is larger than at the upper portion, since in certain cases, rainfall does not clean the sample completely, causing the dust from the upper part to be resettled on the power part [12].

2.4.3. Incidence Angle

Since the earth is constantly rotating and moving through the solar system, the incident angle at which the solar rays meet the glass surface of the solar panel varies. The curve of irradiance losses caused by dust and its dependence on the angle of incidence has a very specific shape.

The minimum transmittance losses occur at solar noon when the incident angle is minimum, and as the angle increases, losses increase slowly, and the growth rate increases with the angle until about 60º, where losses remain almost constant for a window of 10º and then, after a maximum at around 75º, they decrease [4].

This occurs at the first and last hours of the day, when the incidence angle is between 60º and 80º and the irradiance value is about 200 Wm^{-2}. This behavior is related with the proportion of diffuse irradiance to global irradiance in these first and last hours of the day, when this value increases.

On cloudy days, when the global irradiance is mainly diffuse, losses remain almost constant throughout the day, this is because diffuse irradiance has no specific direction and hence losses are not dependent on the incidence angle.

Zero transmittance can be reached at incidence angles less than 90º at higher dust accumulation, where the areas between the particles are totally shaded by the particles themselves.

2.4.4. Dust properties

The physical and chemical composition of the deposited particles has an effect on the panels' surface transmittance. Finer particles settle in a more distributed manner on the panels' surface, hence minimizing the gap for light to pass through. This means that PV module degradation is more affected by smaller particles than larger ones with an equal amount of deposition.

Carbon particulates, which are extra-fine and absorb solar radiation effectively, are proven to have a relatively worse deterioration effect [22,23]. However, unlike coarse particulates, fine depositions do not lead to partial shading since this kind of particulates tend to distribute uniformly as early as their initial deposition [22]. Additionally, different types of particles have different degrees of transparency.

Besides size and density, different dust types exhibit different physical characteristics, which determine how long they can travel in the atmosphere, how fast they deposit and how easily they're cleaned.

The removal efficiency of dust by the wind depends on the relative strength of the adhesion force between surface and particles. The adhesion force is inversely proportional to the particle diameter. Hence, small particles have stronger adhesion forces of adhesion and are less affected by the wind [15,24]. In addition to that, rainfall also has a limited cleaning effect on small particles when compared to larger ones [25].

Depending on the dust nature, increasing sand accumulation can form clusters, stacking several layers of particles. As we've covered, under the effect of the wind, these clusters can be destroyed only to resettle elsewhere on the surface. This does not happen to single layer depositions, which can be promptly blown off the surface by the wind.

2.4.5. Air Mass

Air Mass is a concept that quantifies the amount of atmosphere incident light goes through before

reaching the earth's surface. The power output of a solar panel doesn't depend solely on the intensity of the irradiance, but on the spectral composition of such irradiance as well, both of which are affected by the air mass.

When the sun is 30º above the horizon, the path that the sunlight takes through the atmosphere is about twice as long as the path it takes at solar noon, resulting in higher losses. These can be due to scattering or reflection events in the atmosphere that reduce the irradiance reaching the solar panel.

The efficiency of a solar cell is sensitive to variations in both the power and the spectrum of the incident light. But the air mass's main effect is on the intensity of the light, which is reduced as the air mass increases.

However, it is the variation on the spectral composition of the incident light that relates to soiling, as the accumulated particles will filter differently each part of the spectrum, as we'll see ahead.

2.4.6. Spectral Composition

The sun emits electromagnetic radiation across most of the electromagnetic spectrum. But after being filtered by the atmosphere, only part of the incident radiation reaching the panels will be successfully absorbed and converted to electricity.

Once at ground level, the spectral response of each solar cell will dictate the upper limit of its efficiency. Much like the atmospheric filtering process, the dust accumulated on top of the panel's surface will filter the incoming radiation, affecting certain wavelengths more than others.

The transmittance reduction contributed by dust is then spectrally dependent [26,27], and is more severe at shorter wavelengths [26]. This explains why mono-crystalline PV modules are more sensitive to dust accumulation than amorphous silicon modules [28].

On the other hand, as dust deposition increases, more light is reflected, where the reflectance increment is more pronounced at longer wavelengths than shorter ones [23].

Fortunately, silicon solar cells aren't very sensitive to the portions of the spectrum lost in the atmosphere. The resulting spectrum at the Earth's surface more closely matches the bandgap of silicon, which means silicon solar cells are more efficient at AM1 than AM0.

This apparent counter-intuitive result arises because silicon cells can't convert much of the high radiation which the atmospheres filters out. Even though the efficiency is lower at AM0, the total output power for a typical solar cell is still highest at AM0.

Conversely, the shape of the spectrum does not significantly change with further increases in atmospheric thickness, and hence cell efficiency does not greatly vary for AM numbers above 1.

2.4.7. Temperature

Besides transmittance losses, dust deposition on PV panel surfaces also cause a temperature increase, resulting in the reduction of their conversion efficiency. An increase in solar cell temperature causes a slight increase in short circuit current, but a significant decrease in open circuit voltage. As such, the panels' overall power and efficiency are reduced.

The thermal coefficient defines the degradation of a solar cell's performance as a function of temperature. As every other semiconductor device, solar cells are sensitive to temperature, with each material having its specific thermal response. An appropriate choice of cell material can then reduce the thermal effects of dust on the solar panel performance.

Interestingly, due to the uneven coverage of the glass surface, soiling can give rise to temperature differences along the solar panel of up to 10ºC [32].

2.4.8. Surface Coating and Rugosity

The surface of the panels is an important contributing factor in the soiling deposition process. If the surface is not smooth, it will allow for more soil to accumulate. The rougher the surface is, the harder it will be for the wind and rain to clean it effectively.

Another important aspect concerning the surface of the panels is the coatings. There are various kinds of coatings such as anti-reflection or surface passivation, causing the surface to become sticky and more likely to accumulate dust than smooth surfaces [25].

Dust deposited on this kind of surfaces is less likely to be blown away by wind, resulting in permanent dust settlement on the surface. On the other hand, self-cleaning coatings can reduce the soiling associated transmission by allowing rainfall to wash dust off more effectively [26].

However, the thickness of the coating must be ideal, balancing between its self-cleaning properties and the fact that the coating itself slightly hinders the panels' transmissivity [12].

2.4.9. Shading

The term shading refers to the blocking of sunlight that casts a shadow over the module. This can be a serious problem for PV modules since the shading of just one cell in the module can reduce the power output to zero.

Shading due to soiling is divided in two categories: soft shading, such as caused by accumulated dust, and hard shading which occurs when something blocks the sunlight in a clear and definable manner.

Soft shading mostly affects the current provided by the PV module, decreasing in proportion to the shading. In this case, only the current provided by the system will be significantly affected, while the voltage will remain more or less the same.

Under hard shading, the performance of the PV module depends on whether some or all cells of the module are shaded. If some are shaded, then as long as the unshaded cells receive solar irradiance there will be some output, although there will be a decrease in the voltage output of the PV module.

Soiling tends to fall under the soft shading category, although in addition to the general dust related soft shading, some soil patches such as leaves, bird droppings and dirt that block some cells of a PV module can result in hard shading.

2.4.10. Natural and Artificial Cleaning

Cleaning the glass surface of a solar panel is the fastest way to minimize soiling losses. There are several ways of cleaning the panels, which are essentially divided in two categories: natural cleaning, from nature's own processes, and artificial or human assisted cleaning.

In the first category we have rainfalls, which are free of charge but seasonally volatile. Therefore, the reliability of this cleaning method is questionable when soiling is intensive and rainfall is scarce in either frequency or intensity. However, as previously mentioned, there can be an occasional decline in performance after a light rain.

Besides rainfall, the second most effective natural cleaning agent is wind, which can assist to reduce the soiling to a certain extent, but there is a need for water in order to clean the surface optimally.

On the second category we have manual cleaning, a method that follows the same procedure used to clean the windows of buildings. This process consists in scrubbing the soil off the surface, where specially designed brushes with bristles prevent the scratching of the modules. Some higher end brushes are also connected directly to a water supply to perform the washing and scrubbing simultaneously.

Finally, there's mobile cleaning, a method that utilizes machinery to perform the task without human assistance, but still falling within the scope of this second category. This usually makes use of a water supply or sprinkler system to clean the surface of the modules.

More advanced designs make use of robotic cleaning technologies, removing soiling through a wireless autonomous system. These new technologies are even eliminating the need for water, offering major potential savings on both vehicle and labor costs.

Chapter 3 – Objectives

The aim of this work is the study, characterization and quantification of the influence of soiling on photovoltaic panels deployed near the region of Paris. To this end, five solar modules of different brands and technologies will be studied over the period of one year, aiming to detect and quantify soiling related losses.

Although several studies have been published on this subject, few analyzed soiling through the relation between efficiency and rain, a much more accessible method for those without the need or means to more accurately assess soiling losses.

Among all weather variables, rainfall has the highest cleaning potential, allowing for an energy output recovery of up to 99.5% after the modules are cleaned by rain [11]. For this reason, it's sensible to study the efficiency's behavior during dry periods, where virtually no soiling removal processes occur.

Multiple studies have already found a stark correlation between dry rainless intervals and periods of increased soiling accumulation. And although these were often performed in dry climates, where rainfall is scarce during a pronounced summer season, it seemed reasonable to extend this type of analysis to the region of Paris, characterized by a temperate oceanic climate, with rainfall evenly distributed throughout the year.

Chapter 4 – Methods

This study is divided into roughly three parts. The first, concerning the initial processing of the data, involves the calculation of the module temperatures, their conversion efficiency and their subsequent thermal correction. The bulk of this section concerns the prediction of module temperatures, which would be required to fill any eventual gaps due to thermal sensor failures.

These temperatures will be obtained through the implementation of two thermal models capable of predicting module temperatures. The first, already existent in the literature, is reliant on the air temperature, irradiance and the nominal operating cell temperature. Despite being generally provided by the manufacturer, this value was calculated experimentally, ensuring the model was provided with real, field-measured, nominal operating cell temperatures.

The second model, based on the precise modelling of the heat fluxes between the panel and its surroundings, was created from scratch with the purpose of increasing the estimates' accuracy. The performance and stability of these models will be assessed, contrasting their accuracy and reliability under different conditions.

This will be followed by the calculation of the panels' conversion efficiencies and their thermal correction. This correction is indispensable for the analysis of the soiling induced performance degradation, as it rids the efficiencies of the temperature's influence, allowing for the calculation of the normalized efficiency degradation rates. The latter will also entail a brief analysis of the correction process, assuring the quality and validity of the results.

The second step revolves around the reprocessing of the efficiency values in order to facilitate the detection of soiling related losses and increase the accuracy of the analysis. To this end, the cumulative daily efficiency values were calculated, taking into account the panels' total power production and irradiance received during the day, resulting in a very precise value of the average daily efficiencies. This simplified the soiling analysis through the reduction of the intra-day fluctuations, ensuing a series that more faithfully represented the efficiency's overall trend.

This step will also include the removal of outliers, due to measurement errors or low light conditions, and thus detrimental to the current study.

This will be followed by an analysis of the efficiency variations through the diffuse ratio, as these fluctuations severely hindered the soiling analysis, masking soiling losses, and affecting the extraction and statistical significance of the efficiency degradation rates.

The third step consisted on the identification of the rainless intervals, or periods whose daily amount of rainfall did not significantly interfere with soiling accumulation, and were thus fit for the calculation of the efficiency degradation rates. These rates will be based on a linear regression of the daily efficiencies over these periods.

The use of a linear regression model to predict soiling losses is based on studies of similar nature, which concluded that the observed decline in system performance over dry intervals was approximately linear, steadily decreasing during periods without rainfall and promptly returning to normal levels after a period of rain. [2] These facts suggest that the effects of soiling on PV system performance may be accurately predicted using a linear model of decreasing system performance over time between significant rainfall events.

The quantification of the soiling losses was performed for two types of periods, based on different qualifying criteria. Firstly, only periods whose daily rainfall did not exceed five millimeters were studied. This consisted on the calculation of the efficiency degradation rates for these intervals. Secondly, this threshold was set to a more conservative value, ensuring that no significant cleansing process could have commenced, and the degradation rates were once again calculated.

A special focus was given to longest rainless interval, occurring amidst an unusually dry Parisian summer, during which every panel registered an unequivocal efficiency decrease. The panels' average power degradation rate during this stretch was -0.042%/Day, a value that's in accordance to several other similar studies. [2,3]. Due to its unparalleled duration, spanning thirty-seven days, a particular emphasis was placed on this interval, as it was the longest recorded period of uninterrupted soiling accumulation.

Finally, a brief statistical analysis of the linear regressions was performed, aiming to validate the results. The regression slopes were tested unidirectionally, determining their probability of registering an efficiency decrease during this period. To this end, a one tailed t test was performed for each module, focusing exclusively on the upper confidence interval, revealing the level of confidence with which one can affirm that soiling losses were present for each panel.

4.1. Calculation of Module Temperature

When looking at solar panel efficiency it's necessary to know the real working temperature of the solar modules. Since these records were at times incomplete, and module performance is strongly dependent on their operating temperature, it was deemed essential to estimate this parameter.

To this end, two separate thermal models were tested, aiming to obtain the most reliable temperature records possible. The most precise temperature model will be used, when necessary, in replacing missing temperature data used during the thermal correction of the panels' efficiency.

4.1.1. NOCT Thermal Model

The first simulation of module temperature was based on the nominal operating cell temperature and the equation below (4.1), since it correlates the module's temperature with the outside temperature and irradiance, the two main factors governing cell temperature.

$$T_C = T_{AIR} + (NOCT - 20) \times \frac{G}{800} \tag{4.1}$$

T_c and T_{air} are the cell and the ambient temperatures, respectively, G the irradiance, and NOCT the nominal operating cell temperature.

Whereas the air temperature and irradiance were measured and available, the NOCT was provided by the PV module manufacturers, similarly to the thermal coefficients.

Nonetheless, in order to find the real operating temperature and minimize the error, the NOCT will be experimentally calculated under the modules' real working conditions.

The NOCT is defined, for an open-rack mounted module such as ours, as the mean solar cell junction temperature in the following reference environment:

- Tilt angle: 45º from horizonal

- Total irradiance: 800 W/m^2

- Ambient temperature: 20 ºC

- Wind speed: 1 m/s

- No electrical load: Open circuit

This so-called "primary method" to determine NOCT is an outdoor measurement method used by both IEC 61215 and IEC 61646, and is universally applicable to all PV modules. In the case of modules not designed for open-rack mounting, the primary method may be used to determine the equilibrium mean solar cell junction temperature, with the module mounted as recommended by the manufacturer.

This NOCT determination procedure is based on the fact that the difference between the module and the ambient temperature is largely independent from the air temperature, and linearly proportional to the irradiance at levels above 400 W/m^2.

To calculate the NOCT experimentally, all data points taken during the following conditions were rejected:

- Irradiance < 400 W/m^2

- Wind Speed outside the range 1 ± 0.75 m/s

- Ambient Temperatures outside of 20 ± 15 ºC or varying more than 5ºC, a 10 min

- A 10 min interval after a wind gust of more than 4 m/s and wind direction within ± 20º East or West.

Additionally, all the entries where the temperature was zero were removed, as they corresponded to measurement errors.

From the linear regression of the difference between the module and the ambient temperature against irradiation, a preliminary value of the NOCT was obtained. This value was corrected to 800 W/m^2 and 20ºC. Below is an example of this procedure for the Sharp solar module.

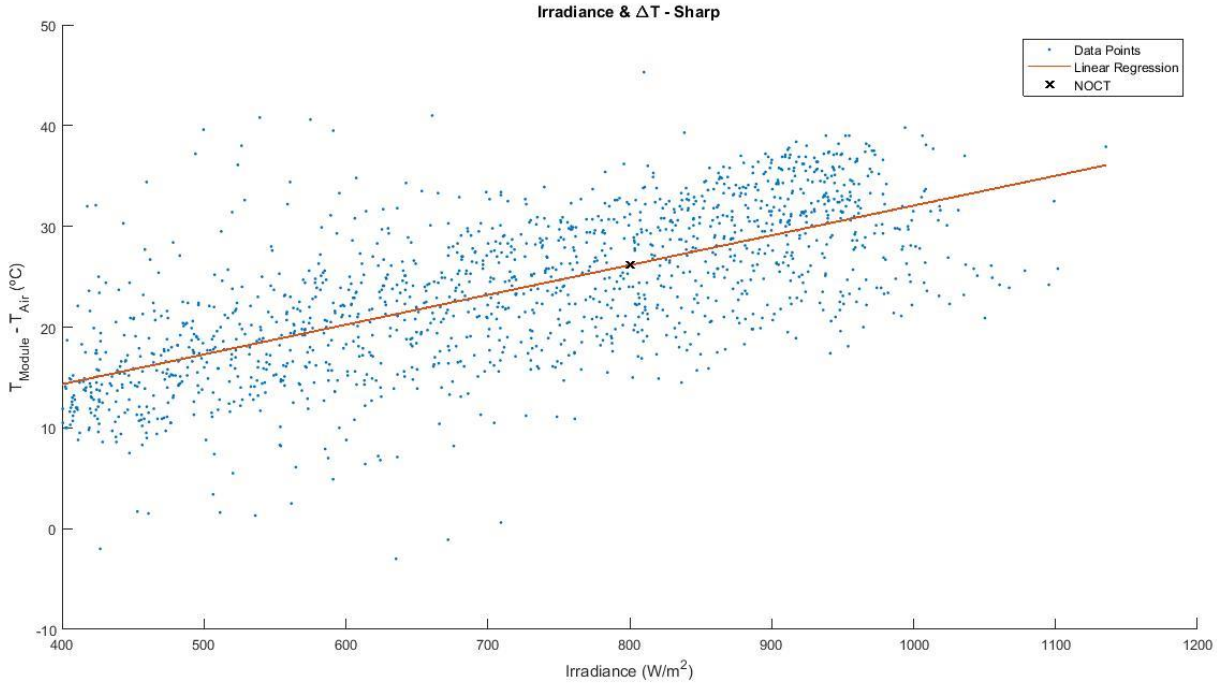

Figure 1: NOCT determination procedure (Sharp)

The temperature differences between the module and the ambient temperatures are higher in the afternoon than in the morning, due to fact that the ambient temperature rises during the day.

For this reason, the NOCT was estimated using the maximum possible data points in the morning and afternoon, giving averaged values more representative of the module's behavior during a day.

Finally, the prediction and confidence intervals were calculated to ensure the statistical significance of the linear regressions.

Confidence intervals consist of a range of values that act as good estimates of the unknown population parameter. With this method, for a pre-determined confidence level, a whole interval of acceptable values for the parameter is given instead of a single value.

The confidence interval is based on the observations from a sample, hence differing with sample size. Smaller samples generate wider intervals, following an inverse square root relationship between confidence intervals and sample sizes.

The prediction and confidence intervals were computed using the following equations.

$$Confidence_{Interval}: y_1 \pm t \times SE \times \sqrt{\frac{1}{length(x)} + \frac{(x_1 - mean(x_1))^2}{sum(x - mean(x))^2}} \quad (4.2)$$

$$Prediction_{Interval}: y_1 \pm t \times SE \times \sqrt{1 + \frac{1}{length(x)} + \frac{(x_1 - mean(x_1))^2}{sum(x - mean(x))^2}} \quad (4.3)$$

The y_1 represents the slope of the linear regression, to which the prediction and confidence intervals will be added. The t denotes the coefficient correspondent to the confidence level, according to the student's t distribution. Finally, SE stands for standard error, while the rest of the values are calculated.

The confidence level was set at 95%, a level deemed adequate for our analysis. This level indicates that there's a 95% chance that any point of the linear regression is within the calculated confidence interval. Conversely, there's also a 95% percent chance that any individual sample point lies within the prediction interval.

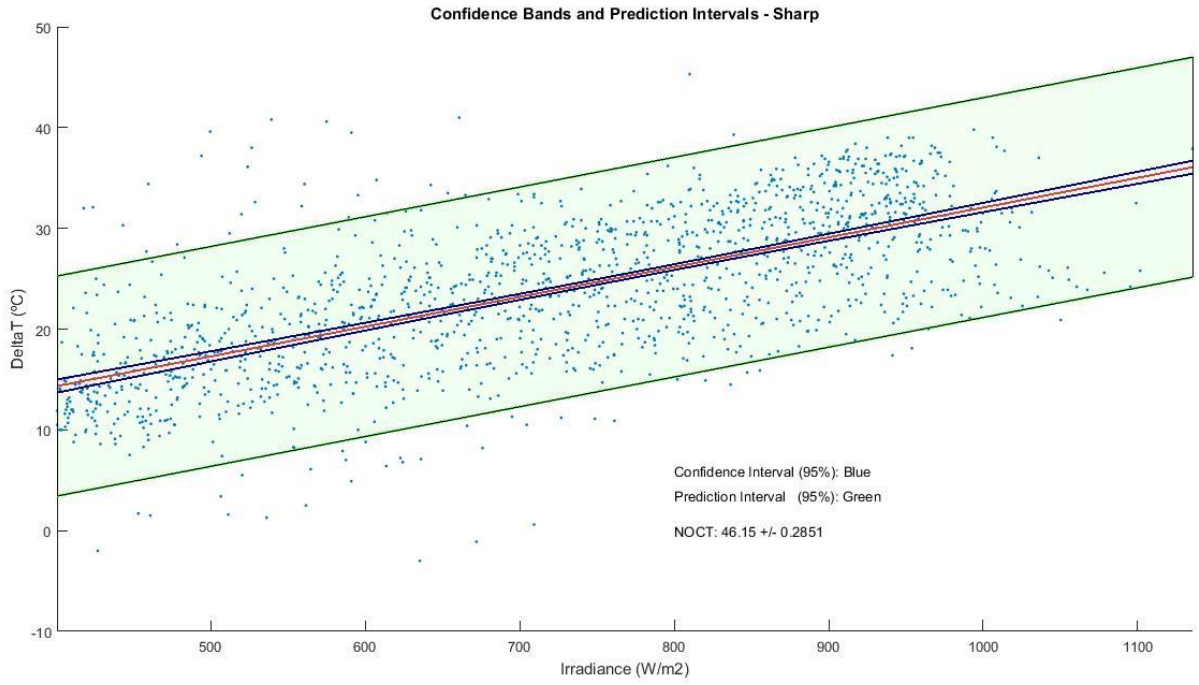

Figure 2: Confidence bands and prediction intervals for the NOCT regression (Sharp)

In the image below are represented both the confidence and the prediction intervals for the linear regression of the Sharp module. The confidence interval of the linear regression is given by the blue lines, which are closing in on both sides of the linear regression marked in red.

Whereas the prediction bands are clearly defined, encompassing a larger area, the confidence intervals are almost undistinguishable from the regression line.

The narrowness of the confidence interval is a product of the large sample size, drawing on over one and a half thousand points to estimate the intervals.

Following the NOCT determination procedures, the value of NOCT is obtained by adjusting the difference between the module and ambient temperatures at 800 W/m^2 to 20 ºC. As such, the uncertainty of this value will be given by the confidence values at this point.

For the Sharp solar panel, with a 95% confidence level, this resulted on a nominal operating cell temperature of 46 ± 0.2851 ºC.

This process was repeated for the other modules, ensuring the statistical relevance of this method.

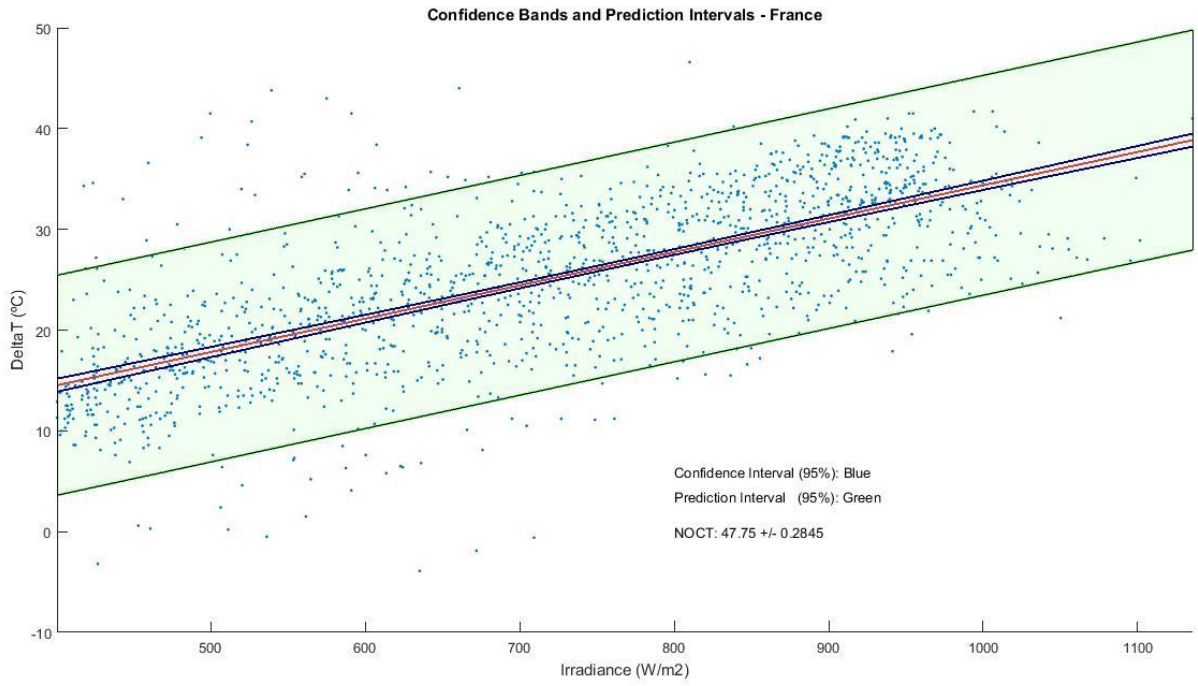

Figure 3: Confidence bands and prediction intervals for the NOCT regression (France Watts)

Once again, the NOCT stayed within a very reasonable interval range, straying less than once percent of its estimated value. The largest confidence interval was found on the Panasonic solar module, whose data sample registered the most dispersion among the panels.

With a sample size of less than half of the other modules, the Panasonic solar panel displayed the largest confidence interval. This was due to the increased dispersion of the data, as hinted by the prediction bands, as well as the reduced sample size.

Nevertheless, its confidence interval remained extremely narrow, well within one percent of the parameter's value.

Despite the small uncertainties in the NOCT calculation, inaccuracies of about ± 3 ºC in the NOCT value do not introduce excessive errors (about ± 1.5%) on the yearly performance estimations, as temperature has a second order influence on module energy output.

Having calculated the NOCT's, it was now possible to determine the module's temperature in function of the irradiance and ambient temperature. The modules' temperature estimates were now available for the entire duration of the study without any gaps.

Then, in order to determine how accurately these new temperature curves described the real ones, the average mean absolute error was calculated. This indicator measures the average magnitude of the errors in our set of predictions, regardless of their direction.

This was done by comparing the measured and the estimated temperature curves, averaging the difference between them over the intervals where they had valid records.

The formula presented below was used in this process.

$$Error\ (ºC) = \frac{\sum_{i=1}^{n} | T_{real}(i) - T_{Estimate}(i) |}{n} \tag{4.4}$$

This formula measures the average distance between these two curves at every single point of our valid domain. The valid domain encompasses all the intervals where the data points were different than zero.

For the Sharp solar module, the mean error was of 3.24 ºC, giving us a very precise estimate of the module's temperature during our study.

This error is close to the minimum possible obtainable error using equation (4.1), as we'll see ahead, which means that it's not possible to get a much more precise temperature estimate using this method.

The NOCT obtained experimentally was 46.15 ºC for the Sharp solar module, which was used to draw the temperature curve. This curve is an accurate representation of the module's thermal behavior; however, another method was employed in order to draw the temperature curves that best matched the real measured data.

These new curves were calculated through an iterative process of altering the NOCT, estimating the module's temperature with equation (4.1), and comparing it to the real measured temperature curve by calculating the error following the same procedure as before.

The best curve fit resultant from this process, nicknamed the ideal temperature, was then the curve that minimized the error, thus best adapting to the real temperature data.

This method yielded the best results, with an average error of 3.23 ºC for the Sharp module. For this reason, the so-called ideal temperatures obtained from this method were prioritized.

The table below summarizes some of the results for the panels studied:

	Sharp	France	Frontier	Panasonic	First
Manufacturers NOCT (ºC)	44	Not Given	47	44	45
Calculated NOCT (ºC)	46.15	47.75	Impossible	54.03	48.10
Ideal NOCT (ºC)	45.48	46.41	54.45	54.27	46.67
Calculated Curve Error (ºC)	3.24	3.59	4.60	9.37	3.17
Ideal Curve Error (ºC)	3.23	3.55	3.77	9.37	3.16

Table 1: NOCT model results. Calculated and ideal NOCT values and their respective temperature curve errors.

There are three types of NOCT values referenced in this table, each obtained through a different method.

The first one is the NOCT provided by the manufacturer in the datasheets. This value is often inadequate for temperature estimations, since in real operating conditions, different factors such as soiling can affect the nominal operating cell temperature. With this in mind, this value remained unused but was still referenced in the table, so as to allow a comparison between NOCT's obtained through different methods.

The two other NOCT values were used to estimate and draw the module temperature curves, and are a product of two different methodologies.

The calculated NOCT was obtained by filtering the data and applying a linear regression, following the NOCT determination procedures designated in the IEC 61216 and IEC 61646. The ideal NOCT, however, was calculated through an iterative process of error minimization between the ideal and the measured temperatures. Having tested different NOCT's over a reasonable interval range, the ideal NOCT was found to be the one that minimized the error, and thus whose resulting temperature curve best defined the real measured thermal behavior of the panels.

Finally on this table, are the calculated and ideal temperature errors. These correspond to the average errors between the real measured temperature points and the ones obtained through each procedure, measuring the success of each method.

While the calculated average error characterizes the average deviation between the measured and the calculated curves, the ideal average error denotes the error between the real measurements and the best possible temperature estimates using the IEC formula (4.1).

It's worth noting that there weren't sufficient reliable temperature records on the Solar Frontier module. As such, instead of calculating its NOCT through a linear regression, the manufacturers NOCT was used to draw the temperature curves for this panel.

In all cases, the ideal and calculated NOCT's were always in close agreement, which suggests that the experimental method for the NOCT calculation is accurate, and that the temperature curves are near the best possible temperature estimates using the IEC NOCT determining procedures.

This precision is illustrated below in figure 4, for the France Watts solar module, where all three temperatures were plotted against each other.

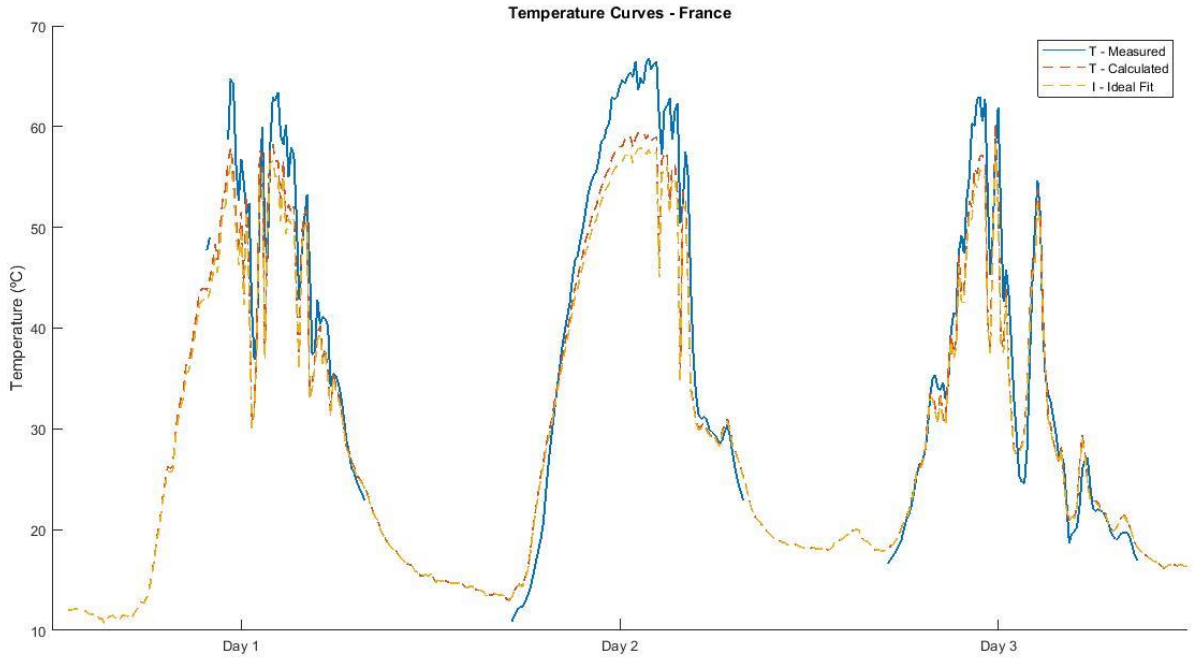

Figure 4: Measured and estimated temperature curves (France Watts)

As evidenced by the graph, there's a very strong correlation between the real and estimated temperatures, which allows us to have continuous records of every module's temperature during the entire duration of this study.

The cell temperature is essentially dependent on two main factors: Irradiance and air temperature. The air temperature heats the panel through conduction and convection, and conditions the minimum temperature the solar modules can achieve.

If it wasn't for the irradiance, the solar modules' temperature would follow the air temperature, with a certain thermal lag, depending on the insulating characteristics and thermal inertia of the panels. As such, the ambient temperature strongly affects the passive cooling of the PV panel, leading to an efficiency increase.

Solar irradiance, on the other hand, heats the panels through radiation, and the amount of heat transferred is proportional to the intensity of the irradiance.

Although there are several ways to minimize the heating effect caused by the Sun's radiation, such as special coatings and better air circulation around the panel, there aren't many solutions to counter the effects of air temperature.

In order to better illustrate this relation, the Sharp panel's real measured temperature was plotted over a day with a narrow ambient temperature variation range, thus allowing for a better visualization of the irradiance module temperature dependency.

The graph below shows the influence of these two parameters for the Sharp branded solar module during a typical summer day.

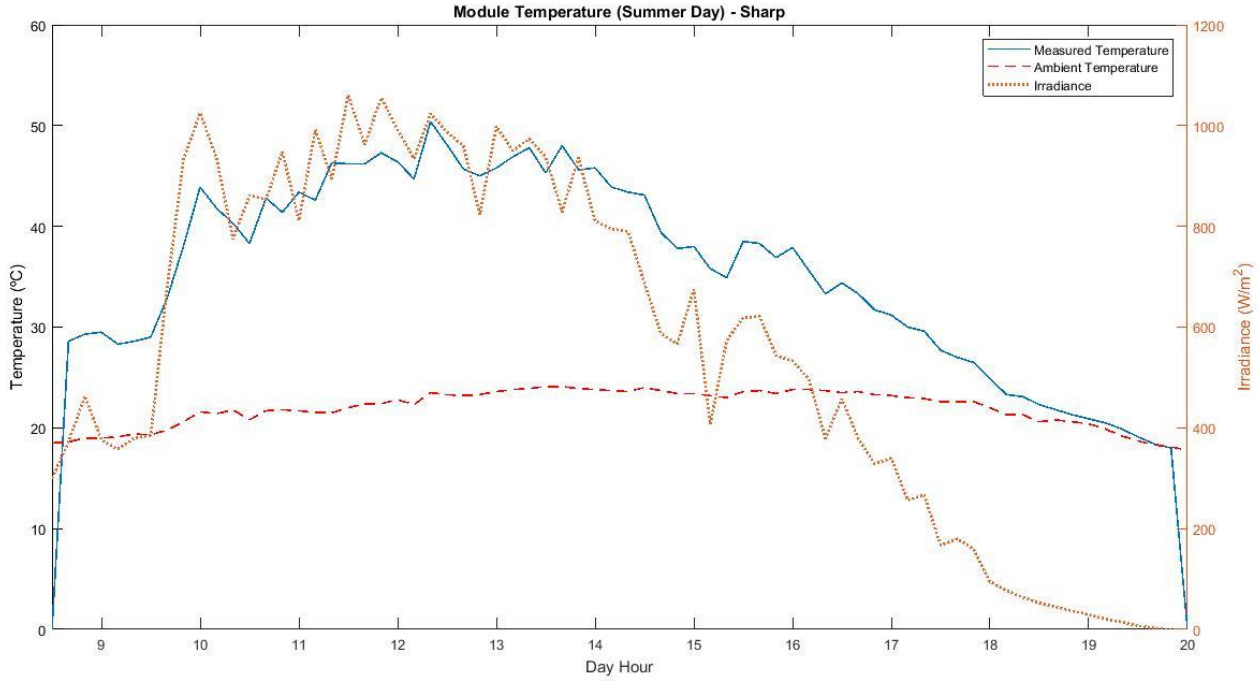

Figure 5: Measured and estimated module temperatures over a day with a narrow ambient temperature variation (Sharp)

As we can observe, the module temperatures are strongly conditioned by the irradiance. This is particularly visible during this specific day due to the low range of the ambient temperatures.

Finally, in order to get a sense of how subtly the ambient temperature influences the module's temperature, the same graph was plotted over the day of lowest irradiance.

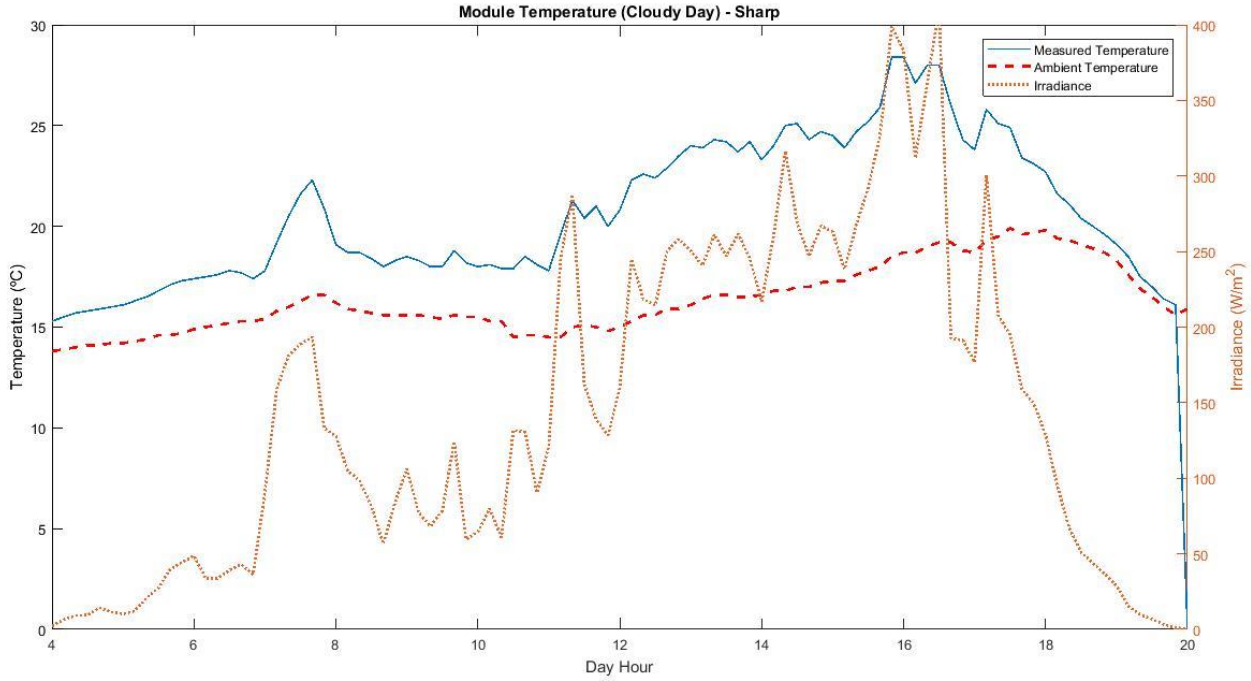

Figure 6: Measured and estimated module temperatures over a day with low irradiance

Despite the record low irradiance values, it's clear that the panel's temperature is strongly influenced by the irradiance, whilst being baselined by the ambient temperature.

4.1.2. HEAT Thermal Model

Since temperature is a key parameter ruling the conversion efficiency, it was deemed important to try to further increase the accuracy of the temperature estimates. This would allow for a better correction of the efficiency values to STC conditions, leading to a more precise estimation of the soiling losses.

The module temperature is dependent upon several factors, making it extremely difficult to obtain an accurate estimate. Simple estimates tend to rely on a few key parameters, such as ambient temperature, irradiance and NOCT. In order to increase the precision of this estimate, it's necessary to increase quality of the model, taking into account the maximum number of relevant parameters, approaching the model to reality.

The HEAT model, as its name suggests, was based on the precise modelling of a panel's energy fluxes. As such, the temperature of the panels will be estimated using a heat balance model, assuming the conservation of energy as follows:

$$Energy_{Input} = Energy_{Output} \tag{4.5}$$

This isn't necessarily true at every single moment, as it's this very imbalance of input and output energy that causes temperature to change, allowing for the estimation of the panels' temperature.

The energy balance equation for our solar panel can be best described by the equation below:

$$Radiative_{Input} = Radiative_{Output} + Convective_{Output} + Electric_{Output} \tag{4.6}$$

This simplified equation characterizes the heat balance of the solar module. The more accurate this model is, the more precise the temperature estimates will be. As evidenced by the equation, there is no mass transfer in our panel, making it a closed system.

In this equation, the radiative input corresponds to the total incident solar radiation on the panel. The radiative, convective and electric output correspond to the net energy transferred to or from the panel through those mechanisms.

These parameters were named outputs because they generally represent energy losses. However, these can be negative at times, when the ground radiation or air temperature heats the panels. Due to their relatively small contribution, the conduction losses were neglected in order to simplify the model.

The first step on the construction of this model was the calculation of the radiative input on the solar panel. For this, the direct, diffuse, and reflected radiation were separated, giving a more detailed estimate of the incident radiation.

The incoming radiation was calculated with the following equation:

|--Direct--| |---Diffuse---| |---------Reflected---------|

$$Radiative_{Input} = B_{NI} \times C_O + D \times C_s \times C_D + G \times R_G \times (1 - C_S) \times C_D \tag{4.7}$$

B_{NI}: Direct Irradiance (W/m^2), C_O: Average Transmissivity of the Glass for the Panel Inclination

D: Diffuse Irradiance (W/m^2), C_S: Fraction of the Maximum Absorbable Diffuse Radiation

C_D: Transmissivity Coefficient, G: Global Irradiance (W/m^2)

R_G: Average Reflective Index of the Surrounding Ground Floor

The transmissivity of the glass for direct radiation was fixed 0.67, which was the value previously calculated by integrating the transmissivities of the whole hemisphere. The transmissivity of the glass for diffuse radiation, on the other hand, is uniform and fixed at 0.8.

Finally, the average reflective index of the surrounding ground floor was fixed at 0.15, and the maximum absorbable fraction for diffuse and reflected radiation were calculated through the following formula:

$$Fraction_{Diffuse} = \frac{\cos(Slope)+1}{2} \quad [3.8]$$

It's worth noting that, in the case of the reflected radiation, the opposite was true, and the maximum absorbable fraction was given by:

$$Fraction_{Reflected} = 1 - \frac{\cos(Slope)+1}{2} \quad [3.9]$$

The image below details the panel's estimated radiative input over two typical days, detailing the contribution of the different types of radiation to the total as well.

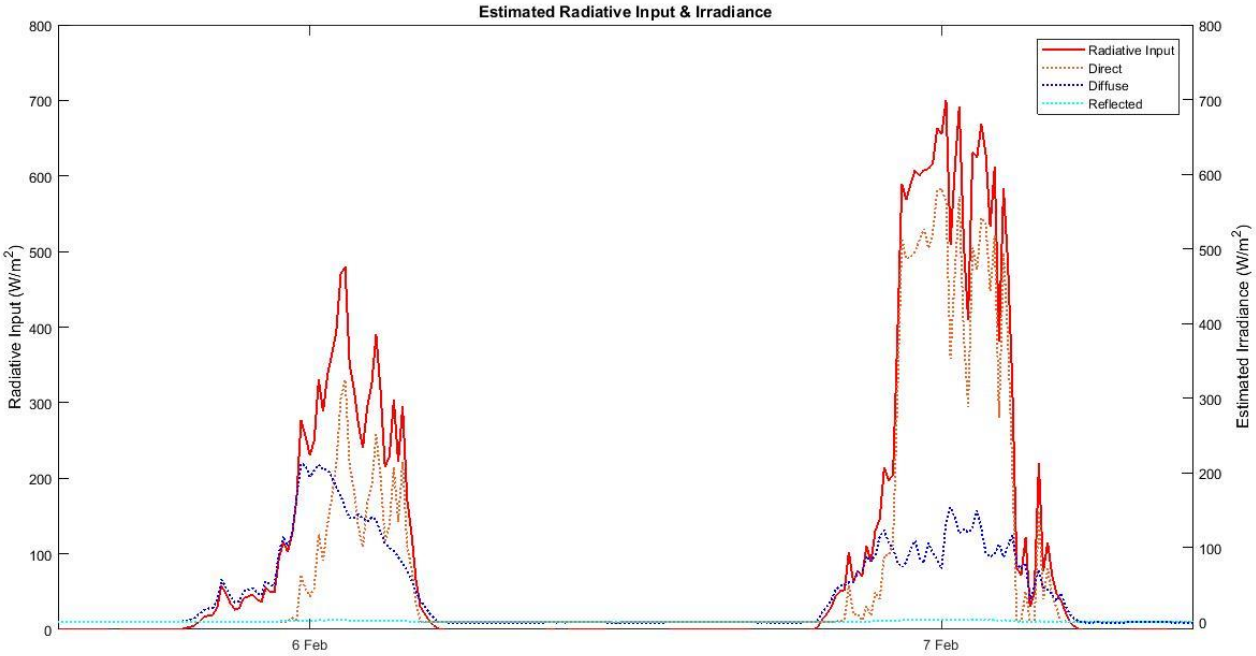

Figure 7: Radiative Input of the HEAT model (France Watts)

The radiative heat exchange between the panel and its surroundings was calculated according to the equation below.

$$Radiative_{Output} = \varepsilon \times \delta \times [\, 2T_m^4 - (T_s^4 - T_g^4)\,] \quad [3.10]$$

|Emission| |Absorption|

ε: Emissivity of the Panel , δ: Stephan Boltzmann Constant (J/m^2K^4)

T_m: Module Temperature (K) , T_s: Sky Temperature (K) , T_g: Ground Temperature (K)

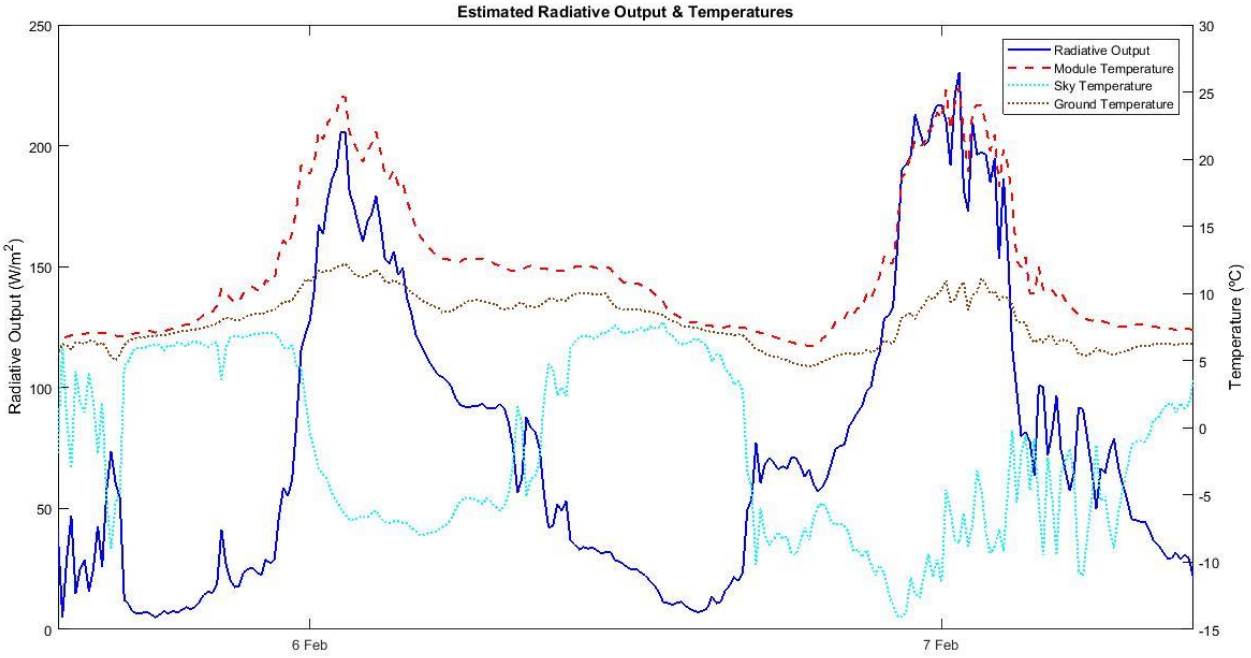

Figure 8: Radiative output of the HEAT Model (France Watts)

A basic temperature estimate was needed for the calibration of the model, and for this task the NOCT model was used.

For simplification purposes, it was assumed that the emissivity did not depend on wavelength, emission angle or temperature, and it was fixed at 0.8, using the so called "Grey Body" approximation.

The ground and sky were extrapolated from the values of the Upwelling and Downwelling longwave horizontal irradiance, using the formulas below.

$$T_g = \left(\frac{Upwelling_{Longwave}}{\delta}\right)^{\frac{1}{4}} \quad (4.11) \qquad T_s = \left(\frac{Downwelling_{Longwave}}{\delta}\right)^{\frac{1}{4}} \quad (4.12)$$

The convective balance of the module was calculated according to the formula below.

|Natural| |-----Wind-----| |Temperature|

$$Convective_{Output} = [\, h_1 + (h_2 \times WS^{Cws}) \,] \times (T_m - T_{Air}) \quad (4.13)$$

h_1: Convective Coefficient (W/m^{2}K) , h_2: Convective Coefficient (W/m^{2}K)

WS: Wind Speed (m/s) , CWS: Coefficient of Convection dependency on Wind Speed

Tm: Module Temperature (ºC) , TAir: Air Temperature (ºC)

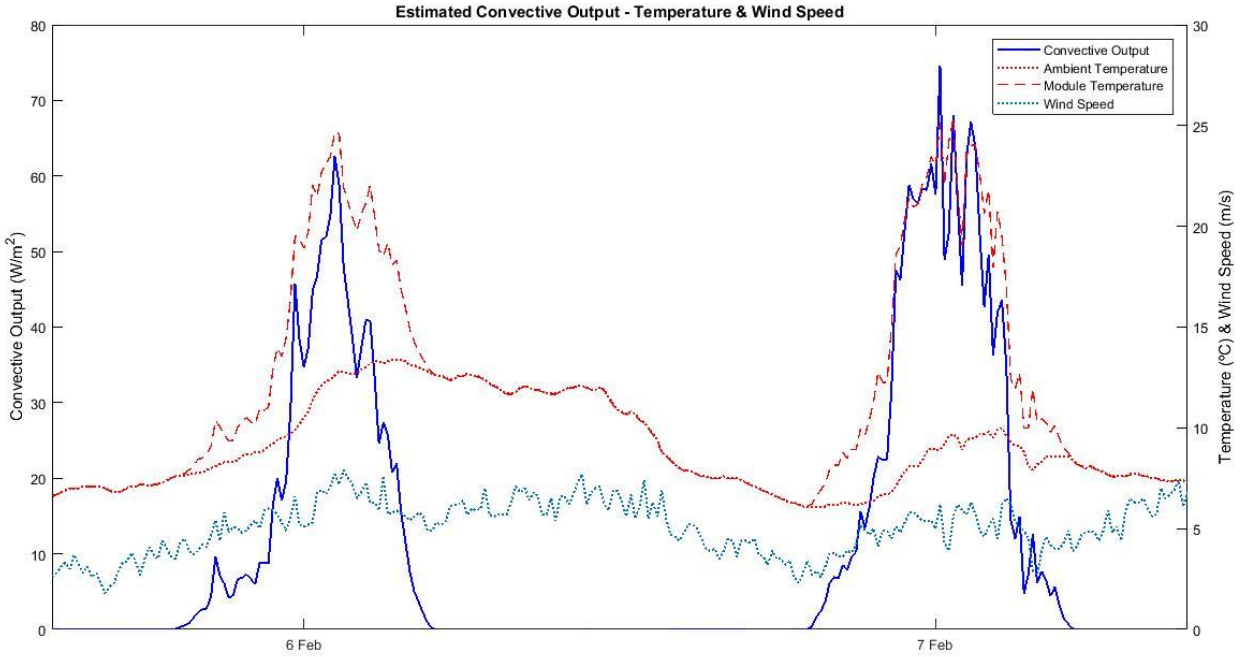

Figure 9: Convective Output of the HEAT Model (France Watts)

As this image suggests, the convective losses are proportional to the temperature difference between the panel and the ambient air. Wind speed is also represented, allowing for a more complete modelling of the panel's thermal behavior.

Finally, the electric output of the panel was calculated with the following formula:

|Efficiency| |-----Correction-----|

$$Electric_{Output} = A \times G \times \eta_{STC} \times [\, 1 + \beta \times (T_m - 25) \,] \times F \qquad [3.14]$$

A: Solar Panel Area (m^2) , G: Radiative Input (W/m^2) , η_{STC}: Module Efficiency at STC (%)

β: Power Correction Coefficient (%/ºC) ,T_m: Module Temperature (ºC) ,

F: Electric Output Adjustment Factor

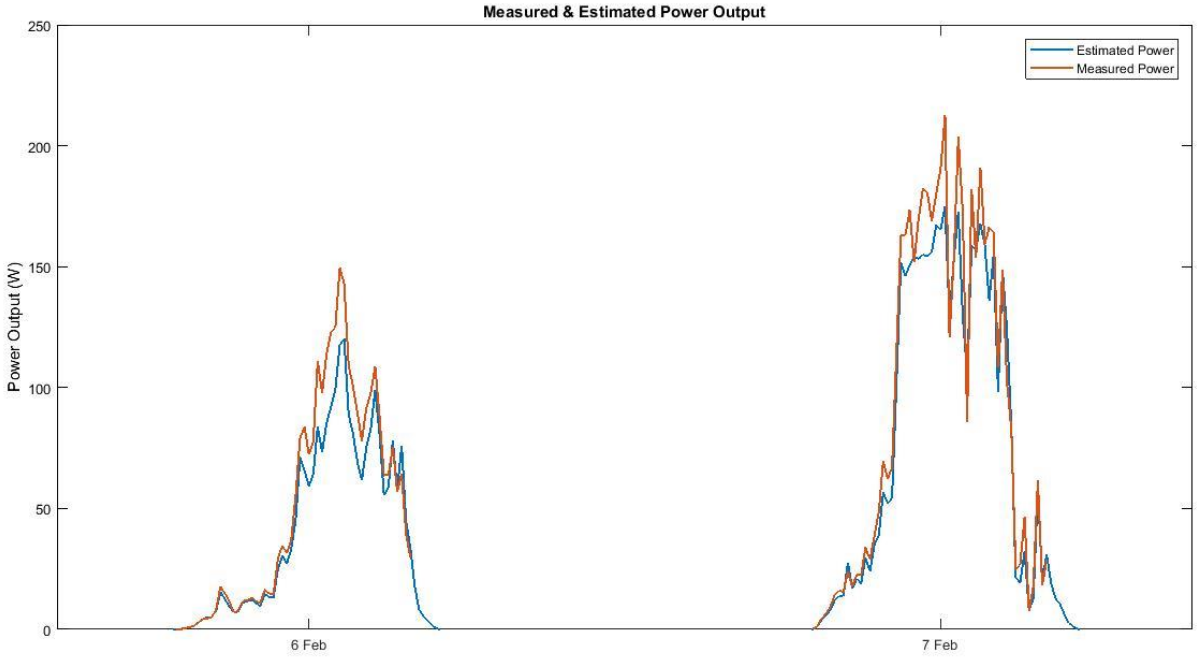

Figure 10: Electric Output of the HEAT Model (France Watts)

Once again, the NOCT model was used to provide temperatures for this model. Ideally, the electric output would be calculated with the estimates resultant from the HEAT model, which would create an infinite loop where temperatures would be calculated and reinserted in the model, only to be recalculated again. For this reason, and similarly to the calculation of the radiative output, the NOCT model was used to provide a basic temperature estimate.

The adjustment factor is present in the formula due to the fact that the panels are not connected to the grid. Instead, they're only briefly connected on regular basis so as to allow measurements to be carried out.

Lastly, both the STC efficiency and the thermal coefficients were extracted directly from the manufacturer's datasheet.

After having revised and refined each member of the heat balance equation, it was possible to start extracting the module temperatures. At this stage, since only the convective parameters and module temperatures were unknown, the convective parameters were isolated, and the module temperature estimated.

$$T_m = \frac{Radiative_{Input} - (Radiative_{Output} + Electric_{Output})}{[\,h1 + (h2 \times WS^{CWS})\,]} + T_{air} \qquad (4.15)$$

Here we have the module temperature described as a function of the heat balance of the solar panel. In order to find the best possible temperature curve, it's necessary to find the parameters that best adjust the estimated curve to the real measured temperature curve.

The module temperature can be calculated by computing the formula above. The best estimate is considered to be the temperature curve that best matches the real measured temperature curve. As such, this estimate is optimized by comparing it to the real data, changing the parameters iteratively in order to find the best possible temperature fit.

Initially, a simpler approach was taken, assuming certain values for the equation terms and optimize only the convection parameters. These parameters were then further simplified, resulting in a single convection coefficient.

This approach was based on estimating all parameters beforehand, such as the transmissivity of the glass or the reflectivity of the ground floor, and obtaining the best temperature estimate whilst varying only the convection parameters. The main advantage of this method lies in its simplicity, ensuring acceptable run times of an otherwise very slow optimization process.

The best temperature estimate was considered to be the one that minimized the following error:

$$Error\ (\%) = \left[\sum_{i=1}^{n} \frac{|T_{Real}(i) - T_{Estimate}(i)|}{T_{Real(i)}}\right] \times \frac{100}{n} \tag{4.16}$$

$$Error\ (\%) = \left|\sum_{i=1}^{n} \frac{Radiative_{Input} - (Radiative_{Output} + Electric_{Output})}{h} + T_{air} - T_{Real}\right| \times \frac{100}{n} \tag{4.17}$$

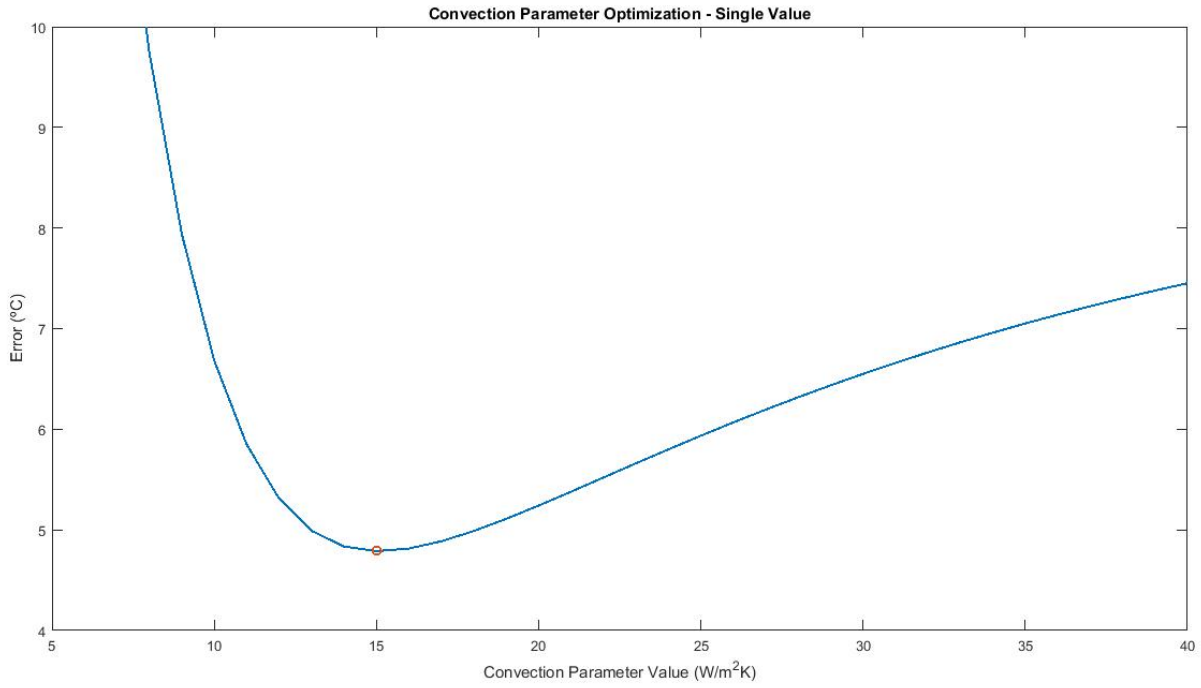

Figure 11: Optimization of the single parameter convection model (France Watts)

The convective parameters that best described the real temperatures were h=15 W/m^{2}K.

The error temperature estimate was of 4.78 ºC on average, a value that is expected to be minimized once the number of convection parameters is increased. In comparison, the traditionally NOCT estimated temperature had an average error of 3.55 ºC.

Both can be considered fairly accurate, since these were calculated point by point, and it's incredibly difficult to obtain detailed temperature estimates.

This precision is illustrated in the graph below, where the daily real measured temperature, the estimated through the thermal model, and the one obtained through the NOCT model.

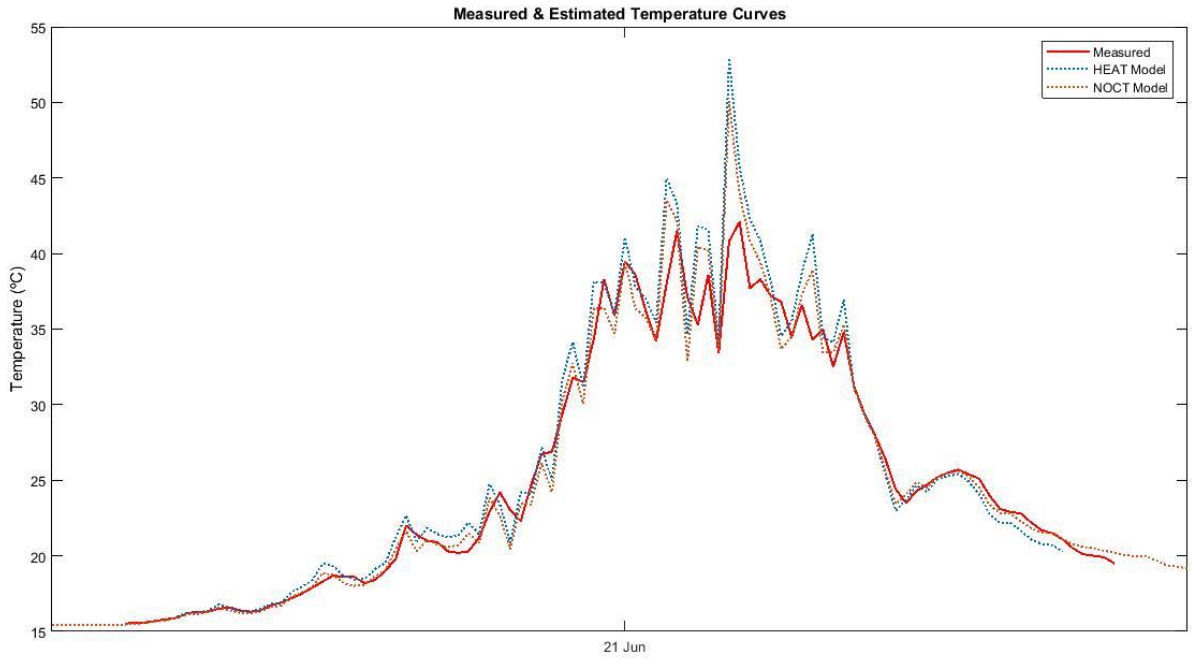

Figure 12: Accuracy comparison between the NOCT and the single parameter convection HEAT model (France Watts)

As we can observe in this figure, both estimates accurately describe the thermal behavior of the solar panel.

As of this moment, the NOCT based temperature estimate was more precise. But as the complexity of the HEAT model increases, so does its prediction capability, theoretically yielding more precise temperature records throughout the day.

In order to achieve this, the convection parameters were refined, and the average error of the model's estimate was now calculated by the following equation:

$$Error = \left| \sum_{i=1}^{n} \frac{Radiative_{Input} - (Radiative_{Output} + Electric_{Output})}{h_1 + (h_2 \times WS^{C_{WS}})} + T_{air} - T_{Real} \right| \times \frac{100}{n} \qquad (4.18)$$

By increasing the complexity of the convection losses equation, going from a single parameter to a multi-parameter convection model, the temperature estimate should in theory be more precise, thus minimizing the error.

However, despite the increase in model complexity, its prediction capabilities did not improve. Different convection parameters were tested, but none exceeded the accuracy of the single parameter model. In fact, the most complex models, which incorporated wind speed as a function of a second convection coefficient, produced higher errors.

This trend suggests that there was problem with the model, and it was necessary to look further into the different terms of the heat balance equation.

To this end, all model parameters were individually varied and tested. Parameters that were previously constant, such as the transmissivity of the glass for direct and diffuse radiation and the average reflectivity of the ground, were now incorporated and tested through an optimization procedure.

It was found that a more accurate temperature estimate was obtained when only the global irradiance was used to estimate the energy input. With this in mind, the radiative input was altered so as to prioritize the global irradiance, and a new heat balance equation was devised.

$$Error = \left| \sum_{i=1}^{n} \frac{(Irradiance_{Global} \times c) - (Radiative_{Output} + Electric_{Output})}{h_1 + (h_2 \times WS^{C_{WS}})} + T_{air} - T_{Real} \right| \times \frac{100}{n} \quad (4.19)$$

This much simpler formula calculated the energy input as a function of the global irradiance, using a coefficient and other variables instead of the reflectivity index to characterize the radiative input. That coefficient is represented by the letter c, and it regulates the amount of radiation the panel receives as a function of the global irradiance.

The best error obtained was in the order of 3.9 ºC, using the most complex convection model. The results also indicated that the more complex the convection model used, the more precise the results, although the difference was almost neglectable.

The same could not be said about the radiative input model, where the best results were attained using the simplest possible model. This consisted in the use of the global irradiance and a single coefficient to calculate the total energy absorbed by the solar panels.

Even though this model allows for an accurate description of the panels' temperature along the year, it is not a truly predictive model. It is so because this model had no physical significance, in the sense that it was not modelled after reality, but simply the best result of a long optimization process aiming to approximate the estimated to the real temperatures.

Naturally, then, this model cannot be applied immediately to any other solar panel since the coefficients were attained through an extensive experimentation process, with no regard for future reproducibility.

Despite this, both models produced comparable results, accurately predicting the module's temperature during the day. Finally, in order to demonstrate the relatively small difference between these two estimates, the yearly power output of the solar panel was calculated using temperatures of both models.

|Efficiency| |------Correction------|

$$Electric_{Output} = A \times G \times \eta_{STC} \times [\,1 + \beta \times (T_m - 25)\,] \quad (4.20)$$

A: Solar Panel Area (m^2), G: Radiative Input (W/m^2), T_m: Module Temperature (ºC)

η_{STC}: Module Efficiency at STC (%), β: Power Correction Coefficient (%/ºC)

Since the temperature has only a second-order influence on the panel's efficiency, and thus on the power output, the differences were minimal. The power output over two typical days can be observed in the graph below for a typical winter day.

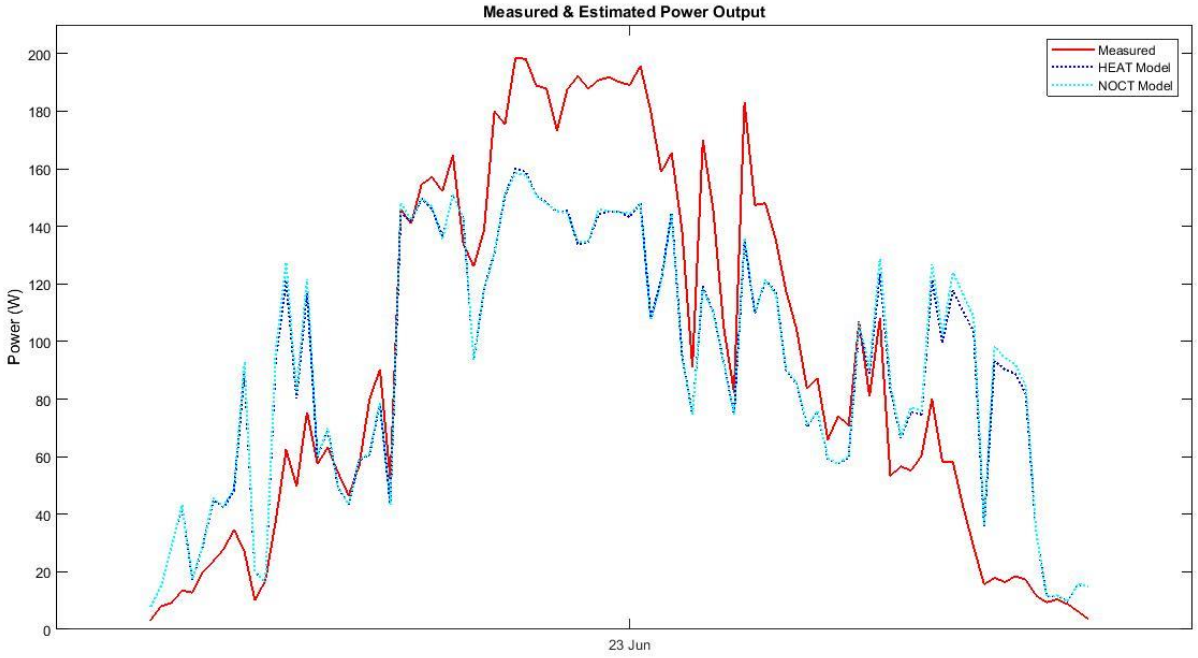

Figure 13: Accuracy comparison between the NOCT and HEAT models (France Watts)

As we can observe, there's a strong correlation between the three power curves. Perhaps most interestingly, is to note that the estimates are virtually indistinguishable.

Since temperature has a limited influence on efficiency, and thus on power generation, it's hardly surprising that such similar temperature estimates would yield almost identical power predictions. In fact, it's only possible to distinguish these two power curves during times of high irradiance, where the models start to diverge slightly.

It's was also generally observed that the power measurements largely exceeded the model predictions during peak hours, where the models tended to underestimate the power output.

On the other hand, this problem was counteracted during the very early and late hours of the day, where the models tended to overestimate the power production. This small discrepancy can be attributed the

oversimplification of the energy input, which ended up being solely based on the global irradiance, no longer taking into consideration the transmissivity of the glass and other relevant factors.

The models were then tested, aiming to determine their accuracy in predicting power generation, using the average daily power production during the day.

In order to ensure a balanced test, certain filters were applied to both the real and the predicted values. These filters consisted in the exclusion of the power output values whenever one of the estimates could not produce one, assuring that the estimates were compared on common points only. This way, if for some reason the real power wasn't measured, or a model did not function during certain hours, these values were excluded for all panels.

Estimate Type:	*Real*	*NOCT*	*HEAT*
Average Daily Power (Wh)	763.8	757.9	802.5
Prediction Error (%)	-	0.76	5.1

Table 2: Prediction error of the NOCT and HEAT models.

The table above indicates the average daily power production using each of the models.

The data is relevant to a period of one year for the France Watts solar module, over which the NOCT model revelated incredibly accurate. Nevertheless, both estimates accurately predicted the power production within a very reasonable margin of error.

These results demonstrate that any of the temperature models can be used to study the panel's efficiency, since their already minor differences translate into even smaller power output or efficiency differences. But more importantly, these results prove that both models can be employed to study the panel's soiling induced efficiency degradation.

4.1.3. Model Testing and Validation

Having tested and compared the thermal models, it was found that the NOCT based model yielded the best results. For this reason, this model was used to estimate the temperatures for the thermal correction of the efficiency values.

Previously, the accuracy of the models was assessed through the absolute mean error, a value which indicated the absolute mean deviation of the estimates from reality. However, despite being a reliable metric for the overall performance of the model, it failed to characterize it beyond a basic level.

Aiming to ensure the reliability of the temperature estimates, it was deemed important to deconstruct and analyze the NOCT model, allowing for a better understanding of its consistency and tolerance under different conditions.

To this effect, key components of the model will be tested and summarized in an effort to identify critical variables and illustrate the model's behavior.

Two of these variables are the estimate's error and the module's temperature above the ambient, whose relation is shown on the graph below.

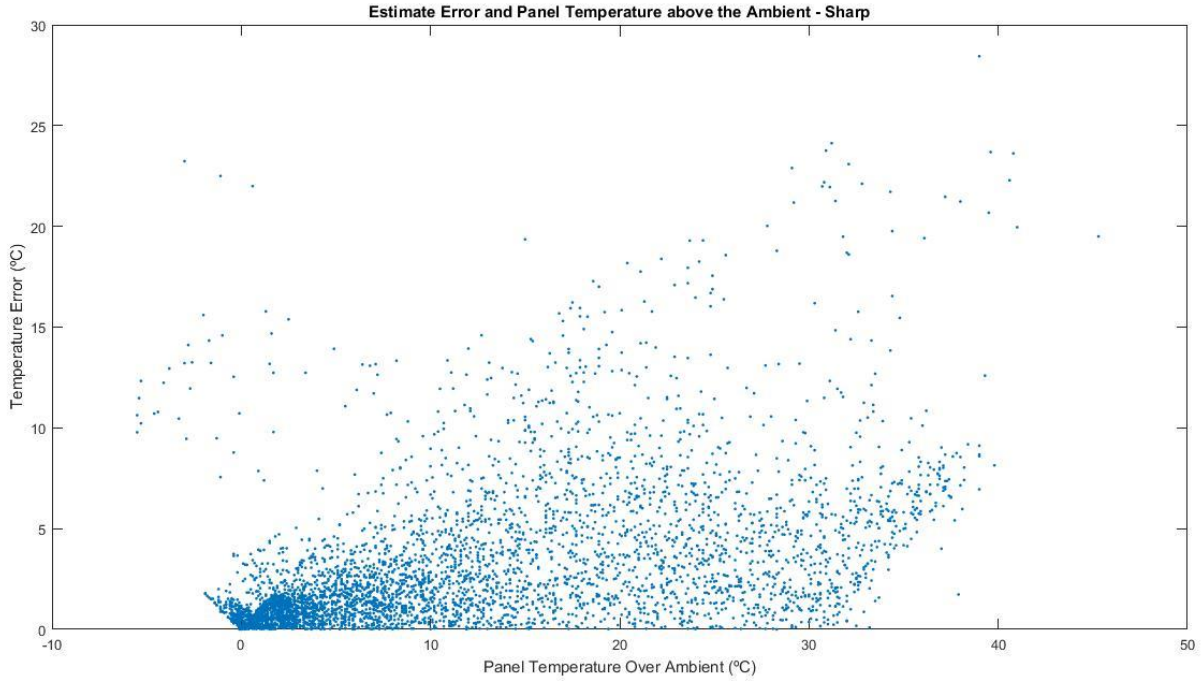

Figure 14: Distribution of the NOCT model's error with module temperature above the ambient (Sharp)

At first glance, there seems to be a correlation between the two. As the module rises above ambient temperature, so does the estimate's error.

This is in accordance with our expectations, given that the module's temperature is based on both the irradiance and ambient temperature, becoming increasingly more reliant on the latter at lower irradiance levels.

The model assumes that both conduction and convection losses increase linearly with irradiation for a given wind speed, provided that the thermal resistance and heat transfer coefficient do not strongly vary with temperature. As such, the ambient temperature's role is fixed, serving only as the baseline upon which the model is built.

It then follows, due to the very nature of this model, that it should be increasingly accurate as the module approaches the ambient temperature, coinciding with progressively lower irradiance levels.

This was partially confirmed in the graph below, where the estimate's error was plotted along the difference between the module temperature and its surroundings.

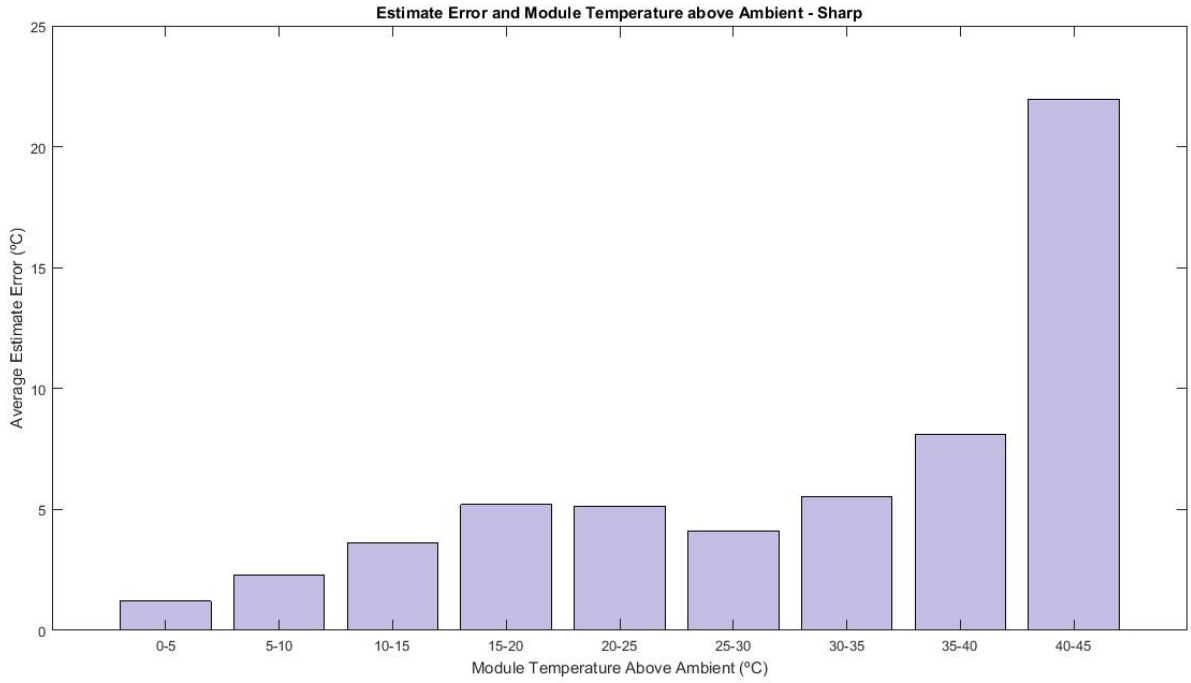

Figure 15: Average NOCT model error with module temperature above ambient (Sharp)

It's evident that the model's accuracy declines at higher levels of irradiance, where the module's temperature is increasingly higher than the ambient temperature.

However, the model didn't behave as predicted, since the estimate's error failed to continuously increase with the temperature difference.

This was hypothesized to be related to our sample size, which might not be sufficiently large to yield a strictly increasing function. The data used in this analysis, belonging to the Sharp solar module, spanned less than two months, thus being relatively short for this kind of analysis.

In order to verify the validity of this assumption, the same graph was plotted using longer set of data, belonging to the France Watts solar module and referent to a year-long period.

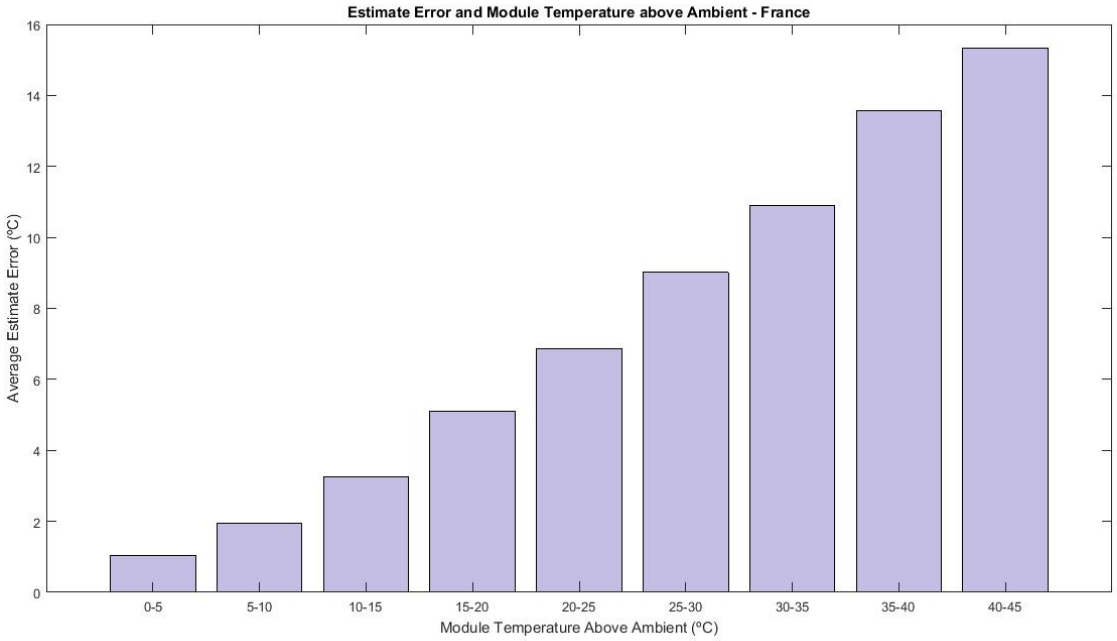

Figure 16: Average NOCT model error with module temperature above ambient (France Watts)

By plotting a longer set of data, we were able to confirm out assumptions that the model's error steadily increases as the module climbs over the ambient temperature.

At lower levels of irradiance, when the module is barely above the ambient temperature, the errors are almost insignificant. But as the day progresses and the modules warm far beyond the temperature of the surrounding air, the errors increase linearly as a function of this temperature difference.

This could pose a problem, depending on the distribution of these temperature differences. If these were mostly concentrated within a reasonably low range, then the model wouldn't introduce significant errors. If, however, the module was consistently far above the ambient temperature, then it would provide slightly inaccurate estimates.

Ideally, then, the panel would stay close to the ambient temperature, as it is at these temperature levels that the model more successfully produces reliable estimates of the panel's thermal behavior. However, during the summer months, where irradiance is at its highest, the module is consistently far beyond the ambient temperature.

Once again looking at the France Watts solar module, the distribution of the module temperatures above the ambient temperature was plotted.

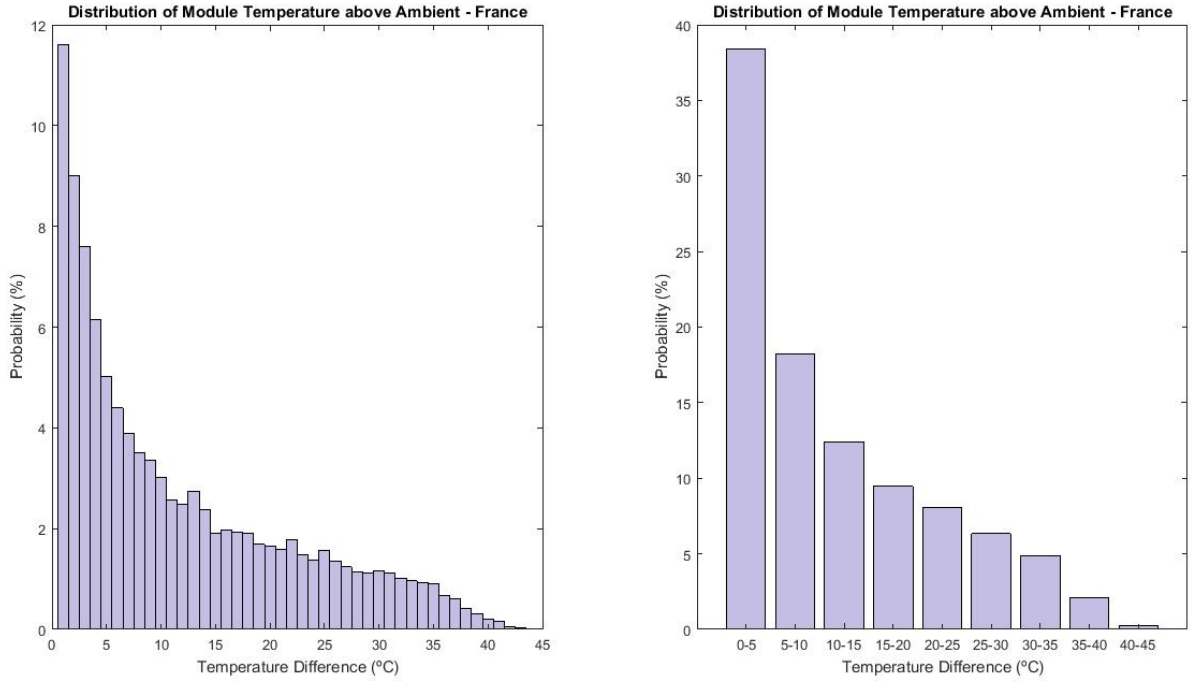

Figure 17: Distribution of the module temperatures above ambient (France Watts)

In this figure, both histograms depict the same distribution, the difference being in the width of the bins. Whereas the left one has single unit bins, each corresponding to a single degree Celsius, the right one groups the data in wider bins.

It's possible to observe in either of them that the module tends to be close to the ambient temperature, being within a ten-degree difference for over half of the time. This indicates that the model will not introduce widespread significant errors.

The more this distribution leans to the left side of the abscissae, the better the model accuracy will be. This stems from the fact that the model's error is proportional to the temperature difference between the module ambient, as seen before.

In order to visualize this phenomenon, the two previous distributions will be combined, giving an overview of the model's behavior at its different levels of irradiance.

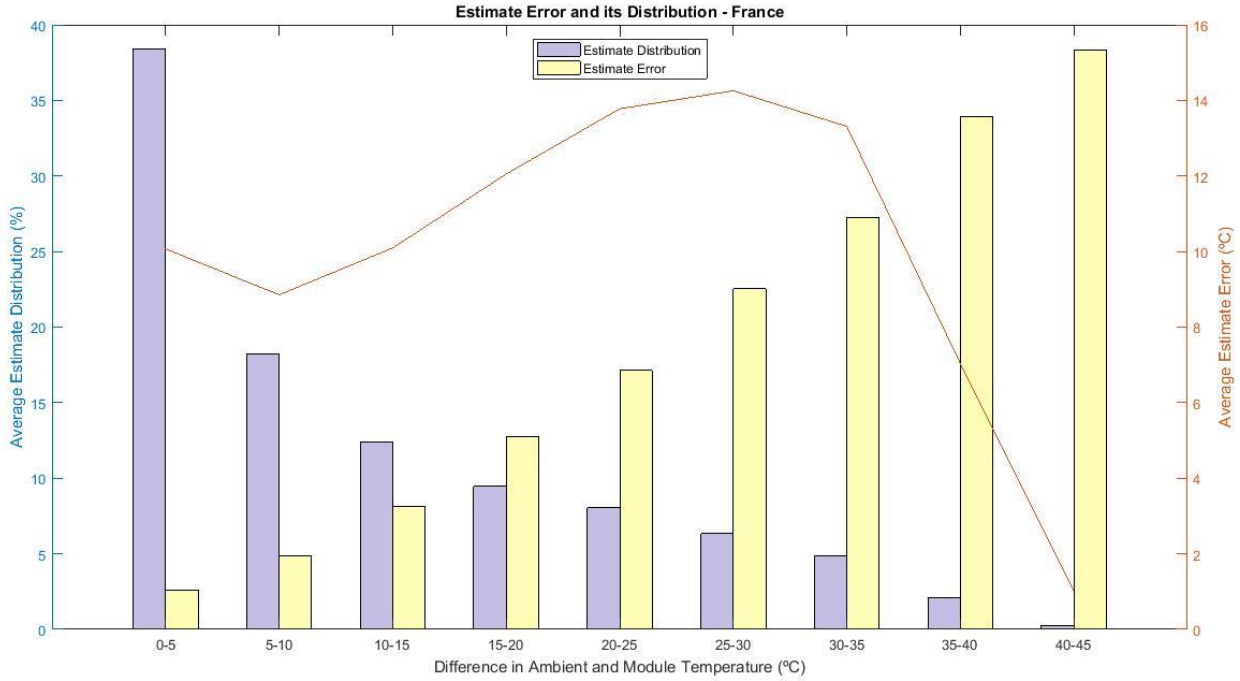

Figure 18: Relative contribution of each temperature range to the estimate's overall error (France Watts)

In this figure are represented two key parameters in the evaluation of the model quality. The first one, represented by the blue bars on the left axis, indicates the distribution of the module temperatures above ambient.

The second, represented by the yellow bars, indicates the average error of the estimate, once again for the various possible module temperatures above ambient.

When combined, they indicate the relative contribution of each temperature range on the estimate's overall error. This was obtained though the multiplication of the probability of the module being within a certain temperature interval over the ambient temperature, by that interval's corresponding average error.

The results of this dimensionless analysis are outlined in red, as a visual aid to assess the relative importance of each bin into the estimate's overall error. As we can see, the relative contribution of each temperature range varied according to these two parameters.

Previously, only the mean absolute error of the whole estimate was known. But having separated the estimates by frequency and their respective average errors for different temperature ranges, it was possible to determine the origin and magnitude of the errors.

Through this analysis, the errors were found to be fairly evenly distributed across the temperature ranges. As the module rises above the air temperature, the frequency of measurements declines at about the same rate at which the average error increases, offsetting each interval range in an analogous way.

This is visible on the first temperature bin, which simultaneously registered the highest number of estimates and the lowest associated average error. Although most errors were found to be at this lower temperature interval, they were of smaller magnitude, and therefore less influential to the estimate's overall prediction error.

Due to their high frequency and sizeable average error, the estimates taken with the module within twenty-five to thirty degrees over the ambient temperature tended to be the most damaging to the model.

On the other hand, estimates taken with the module within forty to forty-five degrees above the ambient temperature proved to be the least damaging for the model. Despite registering the highest average error among the temperature ranges, their extremely low frequency ensured the stability of the model.

This analysis was repeated for the Sharp solar module, yielding comparable results.

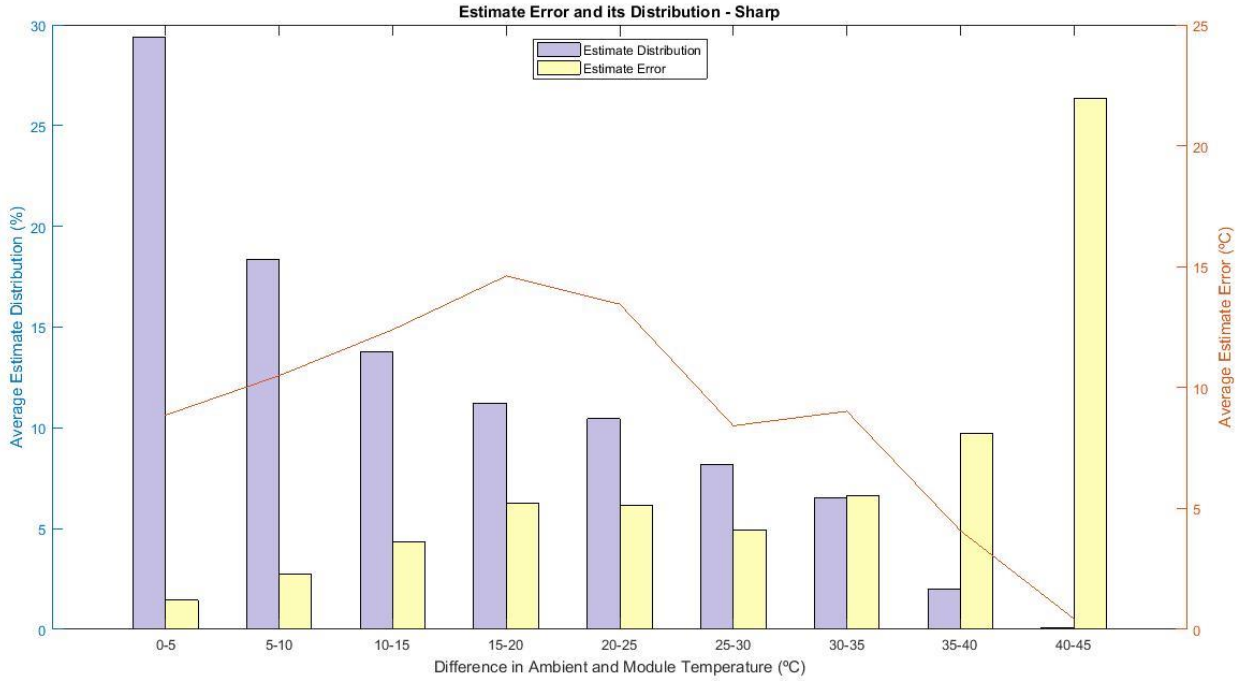

Figure 19: Relative contribution of each temperature range to the estimate's overall error (Sharp)

Once more, the red line exhibited this characteristic shape, reminiscent of a normal distribution curve. Except this line, whose purpose is to outline each bin's relative contribution to the model's overall error, was now slightly dislocated to the left.

This indicates that the most significant contributions to the estimate's overall error were introduced at lower module-ambient temperature differences. On the other hand, the France Watts solar module tended to register its most significant error contributions at higher temperature differences, reflecting its decreased accuracy at these levels.

These figures allow for the detection of several key differences between the modules. Whereas the estimates for the Sharp branded module tended to be accurate throughout the temperature ranges, the accuracy for the France Watts solar module dwindled as its temperature rose.

Additionally, due to differences in their thermal properties, it was found that the Sharp module was on average warmer than the France Watts, consistently registering temperatures farther above ambient. Since the NOCT model works best at lower module temperatures, this impacted negatively its thermal modelling, further hindering its accuracy.

The results showed that the France Watts module registered a smaller overall error, possibly a product of its slightly higher accuracy at lower temperature levels, where the estimates were more densely concentrated.

The final part of this analysis consisted on the assessment of the model quality based on the error distribution. To this end, the frequency of occurrence of each error was sorted by magnitude, once again taking the form of two histograms of different bin widths.

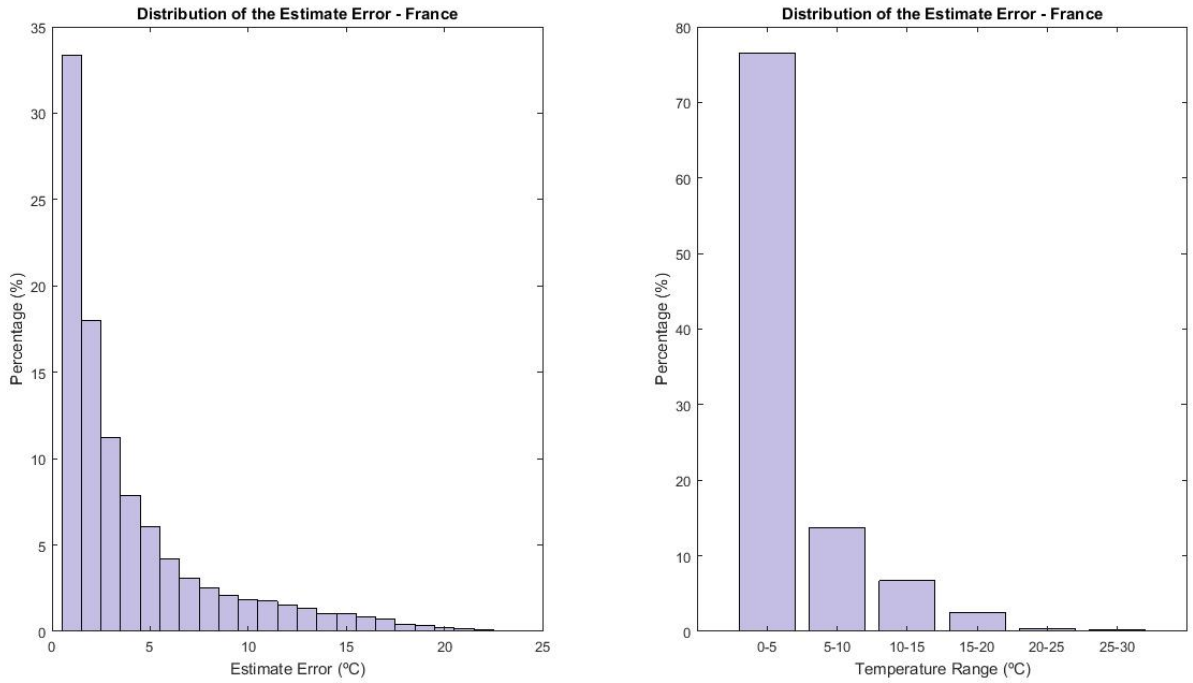

Figure 20: Frequency distribution of the estimate's error (France Watts)

As the figure suggests, the NOCT model accurately predicted the module's temperatures. In fact, around fifty percent of the estimates fell within a two degrees margin of the measured value, and close to eighty percent within five degrees.

This analysis was repeated for the Sharp solar module, yielding almost identical results.

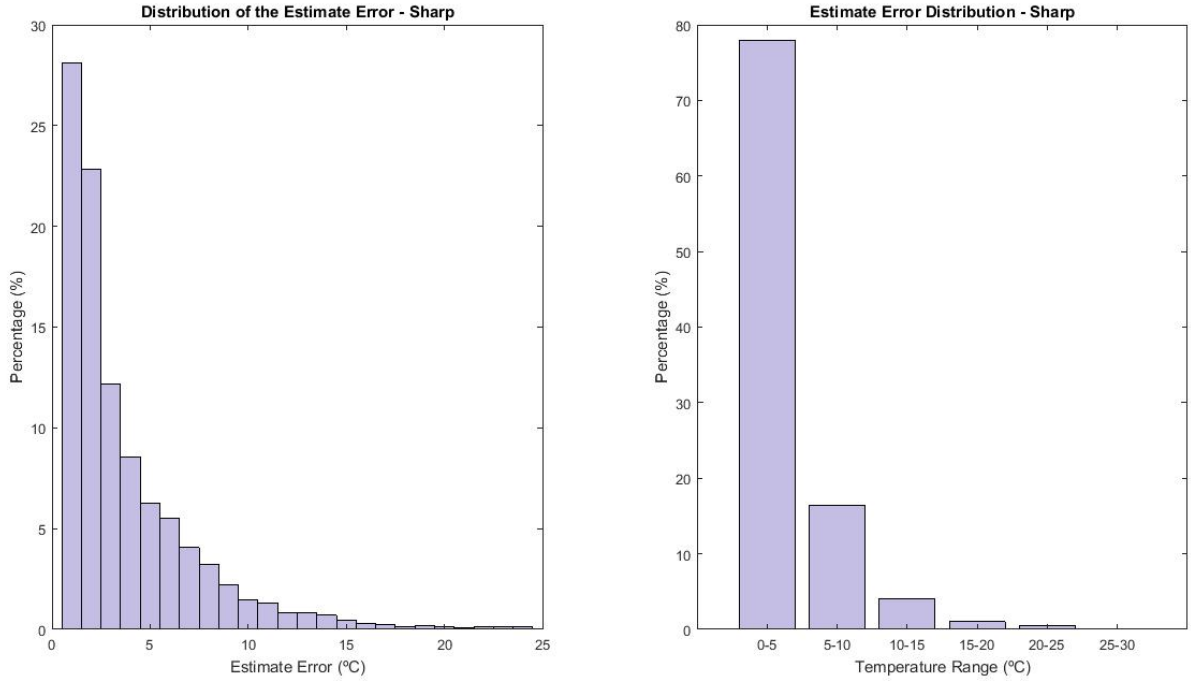

Figure 21: Frequency distribution of the estimate's error (Sharp)

The NOCT model has performed extremely well for both modules, proving it can be employed in the study of the soiling induced performance degradation.

As mentioned before, this model worked best for the France Watts solar panel, whose estimates were more accurate on average. This is particularly visible on the narrow-binned histograms, where a left leaning steeper curve correlates with higher accuracy.

Upon closer inspection it's possible to observe that, on the France Watts solar module, there was a higher frequency of one-degree error estimates. This alone resulted on a sizeable contribution towards an overall more accurate estimate, since these represented about one third of the estimates.

Nevertheless, the NOCT model functioned well for both models, accurately predicting the panel's temperature with minimal inaccuracies.

4.2. Efficiency Calculation

The first step in the study of soiling losses was the calculation of the photovoltaic efficiency. This is solely dependent on two factors, the module's power output and the incoming solar irradiance. The energy output was measured in Watt (W), and the irradiance in Watt per square meter (W/m^2), and subsequently adjusted to the area of the solar panel.

The photovoltaic efficiency was determined by the following formula:

$$Efficiency\ (\%) = \frac{Power\ (W)}{(Irradiance\ \left(\frac{W}{m^2}\right) \times Area\ (m^2)} \times 100 \qquad [3.21]$$

In order to exclude possible efficiency outliers, due measurement errors or very low light conditions, the following data points were excluded from the efficiency calculations:

-Irradiance < 5 W/m^2 ∨ Irradiance > 1500 W/m^2

-Output Power < 3 W

-Efficiency > 35 %

The first two filters assured that no efficiency was calculated in very low light or unrealistic conditions, while the third filter sieved through all the impossible efficiency calculations due to the mismatch between power and irradiance values.

These procedures were applied to all panels, for a period spanning close to twelve months, corresponding to the available data for the panels in question. This resulted in an accurate series of efficiencies, with a ten-minute sampling rate, over a period of three hundred and thirty-two days.

The figure below contains two series plotted independently over the period of a year and a month, respectively, for the Sharp branded solar module, whose results are representative of all experiments.

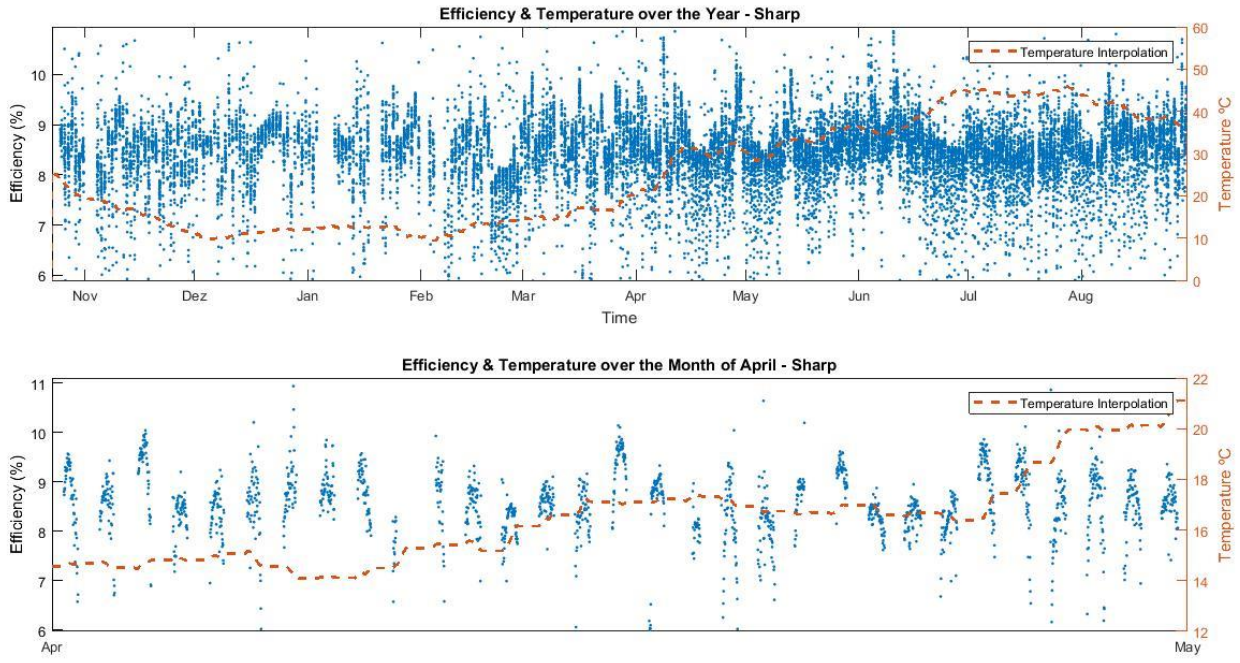

Figure 22: Module efficiency and temperature over a year and a month (Sharp)

On this figure, it's possible to observe that the efficiency for the sharp panel is far from constant. Besides the seasonal variations, caused by the changing average temperature along the year, there are also strong intra-day variations, as evidenced on the second graph.

These daily fluctuations were found among all panels studied. and are a response to both the low incidence angle during sunrise and sunset, as well as variations in the panel's temperature during the day.

Before assessing the impact of soiling on the photovoltaic efficiency, it's necessary to perform the thermal correction of the efficiency values, given that temperature variations severely affect a panel's power output and efficiency.

It is only after this thermal correction is performed that the efficiency becomes an invaluable indicator of a panel's true performance, allowing for the detection of any eventual efficiency degradation regardless of the panel's temperature.

This performance degradation should manifest itself through a slight but consistent decline of efficiency values during dry periods. As particulate matter gradually accumulates on the panel's glass surface, its transmissivity decreases accordingly.

It is therefore worth reminding that the efficiency values displayed in the figure above have yet to be normalized to the panel's temperature. As such, these will not be used in the study of soiling.

Additionally, the temperature interpolation curves displayed on the figure above result from a moving average of all the available ambient temperature records. However, since there were no records of the ambient temperature during the night-time, these temperature curves are slightly inflated.

4.3. Efficiency Correction to STC conditions

Through the application of a correction factor, provided by the module's manufacturer, the panels' efficiencies were corrected to the base temperature of 25ºC, effectively removing the influence of the temperature on the efficiency. Below is a table summarizing each panel's temperature coefficients.

	Sharp	France	Frontier	Panasonic	First
P_{Max} (%/ºC)	-0.24	-0.48	-0.31	-0.29	-0.25
V_{OC} (%/ºC)	-0.30	-0.36	-0.03	-0.131 (V)	-0.27
I_{SC} (%/ºC)	+0.07	+0.02	+0.01	1.76 (mA)	+0.04

Table 3: Thermal characteristics of the panels.

The thermal coefficients displayed on the table will be used to correct each module's efficiency to the standard temperature of 25 ºC. This was achieved through the application of the formula below.

$$Efficiency_{\,T=25ºC} = \frac{Efficiency\,(T)}{[1+\beta\times(T-25)]} \tag{4.22}$$

Where β is the power thermal coefficient, in percentage per degree, and T is the module temperature in degrees Celsius.

Since module temperatures tend to be higher than 25 ºC, the resulting corrected efficiencies will tend to be higher than the measured ones. This trend can be confirmed in the graph below, where both efficiencies were plotted individually.

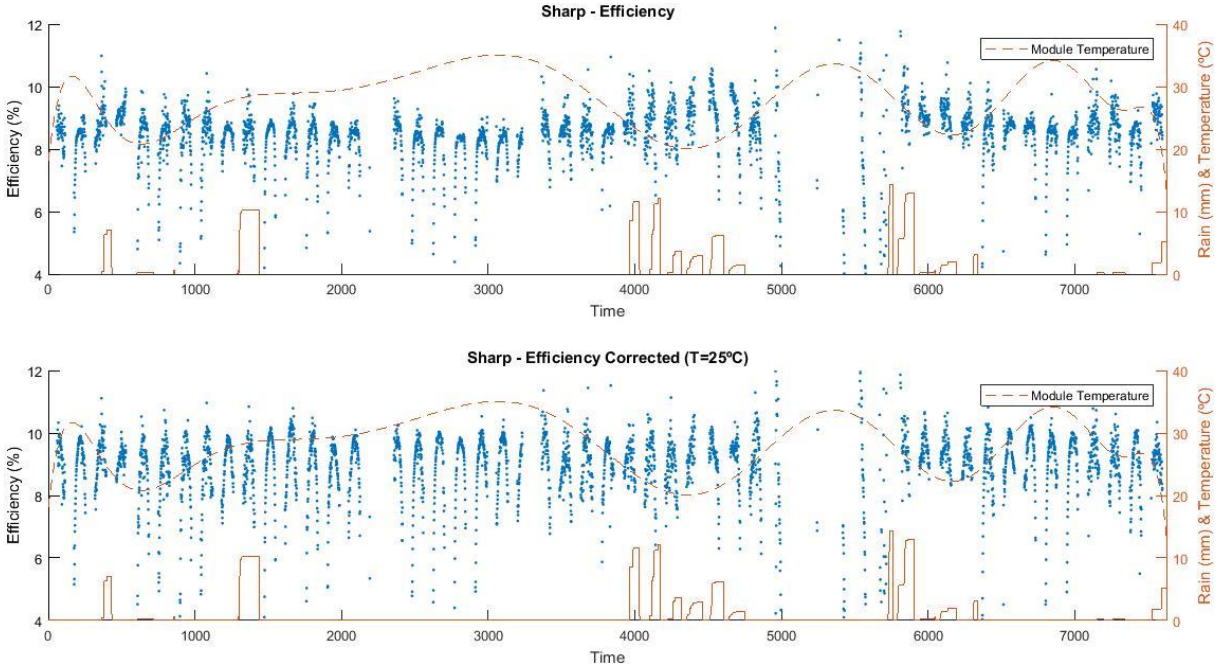

Figure 23: Efficiency correction procedures: Measured and corrected efficiencies with temperature (Sharp)

As predicted, when corrected to STC conditions, the efficiencies were consistently higher than the measured ones, increasing by half of a percentage point on average for the sharp solar panel.

It's worth noting that all panels experienced the same linearization effect, whereas the efficiency increase varied according to the magnitude of the panels' thermal coefficients.

These new corrected efficiencies eliminate nearly all previously unexplained outliers, such as sudden efficiency spikes near periods leading to heavy rains. Additionally, the corrected efficiencies follow a more linear distribution, a product of this temperature compensation.

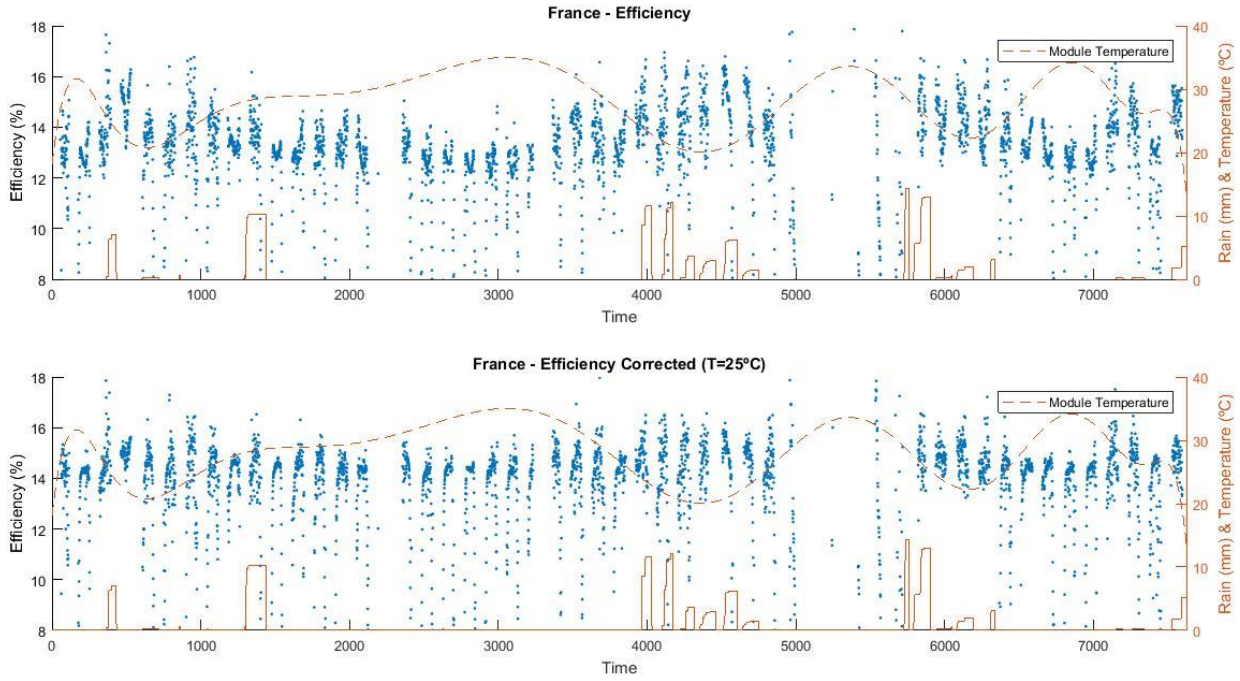

Figure 24: Efficiency correction procedures: Measured and corrected efficiencies with temperature (France Watts)

On most cases, the uncorrected efficiencies registered a slight decrease during the warmest hours of the day, due to the negative values of the thermal coefficients.

This is particularly visible in the daily graphs of the France Watts panel, since it boasted the highest thermal coefficient among the modules studied.

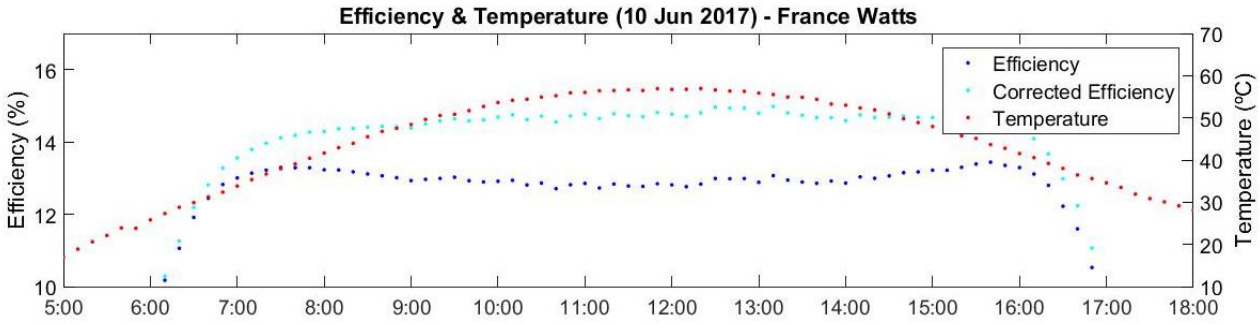

Figure 25: Variation of module efficiency with temperature over a typical day (France Watts)

This graph highlights the negative correlation between temperature and photovoltaic efficiency. Due to this panel's high thermal coefficient, it's possible to observe a short dip in the measured efficiency during the hottest parts of the day, one that was no longer present on the corrected efficiency.

The correction of the efficiencies was performed for all panels studied, with the objective of removing the influence of the temperature over the efficiency. The power thermal coefficients used in this process were the ones given by the manufacturer on the panel's datasheets.

4.4. Analysis of the Quality of the Temperature Correction

Before proceeding with the soiling analysis, it's paramount to verify the quality of the efficiency correction procedure. Assessing the quality of the efficiency correction process serves to assure that no major efficiency fluctuation will be thermally related.

The quality of the correction process can be assessed through the examination of the linearity of the corrected efficiencies over the temperature range. The process is then deemed successful if the resulting efficiencies are systematically within a reasonable range of each other.

In simpler terms, this means that the efficiency values taken with the module at a certain temperature range differ only marginally from the efficiency values taken during any other temperature conditions. If this is verified, the STC correction of the efficiencies is deemed successful.

Although theoretically simple, the degree of success of this process is dependent on both the accuracy of the measurements and the correction coefficients. The aim of this analysis was to verify the reliability of the temperature correction procedures, and not to improve it by experimentally calculating the thermal coefficients.

In order to illustrate the relation between temperature and conversion efficiency, the France Watts solar module was selected due to its unusually high thermal coefficient. With its efficiency decreasing approximately half a percentage point per degree, the France Watts module boasted the highest power thermal coefficient among the panels studied.

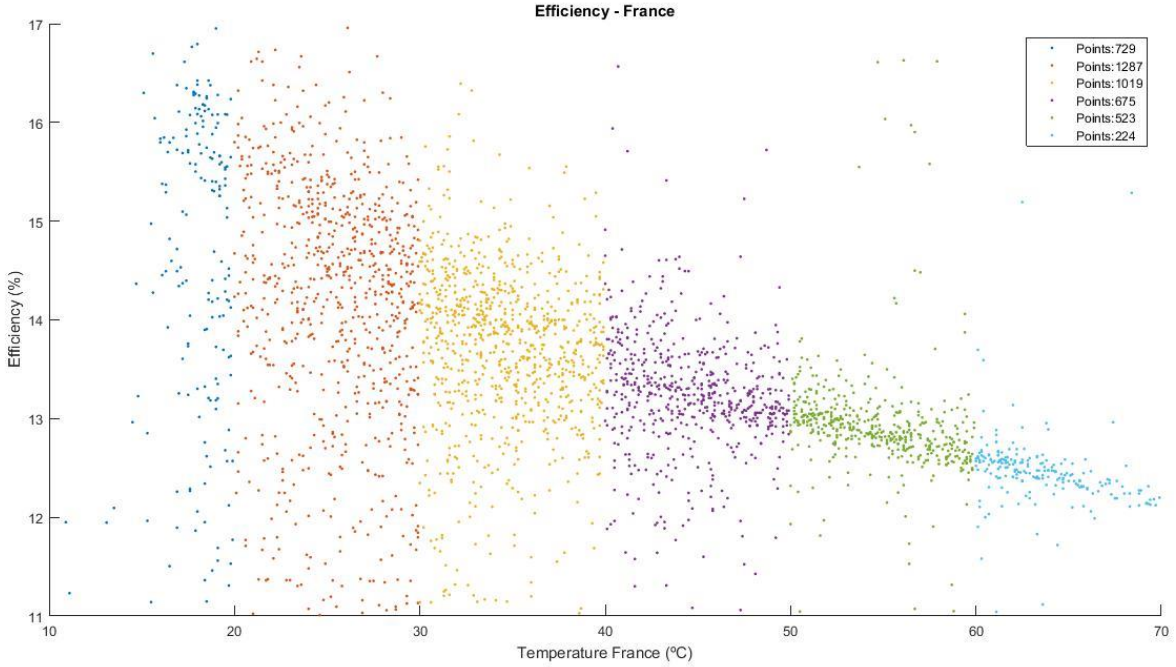

Figure 26: Module efficiency and module temperature (France Watts)

The measured efficiencies of the France Watts module were plotted alongside its temperature. The points are distributed by color, indicating the frequency of measurements registered in each temperature range.

As we can observe, the module's efficiency is negatively affected by its temperature, decreasing as the latter rises. This phenomenon was transversal to all the panels studied, varying only in intensity according to the magnitude of the thermal coefficients.

With its efficiency decreasing by approximately half a percentage point per degree, the France Watts solar module registered the highest power thermal degradation.

However, due to the substantial amount of outliers, corresponding to efficiency values outside the realm of possibilities, it was deemed important to filter the data. These were likely due to the mismatch between power and irradiance measurements, possibly due to passing clouds, resulting in power output values that could not be obtained under those irradiance conditions.

The filtering process consisted solely on the exclusion of efficiency measurements below and above certain fixed values, applying two basic filters to the raw data. This assured the integrity of the analysis, since at no point was the data filtered based on the temperature.

On the figure below are represented both the filtered and unfiltered efficiencies varying with the module temperature.

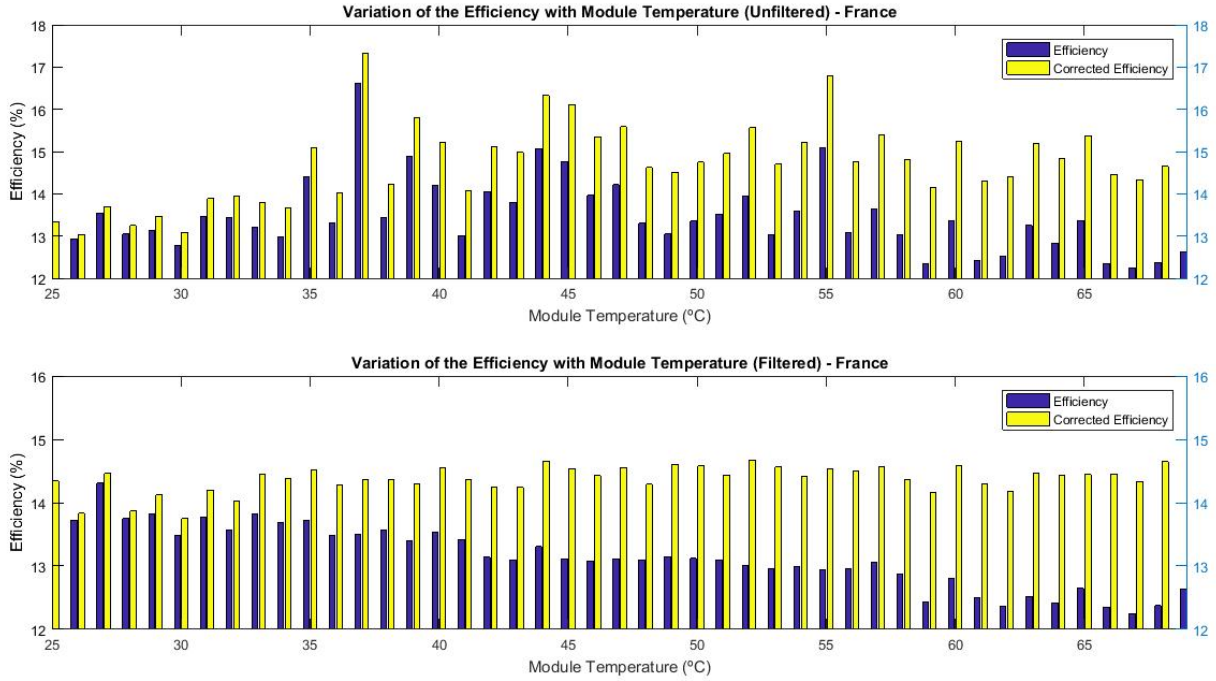

Figure 27: Filtered and unfiltered histograms of module temperature and efficiency (France Watts)

Due to the relatively small number of measurements for this type of analysis, outliers severely affected the results. Inaccurate efficiency measurements at a module temperature of fifty-five degrees, for instance, visibly disrupted the supposedly linear distribution of the efficiencies.

After the filtering process, a more accurate representation of the average efficiency at each temperature level was obtained.

Whereas in the top chart the efficiencies varied wildly across temperature ranges, undoubtedly due to the presence outliers, on the bottom chart the filtered efficiencies follow a much more linear distribution, accurately describing the module's thermal behavior.

In the filtered chart, as expected, the module's efficiency steadily declined as temperature rose. The corrected efficiency, however, remained reasonably constant, as intended. This indicates that the thermal correction was performed reasonably well, and that the power thermal coefficient used in this process was appropriate.

This analysis was repeated for all the panels studied, confirming the quality of the thermal correction procedure.

4.5. Efficiency Processing and Outlier Removal

Previously, the efficiency was severely scattered throughout the day, once again possibly due to the mismatch in the power and irradiance measurements. In order to overcome this and obtain efficiency values that better characterized the panels, a new cumulative daily efficiency was calculated, based on the cumulative sum of the daily power and irradiance values.

$$Efficiency_{Daily}\ (\%) = \frac{\sum Power_{Daily}\ (W)}{\sum Irradiance_{Daily}\left(\frac{W}{m^2}\right) \times Area\ (m^2)} \times 100 \tag{4.20}$$

Whereas the previous efficiency values were calculated at every possible point, allowing for complete overview of the data, this new cumulative daily efficiency is a much more accurate representation of the overall daily efficiency of the panels.

Using this formula, the calculation of the conversion efficiency is done taking into account the total power production and irradiance received by the panel during the day, resulting in a very precise value of the average daily efficiency.

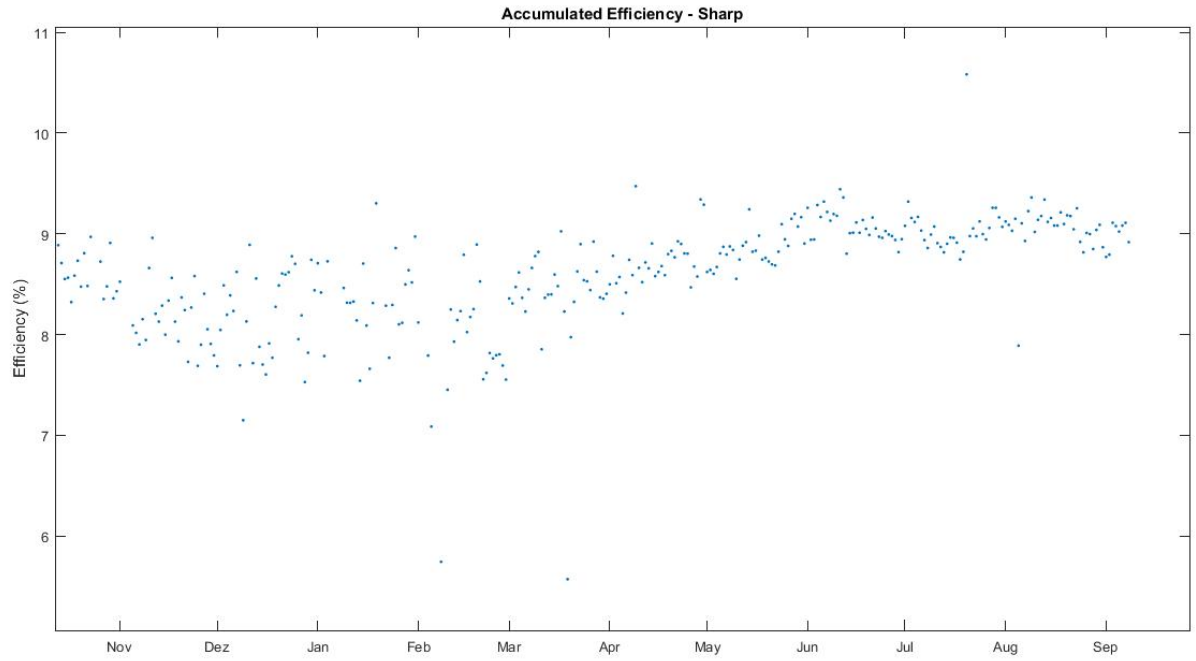

Figure 28: Cumulative Daily Efficiency (Sharp)

By computing the daily efficiency values cumulatively, instead of averaging the efficiencies at every point, we obtain a series that more faithfully represents the real daily efficiency variations.

Not surprisingly, then, the efficiency values followed a much more linear distribution.

Finally, due to the nature of this analysis, involving the use of linear regressions to detect minute variations in efficiency, the correct treatment of outliers was paramount. To this end, it was necessary to identify and remove all values that weren't representative of the panels' true behavior.

It was noticed that several days contained incomplete records of power and irradiance, resulting in daily efficiency values that significantly diverged from the average, as well as their neighboring values. These

anomalies can be attributed to both temperature and the incidence angle, as these vary significantly during the day, impacting the efficiency calculation.

In order to remove these values, all days with incomplete power and irradiance records were removed. Additionally, days where snowfall visibly impacted the efficiency were removed.

A total of eighteen points were removed, corresponding to about one percent of the available data.

4.6. Analysis of the Efficiency Degradation during Dry Intervals

In order to properly assess the impact of soiling on photovoltaic efficiency, it's necessary to maximize the scope of the analysis, extending it to large time frames, thus making the sample size statistically relevant.

Ideally, then, one should study as many periods as possible, aiming to detect a consistent degradation pattern, as many other studies have found [2,10].

For this reason, this analysis will be performed for all panels, on data spanning roughly one year of measurements of identical nature and sampling rate. The availability of the data for the period studied was of 90.88 %.

The data used in this analysis was the previously calculated daily cumulative efficiency values, as they have proven to yield the most reliable efficiency values for the panels, as well as the cumulative daily rainfall seen below.

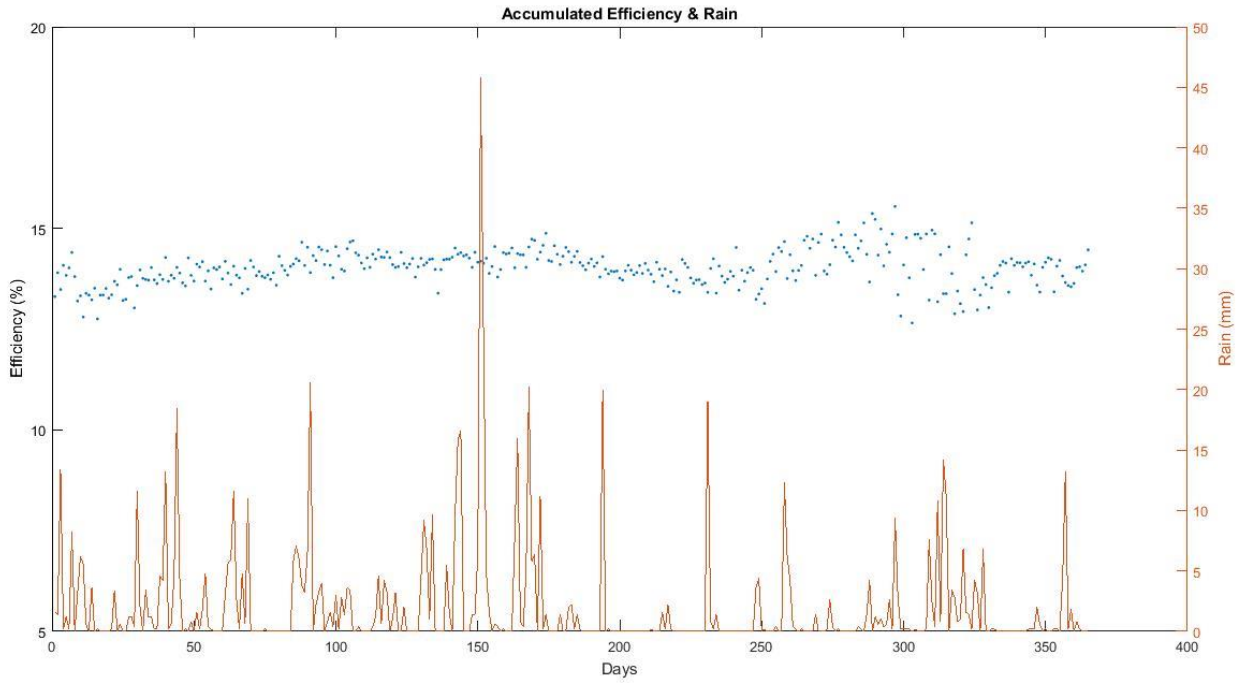

Figure 29: Cumulative daily efficiency and rainfall (Sharp)

4.6.1. Study Period Selection and Cleaning Threshold

Having chosen to use the cumulative daily efficiency values, it was time to select the dry periods over which to perform the analysis. It's worth noting that the so called "dry periods" do not correspond to periods without rainfall, but to periods where rainfall was deemed small enough not to affect the soiling levels of the panels.

The cleansing effect of rain can vary widely due to several factors. The two most important ones being the panel's tilt angle and the intensity of the rains. The latter is characterized by the amount of rain that fell on one occasion and the frequency of such rains.

Different studies agree that at least five millimeters of rain are necessary to start the cleaning process. Otherwise the system will continue to experience power losses due to the dust and soil deposition [5, 11].

Other sources cite lower numbers, likely due to different test conditions, dust properties and panel inclinations [29].

The panels featured in this study were installed at a fixed tilt angle of 27º, at a location just outside the region of Paris. Panel inclinations of these magnitudes tend to negatively affect particle accumulation, resulting in irradiance losses due to soiling of around half of those expected for flat mounted solar panels [30].

Additionally, the effect of the tilt angle on soiling losses is dependent on its surrounding environment, as well as the type of pollutants and intensity of the rain. The activity in the system's immediate environment directly influences their performance, differently affecting their performance recovery and degradation patterns [2].

The panels featured in this study were mounted close to the ground, adjacent to each other, therefore suffering from identical amounts rain and soiling deposition.

Although there is no general consensus on the amount of rainfall required to completely clean solar modules, it's commonly accepted that five millimeters is sufficient to clean photovoltaic systems.

On drier climates, however, rainfall in the order of 5 mm can fail to clean the systems. On a study in northern California, several rainfall events above 5 mm failed to clean the system, and the efficiency continued to drop until a rainfall event of 20 mm was finally able to induce an output recovery of 40% [2].

In the region of Paris, whose climate is characterized by mild but frequent rains, soiling is constantly being removed. For this reason, it seemed sensible to discard the possibility that more than five millimeters of rain would be necessary for an effective module cleaning.

Additionally, it's worth noting that several studies have observed that rainfalls under two millimeters can cause greater losses [29,30]. When there is already a meaningful amount of soiling present in the modules, a rainfall of less than two millimeters may result in the formation of a dirt-like substance. This dirt, created from the combination of soiling and a light rain, might block the irradiance further. However, since the panels studied weren't significantly soiled, this phenomenon can be overlooked.

For the purpose of this study, despite not being possible to determine a precise amount of rainfall that would unequivocally clean the systems, two thresholds were defined as the minimum daily amount of rainfall required to clean the modules.

The first was set at five millimeters, as recommended by most of the literature on the topic, and the second set at one millimeter.

The degradation analyses presented on the next chapter

will be based on these two carefully selected thresholds, starting with the assumption that at least five millimeters of rain are required to effectively clean the modules, followed by a second one defining the threshold which triggers the intensive cleaning process at the more conservative amount of one millimeter.

The first one, based on the assumption that at least five millimeters of rain are required to effectively clean the modules, will study a higher number of periods. This is due to its less restrictive period selection criteria.

The second one, more conservatively set at one millimeter and thus encompassing less periods, serves to ensure that no soiling removal could have taken place during the periods studied.

4.6.2. Implementation of the Linear Regressions

It was now possible to calculate the real soiling induced degradation rates. These rates quantify the impact of soiling on the performance of the panels, measuring the level of performance degradation due to soiling accumulation.

The degradation rates were obtained through the application of a linear regression to the efficiency values of the panels over all dry periods with valid records. The level of performance degradation will then correspond to the slope of these regressions.

Having decided on which periods to study, it was time to perform the first soiling analysis. This consisted on the calculation of the efficiency degradation rates for each period whose total daily rain accumulation did not exceed five millimeters.

The image below contains the results of this year-long soiling analysis for the Sharp Panel.

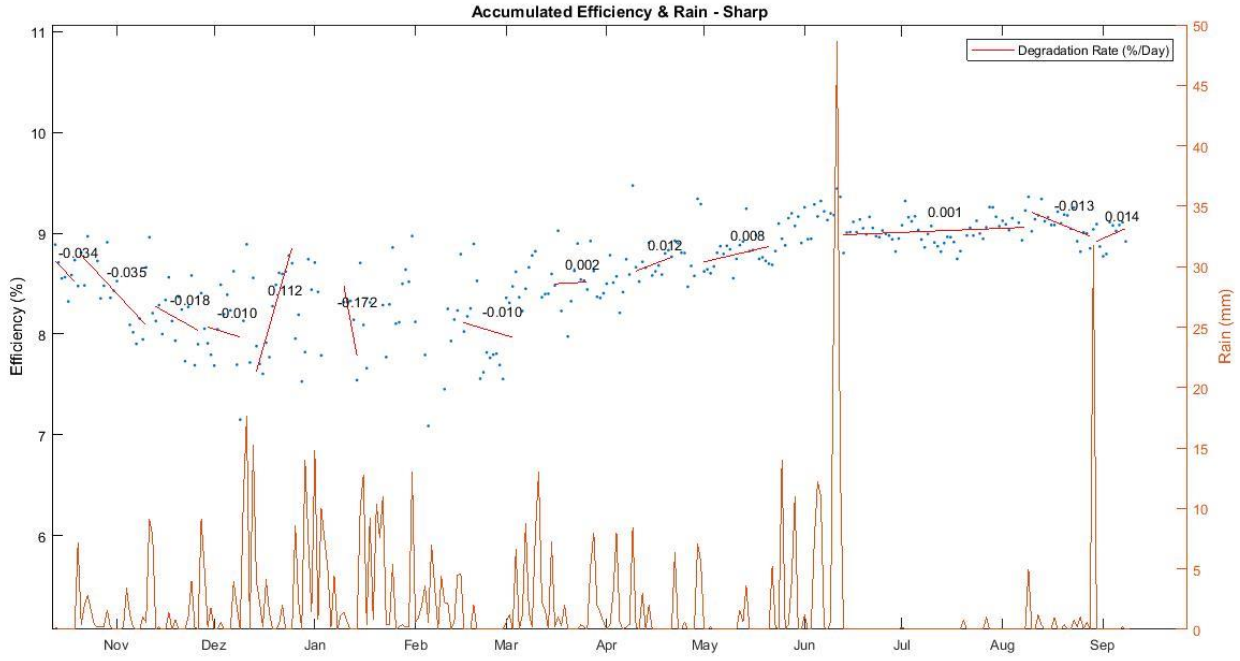

Figure 30: Regression lines for all periods with less than five millimetres of rainfall (Sharp)

The blue dots on this graph correspond to the cumulative daily efficiency values, whereas the red lines are the linear regressions applied to all periods that didn't register rainfall events greater to five millimeters. The slope of each curve is indicated by its respective number in black.

In the case of the Sharp solar panel presented above, it's evident that there's no clear correlation between the two, since the slope of the curves repeatedly alternates from positive to negative throughout the year without a clear pattern.

There was an attempt to filter poorly conditioned linear regressions through the use of two statistical indicators: The R-Squared and RMSE. However, this attempt ultimately proved unsuccessful, and it was not possible to exclude regression lines based on these statistical indicators alone.

This seemingly random alternance of the regression slopes suggests that soiling losses are insignificant when compared to the observed daily efficiency variations. This results in the masking of the soiling losses, rendering them undetectable through this method.

These assumptions were corroborated by the results of the remaining panels presented below.

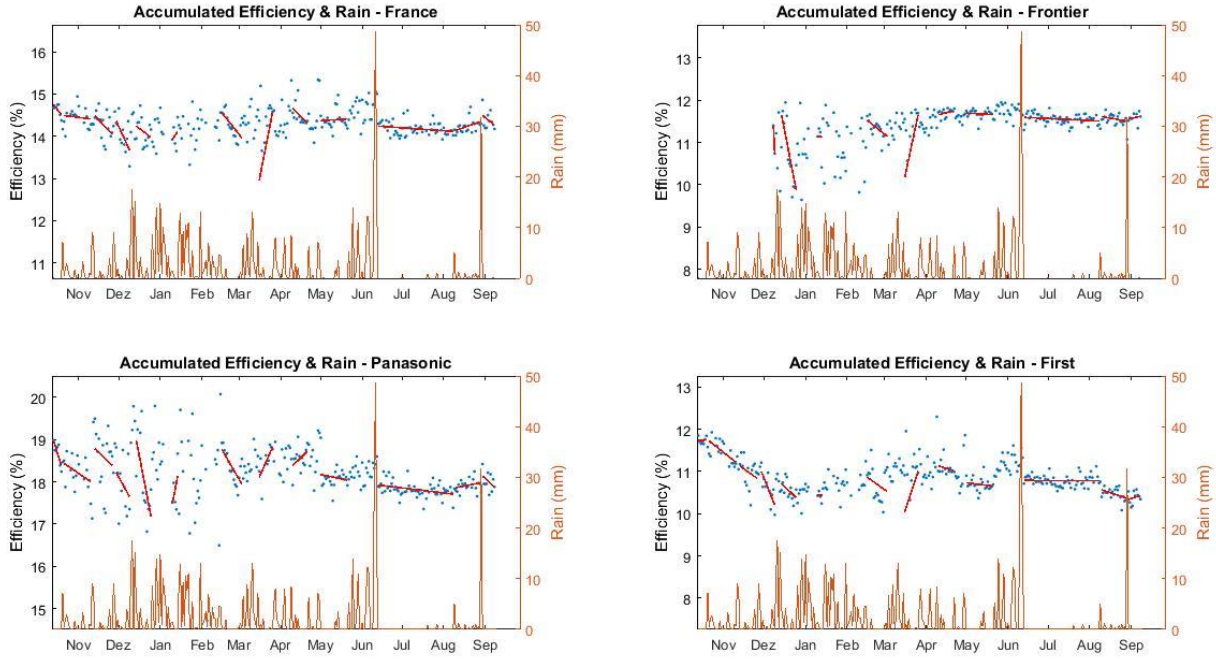

Figure 31: Regression lines for all periods with less than five millimetres of rainfall for the remainder of the panels

Once again, it's possible to observe that the regression slopes followed no clear pattern.

In theory, one should find a slight but consistent efficiency degradation during dry periods, caused by the gradual accumulation of particles on the module surfaces. The efficiency degradation rates should also be consistently within a narrow range of each other, as soiling tends to affect the panels uniformly. This could not be achieved due to several factors.

The first, concerning the efficiency, centers around the fact that these values varied substantially from day to day, not allowing for the detection of the minute efficiency decreases due to soiling.

Additionally, it's worth noting that the daily efficiencies were severely scattered during the first semester, rendering the identification of soiling losses during this period an even harder task. This phenomenon was consistent across all panels, and it was due to the panels' response to diffuse radiation during cloudy days.

The second, related to the Parisian climate, was the high frequency of rainfall. The duration of the dry periods in this first analysis was relatively short, ranging from seven to twenty-one days, with the notable exception of a single fifty-seven-day long period during the summer, during which no rainfall event over five millimeters took place.

This had a two-fold effect on our analysis. Firstly, the relatively short duration of the dry periods severely impacted the statistical significance of the degradation rates, rendering the linear regressions meaningless. Secondly, the high frequency of rainfall negated any meaningful soiling accumulation.

These, allied with the strong daily efficiency fluctuations, caused the regression slopes to vary widely, ultimately proving that in such conditions the study of soiling losses is not possible through this method.

Nevertheless, this problem could be overcome by studying soiling losses over longer dry periods, where soiling losses are more pronounced. This would not only allow for a better averaging of the efficiency

variations that so strongly cripple short term analyses, but for the increase of their statistical significance as well.

Perhaps, then, it is more revealing to focus on the single longest dry interval recorded, stretching from mid-June to August, encompassing fifty-seven days. Throughout the span of these two months there were two recorded rain events, and none superior to one millimeter.

During this period, only the Sharp branded solar module registered an efficiency increase, lending to the idea that the panels might be soiled.

However, upon closer inspection, it was found that these two small rain events strongly correlated with efficiency variations, and on several cases with a noticeable efficiency increase. These events were of zero point eight and two millimeters, respectively.

This fell within our expectations, since in theory even one millimeter of rain is able to produce a cleaning effect, removing material deposited onto solar panel surfaces.

Additionally, it could be argued that, for a variety of reasons ranging from particle size to solar panel inclination, the threshold at which the cleaning process begins was set too high. In that case, it's assumed that the panel is being cleaned by amounts of rain smaller than one millimeter, thus minimizing the effects of soiling.

To substantiate these findings, the longest period was divided into three parts, each corresponding to a rainless interval. Then, linear regressions were applied to the exclusively dry periods, aiming to verify these efficiency gains.

The figure below displays the results of this analysis for the Sharp and Solar Frontier panels, whose results better illustrated this phenomenon.

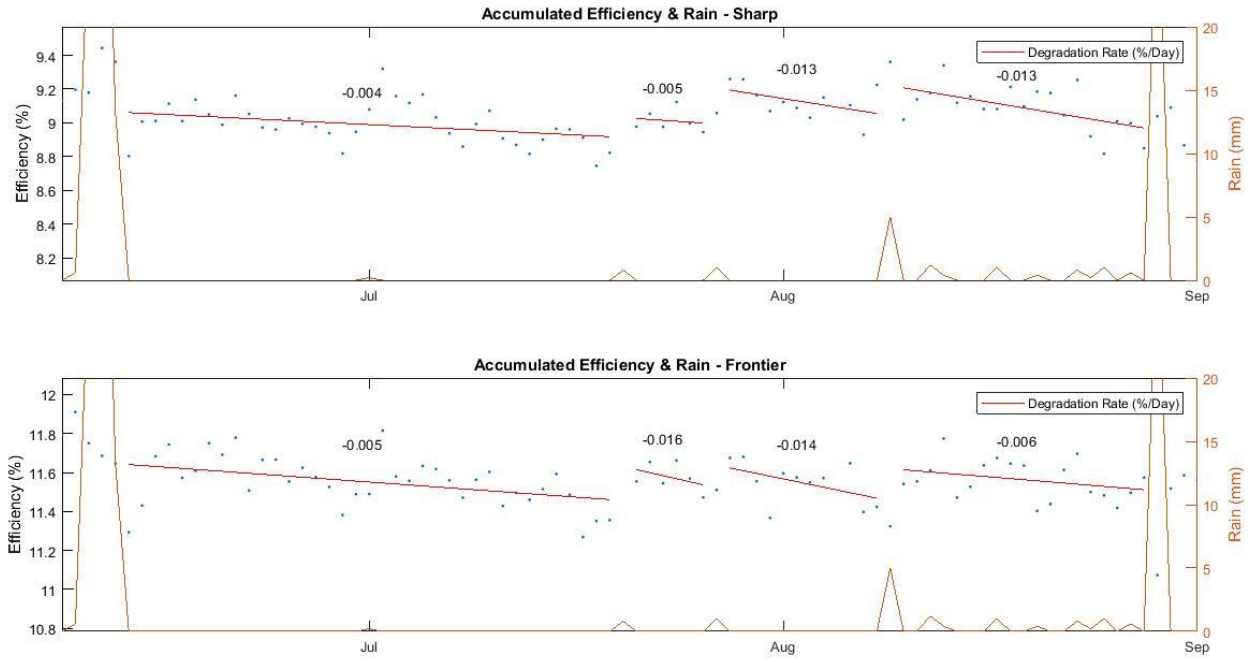

Figure 32: Regression lines for the exclusively dry periods during the summer months (Sharp and Frontier)

These findings point towards a possible influence of such rains in the systems' performance, making it necessary to study soiling losses during exclusively dry periods. This way, we'll be able to determine the soiling induced efficiency degradation rates free of the rain's influence.

In order to determine the validity of such assertions, the efficiency degradation rates were recalculated under different conditions, comprising periods of less than zero point two millimeters of daily rainfall, and assuring that the panels are not being cleaned by rain.

On this second analysis, the rain threshold couldn't be set to zero, and was instead set to zero point two millimeters. This was due to the occurrence of two rainfall events of such magnitude during key periods of our analysis, that would otherwise have broken the continuity of the longest linear regressions.

It's safe to assume that zero point two millimeters of rain won't severely affect the soiling deposition density, particularly when considering that this volume is often a product of multiple separate rains dispersed throughout the day. For practical purposes, then, this interval was referred as the dry period.

Setting the threshold well below the already conservative five-millimeter value, served to ensure that no significant cleansing process could have commenced.

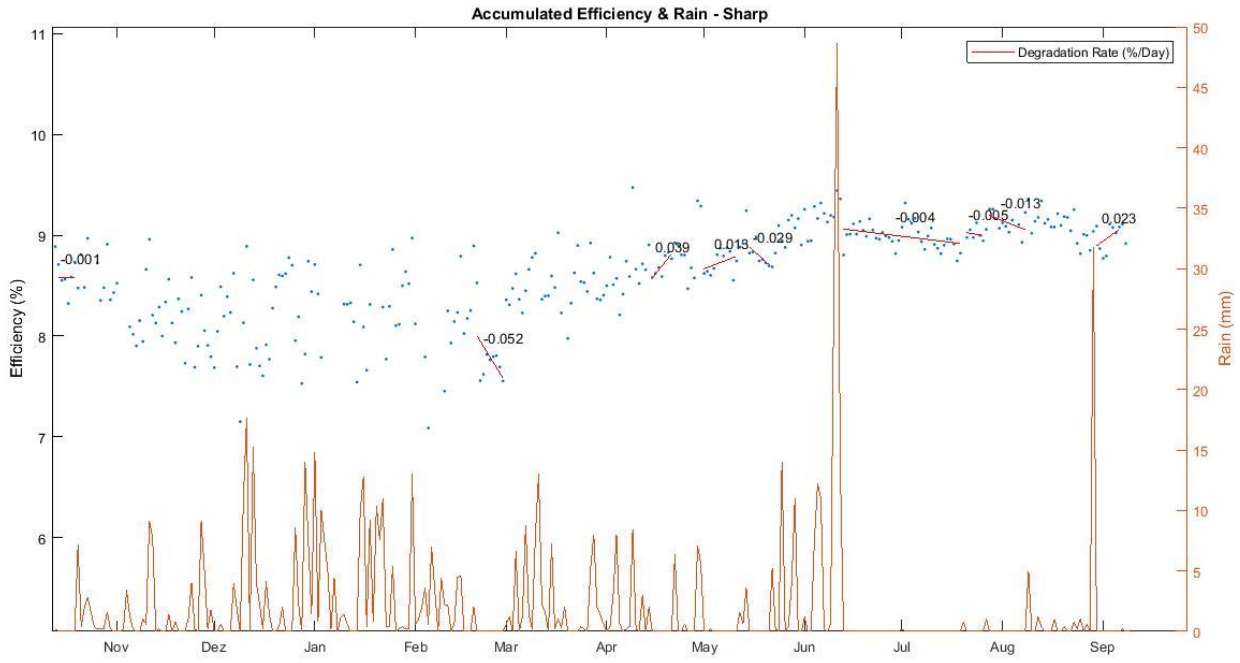

Figure 33: Regression lines for all periods with less than zero point two millimetres of rainfall (Sharp)

This subsequent analysis once again revealed no signs performance degradation during dry periods. In fact, the slope of the linear regressions alternated from positive to negative, failing to exhibit a consistent pattern of efficiency degradation.

Once more, this was likely a product of the severe daily efficiency fluctuations, which have the effect of masking the soiling induced efficiency losses. These losses tend to be incredibly small, therefore requiring a very precise plotting of the efficiencies in order to detect them.

The figure below displays the results of this second analysis for the remainder of the panels.

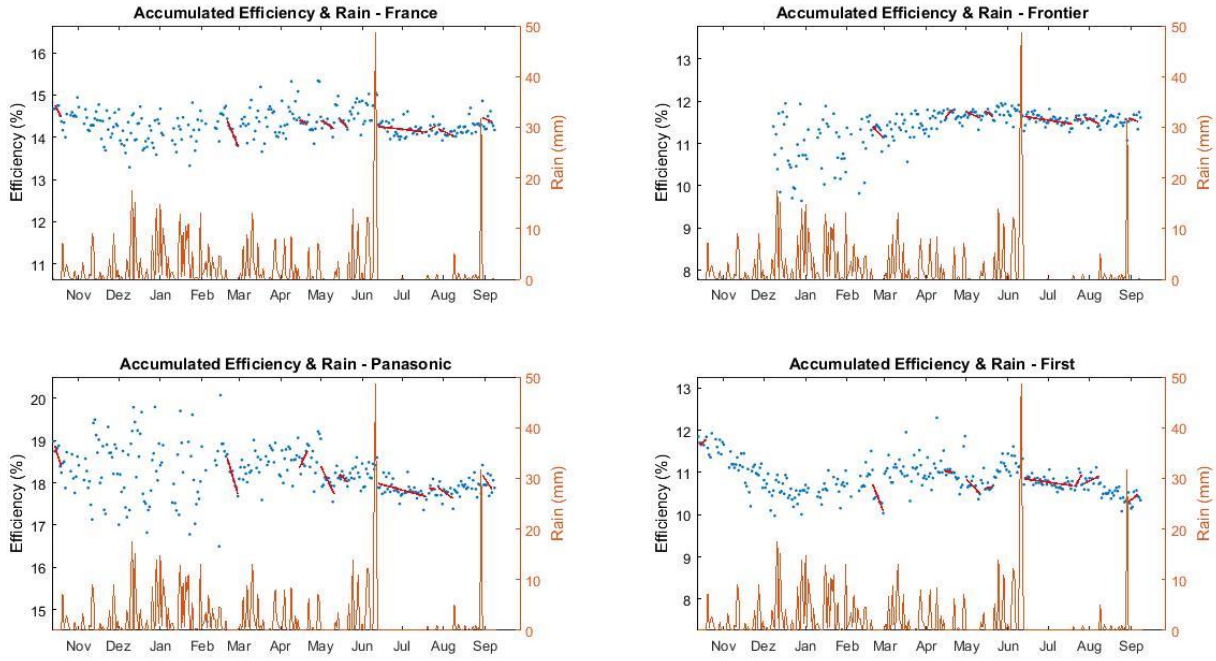

Figure 34: Regression lines for all periods with less than zero points two millimetres of rainfall for the remainder of the panels

Just as before, the daily efficiencies varied substantially from day to day, rendering this type of analysis unsuitable for the study of soiling over brief periods.

For this analysis to succeed in our context, it would require either higher soiling rates or longer dry periods, both of which would aid in the detection of soiling through this method. But as the region of Paris is very rainy, it is only the second possibility the concerns us. Had it rained less during this period, the performance degradation of the systems in question might have been detected despite the efficiency's inherent variability.

In the region of our study, characterized by mild but frequent rainfall, soiling accumulation is severely hindered, thus mitigating the negative impact of soiling on the conversion efficiency.

For this reason, it seemed sensible to once again focus on the longest dry period, this time spanning thirty-seven days, aiming to obtain the efficiency degradation rates for the longest period of uninterrupted soiling accumulation.

During this interval, despite the efficiency fluctuations, all panels registered a marked efficiency decrease, as evidenced by the negative slope of the curves. This was postulated to be due to the effect of soiling, which was able to accumulate over this unusually dry period.

In order to assess the statistical significance of these rates, the confidence intervals were calculated for each slope. These were drawn for a confidence level of ninety-five percent, thus indicating that such is the probability that the true best-fit line lies inside the calculated interval.

Finally, the regression's R-squared and RMSE values were added, and the results displayed below.

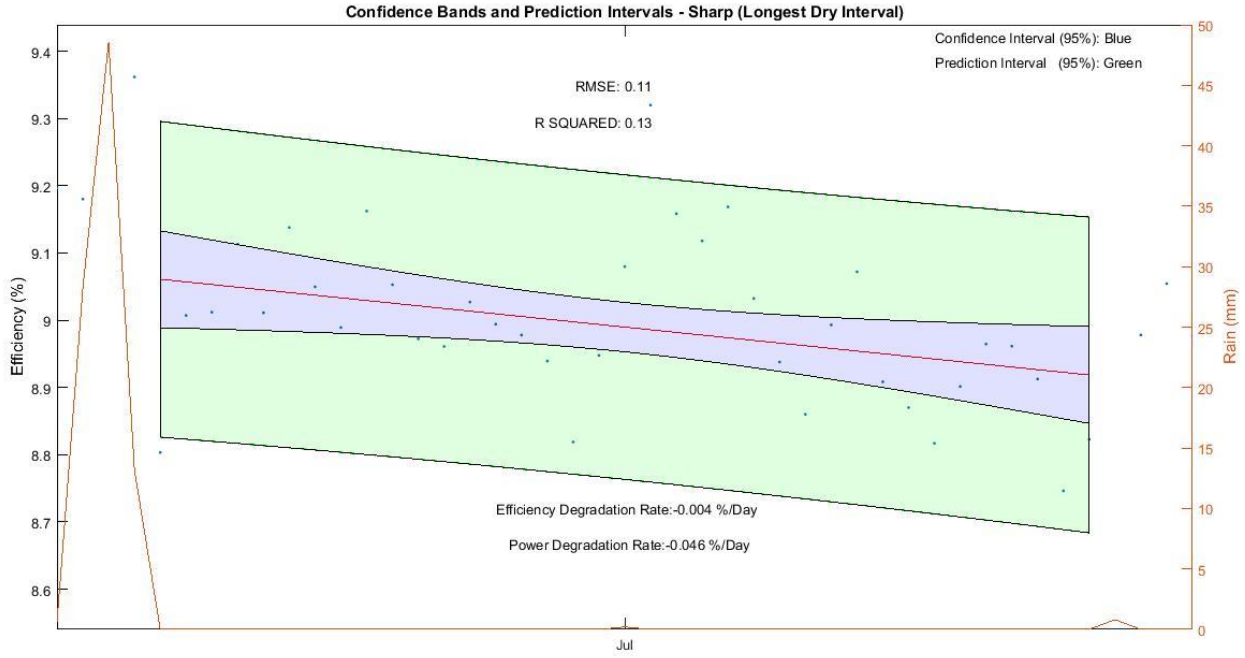

Figure 35: Confidence bands and prediction intervals for the regression line of the longest dry interval (Sharp)

On this figure, the prediction and confidence intervals are highlighted in green and blue, respectively, for the Sharp solar module.

The prediction bands illustrate the efficiency's inherent variability, depicting the interval inside which ninety-five percent of future observations should fall. The width of this interval correlates with the magnitude of the daily efficiency variations.

The confidence bands surrounding the regression line delineate the boundaries within which the true best-fit line will fall, for the chosen confidence level.

Given the assumptions of the linear regression, there is a ninety-five percent chance that the two curved confidence bands enclose the regression line, leaving a five percent chance that the true line lies outside those boundaries.

The confidence and prediction intervals for the other panels are displayed below.

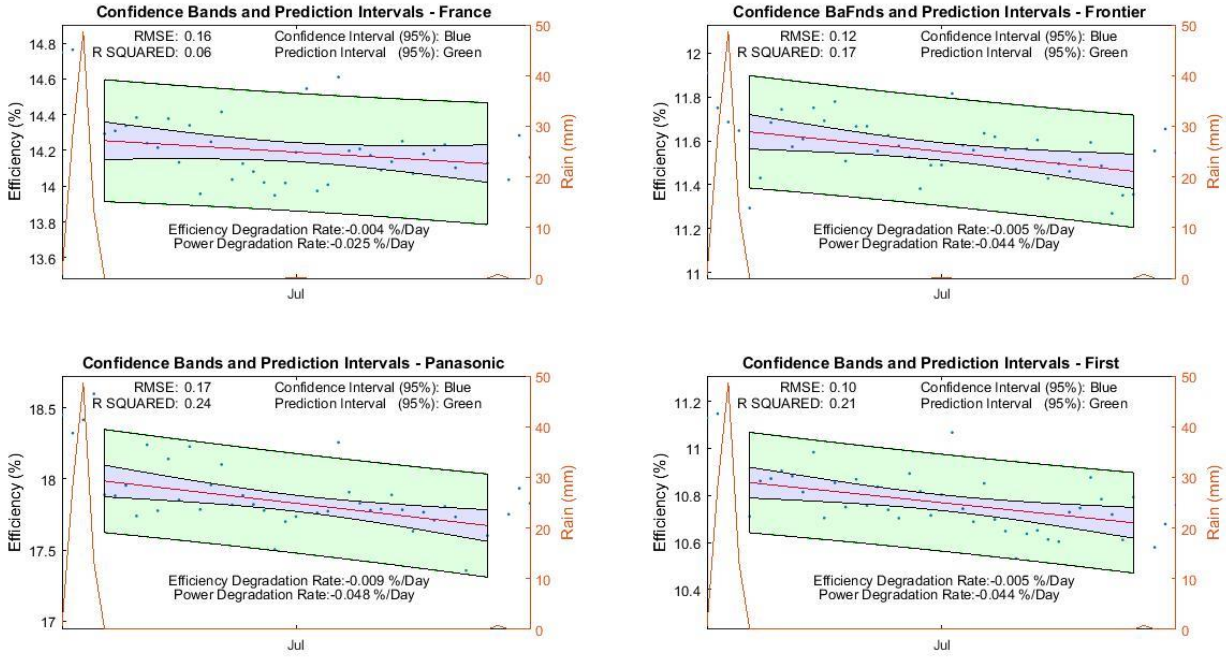

Figure 36: Confidence bands and prediction intervals for the regression lines of the longest recorded dry interval for the remainder of the panels

This figure demonstrates that all panels suffered a sustained efficiency decrease, for a very high confidence level. It's also possible to observe that the width of the prediction bands varied slightly, reflecting the level of dispersion of the observations.

Although the highest efficiency variations belonged to the Panasonic panel, as evidenced by its prediction bands, the highest power fluctuations were found on the France Watts module. This was corroborated by its unusually low R-Squared indicator.

This may be the reason behind this panel's below-average power degradation rate, since all others registered nearly identical rates.

Additionally, the France Watts was the only panel whose power degradation rate was capable of assuming a positive value within the ninety-five percent confidence level. All others assumed an exclusively negative degradation slope within this confidence range.

The results of this analysis were summarized on the table below.

	Sharp	France	Frontier	Panasonic	First	Average
Efficiency Rate (%/Day)	**-0.0040**	**-0.0036**	**-0.0050**	**-0.0078**	**-0.0047**	**-0.0050**
Margin of Error (95%)	±0.0036	±0.0052	±0.0037	±0.0055	±0.0032	±0.0035
Power Rate (%/Day)	**-0.0463**	**-0.0253**	**-0.0443**	**-0.0435**	**-0.0443**	**-0.0442**
RMSE	0.11	0.16	0.12	0.17	0.10	0.132
R-Squared	**0.13**	**0.06**	**0.17**	**0.24**	**0.21**	**0.162**
Nº of Regression Points	**37**	**35**	**37**	**36**	**37**	**36.4**

Table 4: Summary of the degradation analysis for the longest dry period.

The first line of the table indicates each panel's measured efficiency degradation rate. They varied among panels due to their different build quality and solar cell technology. These were followed by their respective confidence intervals, aiding in the characterization of these rates.

The power degradation rates, displayed on the third line of the table, represent the panel's daily power loss during this period. This rate was normalized to the panel's average efficiency, allowing for the comparison of rates among the panels.

With the exception of the France Watts, all panels registered incredibly similar power degradation rates. This might have been a product of this panel's efficiency fluctuations, whose volatility during this longest dry period revealed unusually high.

Despite this slight discrepancy, there was overwhelming consensus towards an efficiency decrease during this dry interval.

The fact the power degradation rates were closely matched is suggestive of the presence of soiling, as the accumulation of dust should be uniform among panels, equally affecting the incoming irradiance of each panel. Additionally, degradation values of this magnitude correspond to typical soiling related losses [2,4].

This table also indicates the regressions' RMSE and R-Squared, both of which proved unfit in the assessment of the statistical significance for this type of analysis.

Finally, the last line of the table shows the number of efficiency points encompassed by each regression line during the thirty-seven-day long period.

Despite having been previously filtered, it was necessary to further exclude a total of three points which visibly compromised the quality of the linear regressions.

These corresponded to efficiency values that strayed too far from the average, not representing plausible efficiencies for the panels affected. On average, each panel registered a couple of these along the year, and although most were filtered by the removal of incomplete days, some had to be manually excluded.

During the longest period, only the France Watts and Panasonic modules were affected by the presence of efficiency outliers. These represented less than two percent of the sample for this period.

On the first module, there were two consecutive days with efficiency values far below the average, that could not possible correspond to the daily photovoltaic efficiency. These were ten and twenty-five percent below the average for the same period. Similarly, the Panasonic solar module registered an outlier with an efficiency over twenty-five percent below average on an otherwise incredibly linear dry period.

Previously, the confidence intervals were determined for a two-tailed t test, testing the possibility of the regression slope in both directions. This allowed for an overview of each panel's likely degradation rate, better characterizing the soiling losses.

However, in the context of this analysis, it's particularly relevant to test for negative slopes, as these are indicative of soiling losses. It is for this reason that it was considered appropriate to test these same slopes unidirectionally, aiming to determine the probability of registering an efficiency decrease during this period.

To this end, a one-tailed t test will be performed to each regression line, focusing exclusively on the upper confidence interval. Any effects towards a slope increase will be neglected, as the aim is to ascertain the probability of the occurrence of a soiling related loss.

In simpler terms, this test will reveal the level of confidence with which one can affirm that soiling losses were present.

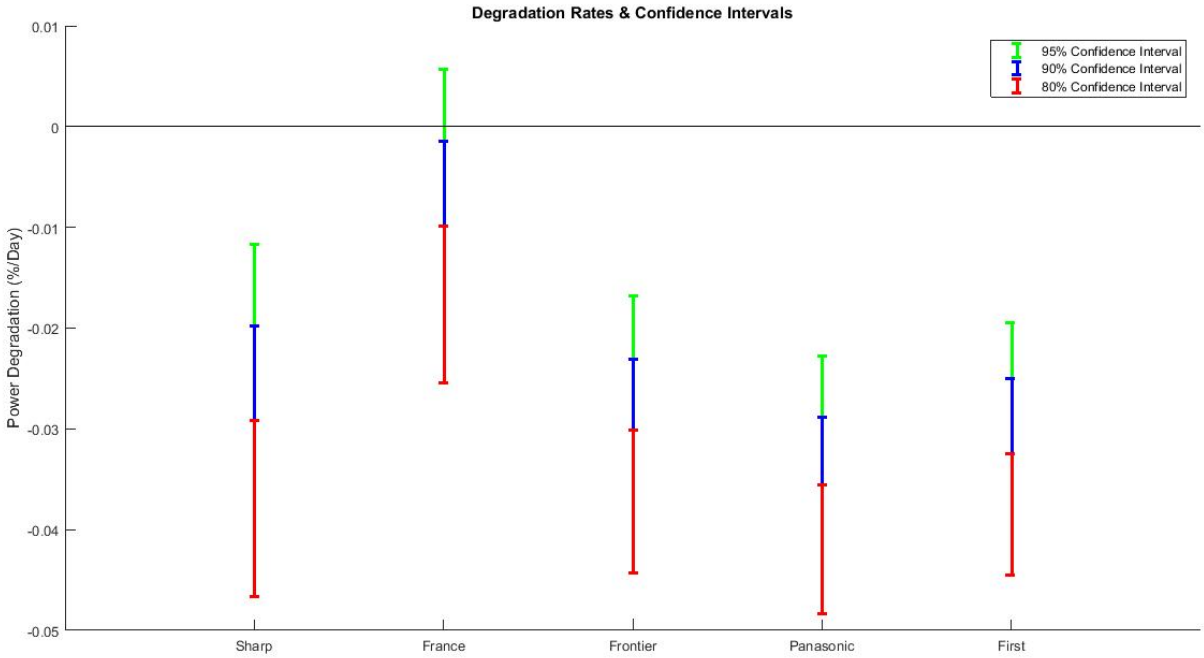

Figure 37: Error bars displaying the power degradation values for three confidence levels

The bars in this figure enclose each panel's possible power degradation values for a certain confidence level. Three different confidence levels were tested, and to each assigned a color.

It's worth mentioning that the higher confidence intervals contain the smaller ones. This means that the 95% interval represented in green encompasses the other two as well.

Finally, since this was a one-tailed t test, the regression results are represented at the bottom of each error bar, with their confidence levels displayed unilaterally towards the positive side.

This figure shows that all panels registered an efficiency decrease for a confidence interval of ninety percent, and for a level of over ninety five percent for four of the panels.

Finally, it's important to observe how closely matched the rates were, varying only slightly from each other. The lowest rate, corresponding to the France Watts panel, was about 38% below the average, and the average deviation from the mean was of 12.5%.

This analysis was made possible by the abnormal rainfall distribution during the year of our study, which culminated in the thirty-seven-day long period during which this study took place.

With its temperate oceanic climate, Paris tends to have rainfall evenly distributed throughout the year, thus severely mitigating the impacts of soiling. During the year of our study, however, the rainfall distribution was somewhat abnormal, with unusually low rainfall during summer months.

It was this unusual precipitation pattern that allowed for the detection of the soiling losses.

Since the quality and precision of these estimates is proportional to the length of the period studied, these rates benefited from an unusually high confidence level, allowing for the detection of soiling losses with a confidence level of over ninety percent.

4.7. Analysis of the Efficiency Degradation during Pollution Peaks

It was postulated that an above average soiling deposition could occur during intense pollution episodes, a phenomenon already well documented in the literature [33,34].

The atmospheric particulate matter (PM) has the potential to diminish the solar energy production by both directly attenuating the incoming radiation, and by being deposited on panel surfaces, thereby reducing the transmittance of the glass cover. In certain parts of the globe, where pollution is most intense, the accumulation of particulate matter on solar panels can severely curtail the energy output of solar panels.

However, whereas the effect of air-borne particles can't be detected through the analysis of the efficiency, since it would simply attenuate the irradiance and power, any particle accumulation might.

Manmade soiling tends to be smaller in size when compared to other traditional pollution sources, resulting in a greater energy loss [22, 23]. Additionally, these types of contaminants tend to be stickier, making their removal by rain a much more difficult process.

In certain parts of India, China and the Arabian Peninsula, air pollutants can account for energy output reductions between 17%-25%, with roughly equal contributions from ambient PM and PM deposited onto photovoltaic surfaces [31].

In recent years, Paris has suffered some of the worse air pollution episodes ever recorded. In fact, these events have gotten so acute that city officials have at times issued drastic measures to address this problem.

Given the pollution levels that Paris occasionally encounters, it wouldn't be unreasonable to expect that soiling deposition rates would be heightened during these periods. In order to corroborate this assumption, a new analysis was performed.

Working with the year-long data referent to the France Watts solar module, the periods of peak pollution were mapped separately. These corresponded to periods of unusually high PM10, provided by the observation pole of the IPSL.

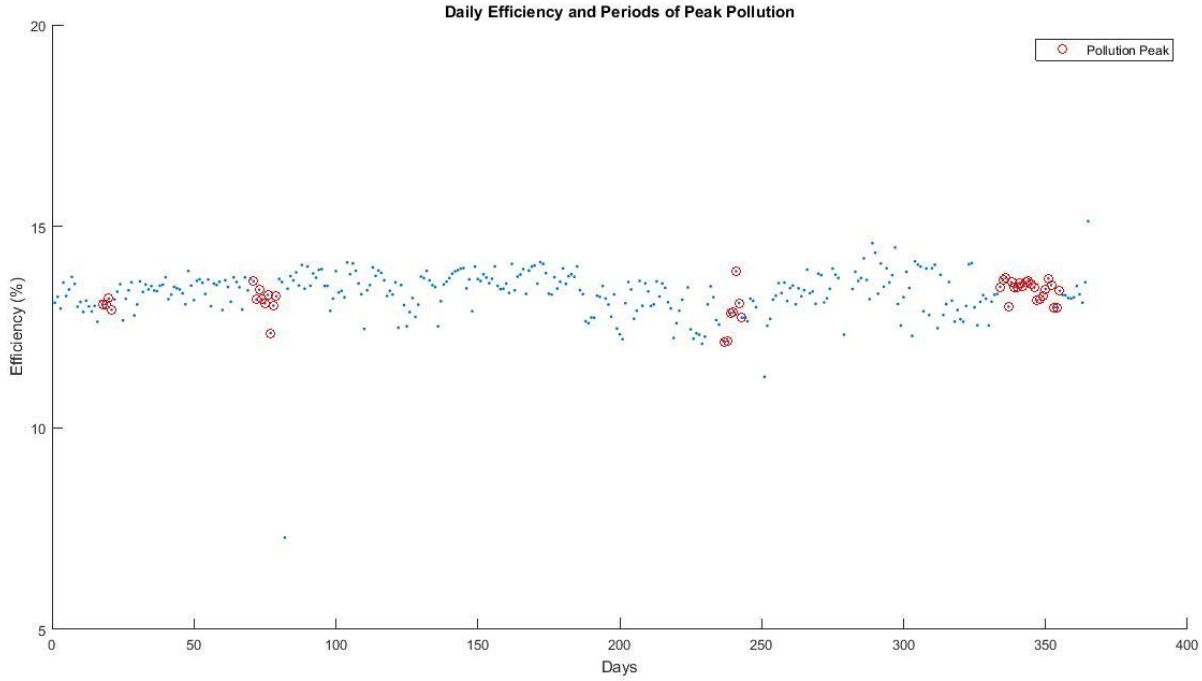

Figure 38: Cumulative daily efficiency and periods of peak pollution (France Watts)

At a glance, the pollution peaks seem to have no effect on the efficiency. This was theorized to be due to the relatively short duration of the peaks, which may not have been sufficient so as to result in any significant soiling accumulation.

The last pollution peak, however, lasted around twenty days, a period deemed long enough to enable PM deposition. For this reason, a new method was implemented in order to study the effects of particulate pollution on photovoltaic efficiency.

This method consisted on the analysis of the module efficiencies during the pollution peaks, aiming to detect an efficiency decrease during these events. This analysis was performed for the two longest and most intense pollution peaks.

The image below contrasts both module efficiency and PM 10 concentration over the longest registered pollution period, spanning just over a month.

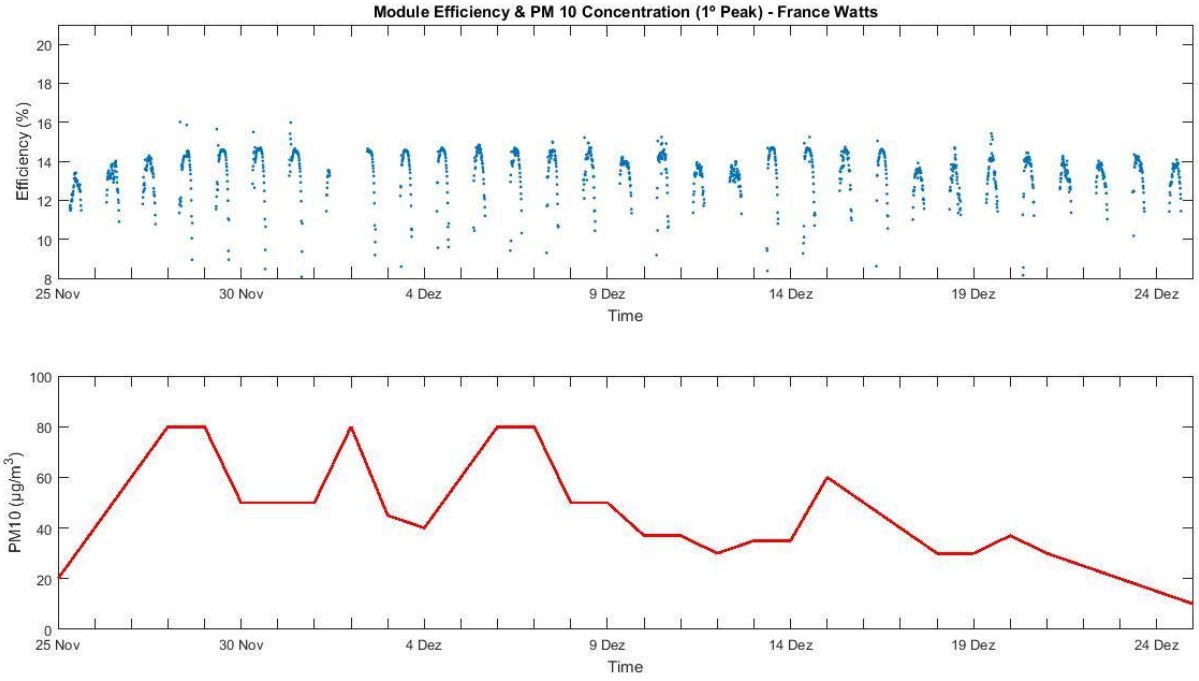

Figure 39: Module Efficiency and PM10 concentration during the first pollution peak (France Watts)

Despite the rising level of PM10, the pane's daily cumulative efficiency remained fairly constant throughout the episode. These results, although preliminary, seem to suggest that the soiling rate has not significantly increased in response to this episode so as to allow for substantial soiling accumulation.

By interpolating both the panel's efficiency and the particulate matter concentration, it was possible to obtain a simpler view of the panel's behavior under these circumstances.

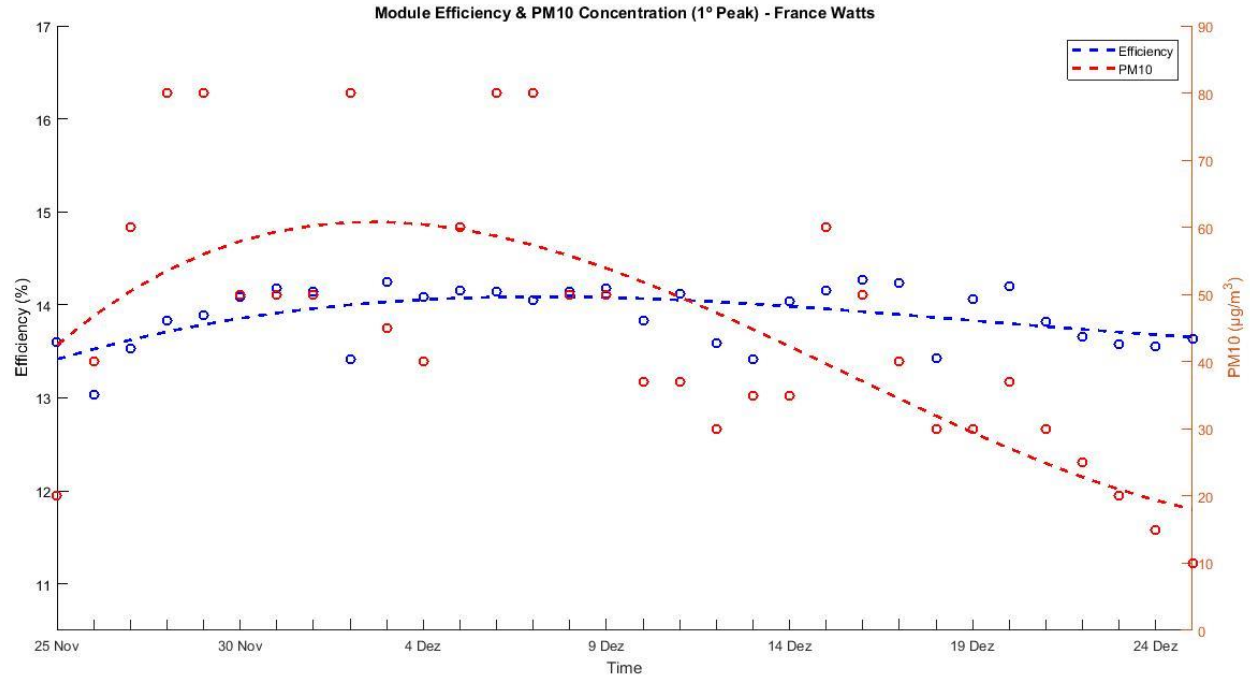

Figure 40: Interpolation of module efficiency and PM10 concentration during the first pollution Peak (France Watts)

Upon further analysis, it became clear that the panel's efficiency was not correlated with the PM 10 concentration. If there were to be a correlation, then the curves should have been inversely proportional, where a rise in PM 10 concentration would result in a decrease in efficiency.

Below is another example of this behavior, where the efficiency remained constant despite the increase of particulate concentration.

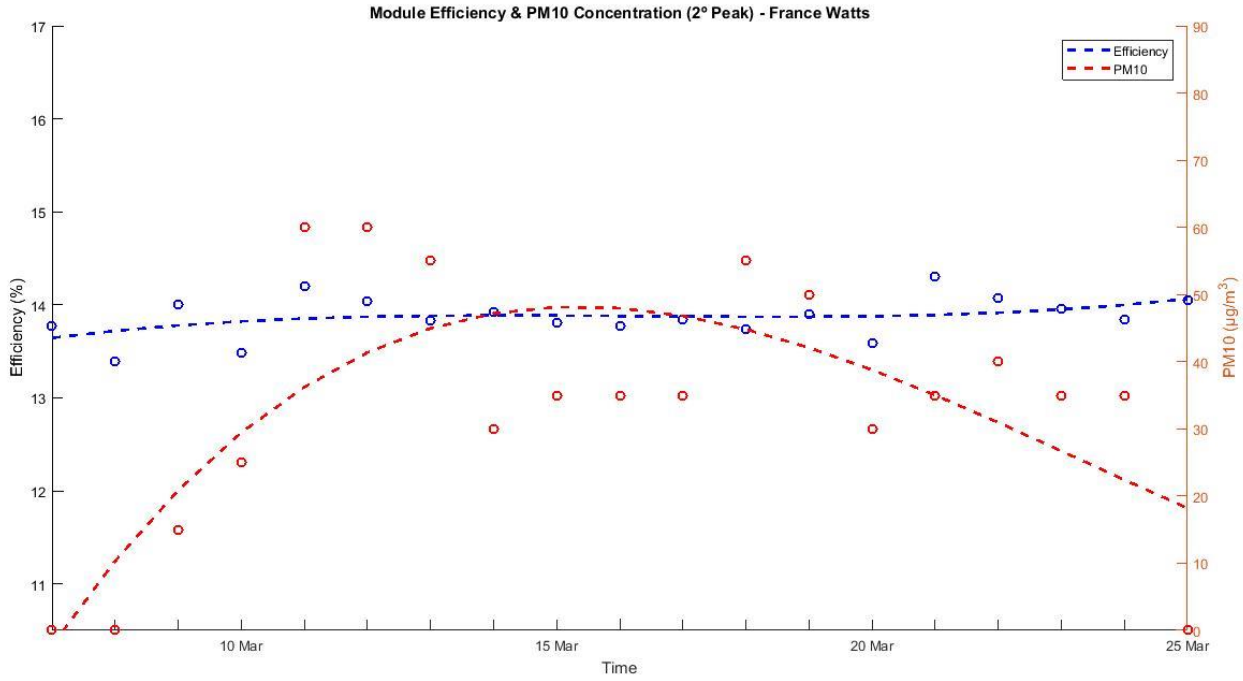

Figure 41: Interpolation of module efficiency and PM10 concentration during the second pollution peak (France Watts)

Once more the particulate levels rose and fell, all the while bearing no relation to the efficiency values. Further studies confirmed this trend, lending to the idea that the pollution episodes were insufficient for any significant soiling accumulation.

These results seem to indicate that the soiling rate has not significantly increased in response to these episodes. Any substantial soiling accumulation would have been reflected in the slopes of the curves, which would have been inversely correlated.

That is not to say that the air pollution was insufficient to negatively influence the solar panels, but simply that it did not affect their energy output through soiling. These results are, however, far from conclusive. Since the pollution episodes affect both the panels and the pyranometer simultaneously, it's possible that the soiling losses went undetected.

It could be argued that the pyranometer was not regularly cleaned, therefore registering soiling accumulation levels similar to those of the panels. If this were to be true, it the detection of soiling losses would not be possible through this method.

Chapter 5 - Diffuse Ratio and Module Efficiency

The daily efficiency values varied considerably during the first semester of this study. This impacted the soiling analysis, negatively affecting the extraction of the efficiency degradation rates.

Since the efficiency variations were most severe during the first semester of the analysis, which coincided with the winter months, this scattering effect was hypothesized to be due to the cloudy weather conditions characteristic of this period.

Clouds block a part of the visible, ultra-violet and infra-red light, depending on several factors such as the type, thickness and altitude of the cloud. At the same time, the presence of clouds in the sky leads to an increase of the diffuse to direct radiation ratio reaching the earth's surface, altering the spectrum of incident light. For this reason, it's possible to obtain a basic characterization of the weather conditions based on the diffuse ratio.

Since the panels' efficiency is sensitive to variations in the solar spectrum, the relation between the diffuse ratio and efficiency dispersion will be studied.

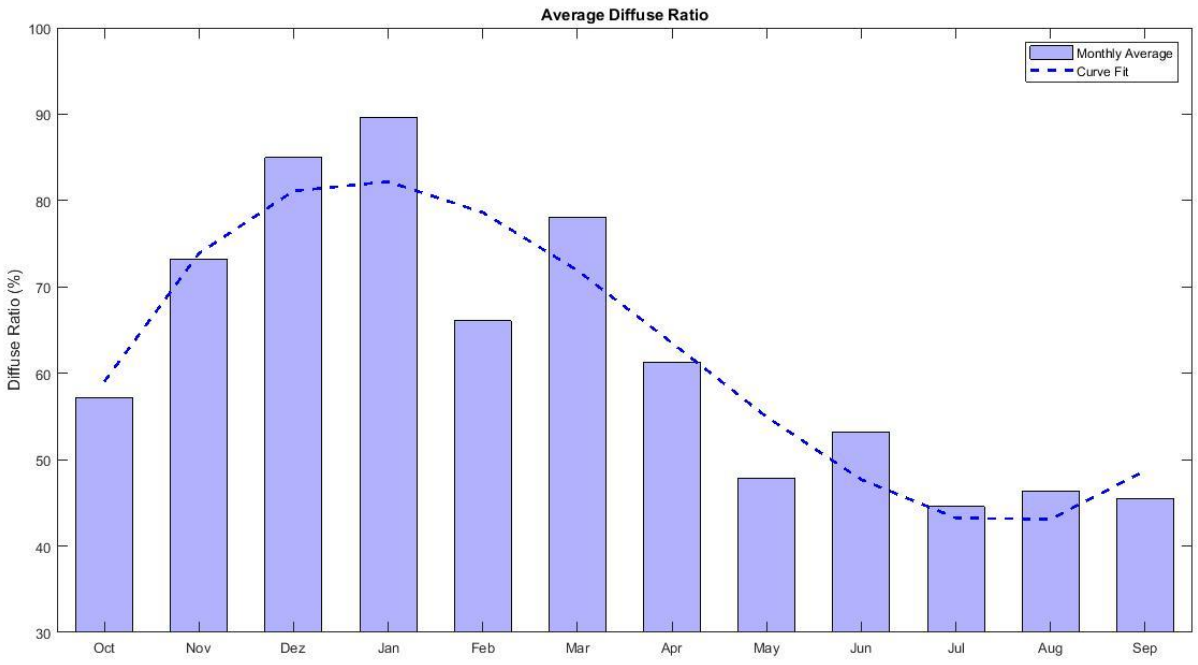

Figure 42: Average monthly diffuse ratio and trendline

This figure displays each month's average diffuse ratio, as well as a trendline highlighting its seasonal variation.

The blue bars show a marked increase of the diffuse ratio during the winter months, followed by a decrease throughout the summer months, roughly coinciding with periods of high and low efficiency dispersion. This preliminary analysis lends to the idea the dispersion is correlated with the diffuse ratio.

In order to test this hypothesis, the daily efficiency values were sorted into three groups: sunny, normal and cloudy days, and to each was assigned a single color. These groups were comprised of efficiency

points whose average daily diffuse ratio was below thirty percent, between thirty and seventy percent, and above seventy percent, respectively.

The resulting color-coded scatter plot can be seen below, for the Sharp branded solar module.

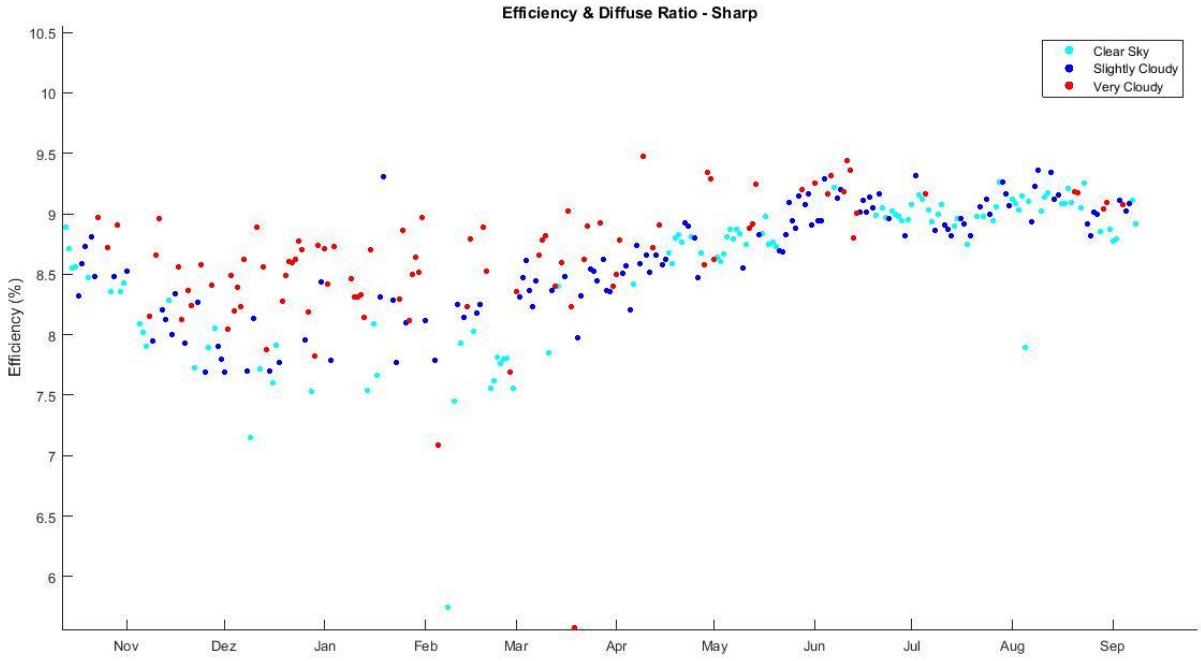

Figure 43: Cumulative daily efficiency and average daily diffuse ratio (Sharp)

In this figure it's possible to observe the daily efficiency for each day, as well as the weather conditions based on the diffuse ratio. Besides the seasonal variation, this image highlights the increased levels of efficiency dispersion during the winter months.

At a glance, the level of dispersion seems to be correlated with the diffuse ratio. During the winter months, where cloudy days were the norm, the efficiencies were much more scattered. On the other hand, during the summer months where sunny days abounded, the efficiency values followed a very linear pattern, hardly straying from the average. This pattern was common to all modules.

Below is the color-coded scatter plot for the remainder of the panels.

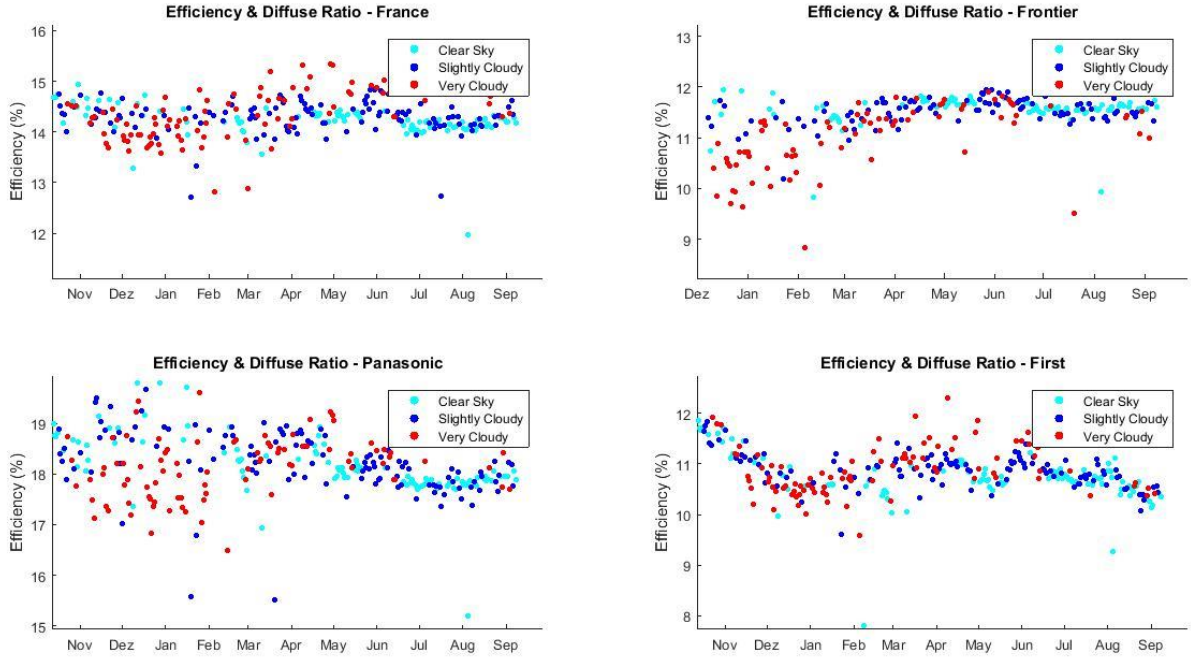

Figure 44: Cumulative daily efficiency and average daily diffuse ratio for the remainder of the panels

Although the dispersion varied in intensity, it was clear that the first semester registered an unusual efficiency spread. Conversely, the summer months registered very little efficiency dispersion, with its linearly distributed values rarely straying from their neighbors.

In order to study the dispersion of the efficiency values, the standard deviation was employed. This measure will quantify the amount of variation present in the efficiency values. A low standard deviation will indicate that the daily efficiencies tend to be close to the mean, whereas a high one that the efficiencies are spread over a wider range of values.

Since this indicator quantifies the dispersion of a data set relative to their mean, the average standard deviation was calculated on a monthly basis, for each day type, so as to bypass the effect of the seasonal variation. The results of this analysis for the Sharp branded solar panel are displayed on the figure below.

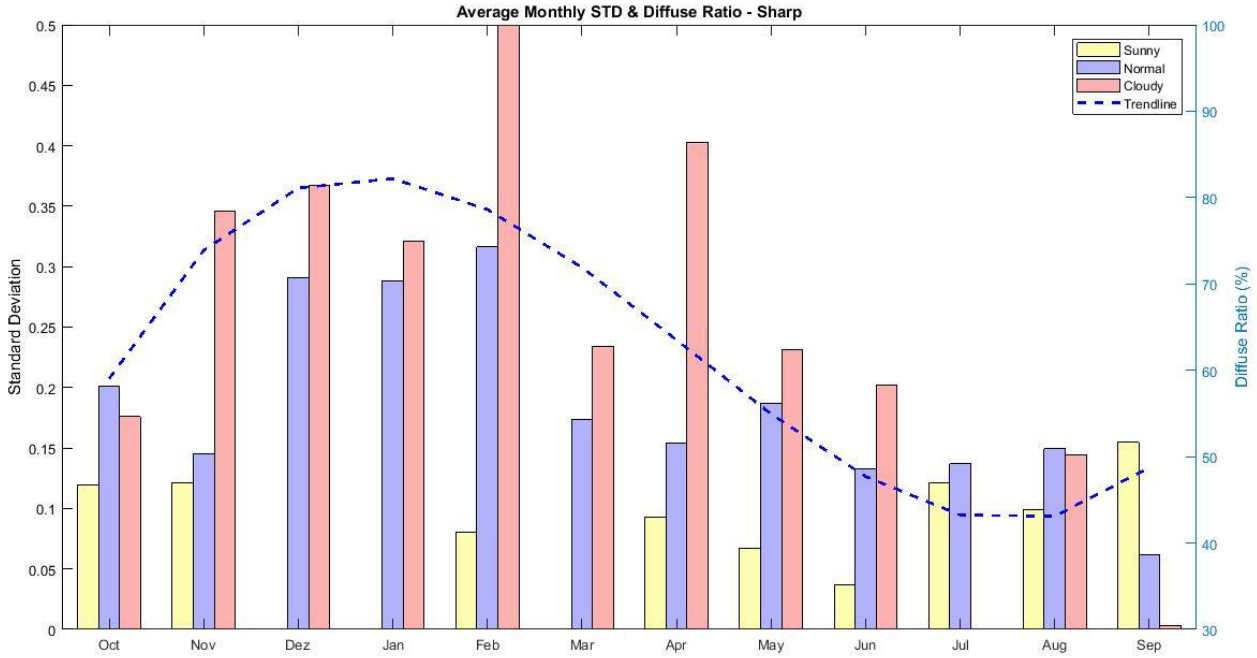

Figure 45: Average monthly standard deviation of the efficiency for each day type (Sharp)

As predicted, the efficiencies registered much less dispersion on clear days, where the diffuse ratio was lower. During overcast days, however, the efficiencies tended to be much more scattered.

With the exception of September, all months registered the least efficiency scattering on sunny days. Similarly, the highest dispersion values frequently coincided with cloudy days.

This trend was present across all panels studied, suggesting that photovoltaic efficiency dispersion is at least partly correlated with the diffuse ratio. Although not unequivocal, this research indicates that the dispersion of the daily efficiencies increases with the diffuse ratio.

It's postulated that the relatively small size of the sample was to blame for the lack of unanimity of the results. Some months registered only a few days of a certain type, not allowing for a comprehensive analysis of the standard deviation.

The month of September, for instance, the only whose standard deviation was higher on sunny weather, had no more than a couple days of this type, thus severely compromising its statistical significance.

This was ultimately due to the seasonal variations, which did not allow for the calculation of a yearly standard deviation for each day type. Since the standard deviation is always relative to the sample's mean, it would be unfit to calculate the yearly dispersion levels for each day type, as in some months the efficiencies were densely packed but far away from the yearly mean due to seasonal effects.

In order to obtain a more reliable assessment of each day type's dispersion, a weighted average of the monthly standard deviation was performed. This procedure ensured that the final values properly reflected each months' relative importance, prioritizing those with larger data sets of a certain day type, thus yielding a more representative value of the standard deviation.

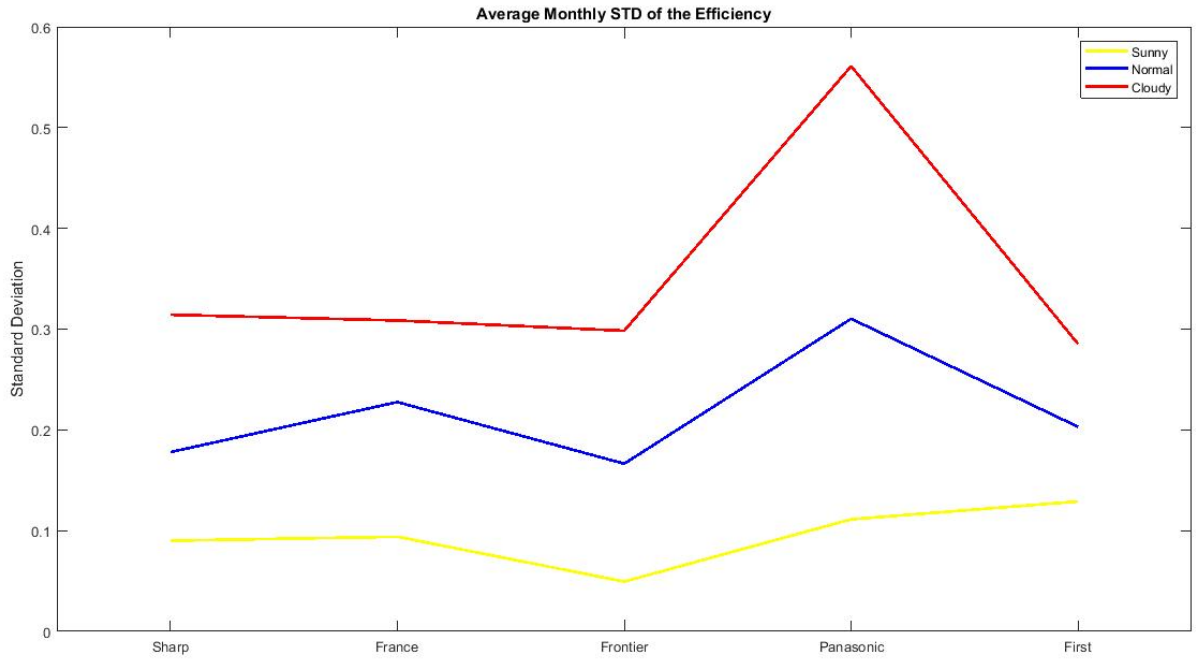

Figure 46: Average standard deviation of the efficiency for each day type

This figure shows the average standard deviation of the efficiency values for each panel. Colored lines were assigned to each day type, as denoted in the legend, allowing for a comparative analysis of the efficiency dispersion levels under different weather conditions.

The yellow line measures the dispersion levels registered under mostly clear-sky conditions, corresponding to measurements taken under diffuse ratios below or equal to thirty percent. The blue and red lines reflect the dispersion levels of efficiency measurements taken between thirty to seventy percent, and above seventy percent, respectively.

This analysis revealed that the least dispersion occurred on sunny days, where direct radiation predominated over the diffuse. Conversely, the highest levels of dispersion coincided with overcast days, during which thick clouds covered most of the sky.

Perhaps most importantly, is to notice that at no time did the lines overlap. This indicates that the panels' dispersion was consistently correlated with the diffuse ratio, increasing with the latter.

This analysis successfully confirmed our hypothesis, proving that the level of efficiency dispersion is proportional to the diffuse ratio.

Finally, it's also possible to conclude that the study of soiling is severely hindered by the varying atmospheric conditions. During the winter months, where the diffuse ratio was higher, the efficiency fluctuations masked any soiling degradation effect. On the other hand, during the summer where the diffuse ratio was consistently low, the efficiencies followed a very linear pattern, hardly straying from the average, aiding in the detection of the minute soiling degradation effects.

Chapter 6 – Conclusions and Future Work

This study analyzed the soiling losses of five solar modules of different brands and technologies in the region of Palaiseau, just outside Paris.

Results showed a consistent efficiency decrease across all panels during the longest recorded dry period, with an average power degradation rate of -0.042%/Day. The power degradation was approximately linear with time and fairly uniform among panels.

For all other periods, it was not possible to obtain reliable estimates of the panels' soiling losses. This was attributed to the significant day-to-day efficiency variations, which persisted despite the thermal correction of the efficiency values.

It was concluded that the linear regression method employed was unfit to estimate soiling losses over short rainless intervals, as these were insignificant compared to the observed daily efficiency variations, rendering these losses undetectable through this method.

For the thermal correction procedure, the accuracy of two thermal models was tested, aiming to obtain the most reliable module temperature records. The first, already existent in the literature and based on the panels' NOCT yielded the best results, with an average error of 3.55 ºC. The second, based on the precise modelling of the panels' heat fluxes, proved less practical and reliable, yielding a slightly average error in the order of 3.9 ºC.

In Palaiseau, due to the high frequency of rainfall, soiling losses appeared to be greatly minimized. Additionally, the combination of low particle deposition rates and moderate panel inclination likely negated any meaningful particle accumulation in this area. This suggested that panel cleaning could be neglected in this region.

It was also found that the weather conditions play an important role in the analysis of soiling losses. The dispersion of the daily efficiency values was observed to increase with the diffuse ratio, severely hindering the analysis of soiling losses through the linear regression method. This method is then better adapted for dry sunny climates, where rainfall is scarce during a pronounced dry season.

Additional efficiency fluctuations could have been introduced by both the panels' behavior at low levels of irradiance, as well as the thermal correction of the panels' efficiencies. Low light behavior depends on each panel's characteristics and cell type, resulting in module efficiencies that aren't constant across all irradiance levels, instead decreasing at progressively lower irradiance levels. Finally, the manufacturer's thermal coefficient used in the correction of the photovoltaic efficiencies to STC conditions may have also contributed to the increase of this dispersion, as these may be slightly inaccurate. Further research into these issues is warranted.

For the study of soiling losses on rainy climates characterized by short dry intervals, without a regularly cleaned control module, the author suggests further studies into a method based on the average of the slopes between individual days instead of a linear regression for the whole interval. This method may be a better predictor of trend, bypassing the daily efficiency variations, and producing a better estimate of the efficiency degradation by allowing outlier values to offset each other.

Annex

Parameters	Units	Sharp	France Watts	Solar Frontier	Panasonic	First Solar
Max. Power	P_{MAX} (Wp)	128	250	150	240	82.5
Power Tolerance	P_{NOM} (%)	+10/-5	±3	+10/-5	+10/-5	±5
MPP Voltage	V_{MPP} (V)	48.6	30.52	79	43.7	48.3
MPP Current	I_{MPP} (A)	3.10	8.21	1.9	5.51	1.71
Open Circuit Voltage	V_{OC} (V)	60.8	37.67	110	52.4	60.8
Short Circuit Current	I_{SC} (A)	3.54	8.64	2.10	5.85	1.94
Efficiency	H (%)	9.5	15	12.2	19	11.4
Temperature Coefficient (P_{MAX})	Γ (%/ºC)	-0.24	-0.48	-0.31	-0.29	-0.25
Temperature Coefficient (V_{OC})	B (%/ºC)	-0.30	-0.36	-0.30	-0.13 V/ºC	-0.27
Temperature Coefficient (I_{SC})	α (%/ºC)	+0.07	0.02	0.01	1.76 mA/ºC	0.04
Module Area	A (m^2)	1.42	1.65	1.228	1.26	0.72
Número de Células	-	180	60		72	154
Tecnologia	-	α & µC-Si	C-Si	CIS	HIT	CdTe

Table 5: Technical characteristics of the photovoltaic modules used in STC conditions.

References

[1] Badossa J., et al, “Deployment of a multi-technology photovoltaic module test bench on the SIRTA meteorological and climate observatory”, 31st European PV Solar Energy Conference.

[2] Kimber A, Mitchell L, Nogradi S, Wenger H. The effect of Soiling on Large Grid-Connected Photovoltaic Systems in California and the Southwest Region of the United States. IEEE 4th World Conference 2006.

[3] Study with similar soiling degradation rates

[4] Zorrilla-Casanova J, Piliougine M, Carretero J, Bernaola P, Carpena P. Analysis of

dust losses in photovoltaic modules. In: Proc of WREC, Linköping, Sweden; 2011. p. 2985–92.

[5] Appels R, Lefevre B, Herteleer B, Goverde H. Effect of soiling on photovoltaic

modules. Sol Energy 2013;96:283–91. http://dx.doi.org/10.1016/j.solener. 2013.07.017.

[6] Kymakis E, Kalykakis S, Papazoglou TM. Performance analysis of a grid

connected photovoltaic park on the island of Crete. Energy Convers Manag

2009;50:433–8. http://dx.doi.org/10.1016/j.enconman.2008.12.009.

[7] Massi Pavan a, Mellit a, De Pieri D. The effect of soiling on energy production

for large-scale photovoltaic plants. Sol Energy 2011;85:1128–36. http://dx.doi.

org/10.1016/j.solener.2011.03.006.

[8] Schill C, Brachmann S, Koehl M. Impact of soiling on IV-curves and efficiency of

PV-modules. Sol Energy 2015;112:259–62. http://dx.doi.org/10.1016/j.solener.2014.12.003.

[9] Al-Otaibi A, Al-Qattan A, Fairouz F, Al-Mulla A. Performance evaluation of

photovoltaic systems on Kuwaiti schools rooftop. Energy Convers Manag

2015;95:110–9. http://dx.doi.org/10.1016/j.enconman.2015.02.039.

[10] Townsend TU, Hutchinson PA. Soiling analysis at PVUSA. In: Proc of ASES-

2000, Madison, WI; 2000.

[11] Hammond R, Srinivasan D, Harris A, Whitfield K, Wohlgemuth J. Effects of soiling on PV module and radiometer performance. In: Proceedings of the twenty-sixth IEEE photovoltaic specialists conference; 1997.p.1121–1124.

[12] Hee JY, KumarL V, Danner AJ, Yang H, Bhatia CS. The effect of dust on trans- mission and self-cleaning property of solar panels. Energy Procedia 2012;15:421–7.

[13] Elminir HK, Ghitas AE, Hamid RH, El-Hussainy F, Beheary MM, Abdel-Moneim KM. Effect of dust on the transparent cover of solar collectors. Energy Convers Manag 2006;47:3192–203.

[14] Goossens D, Van Kerschaever E. A eolian dust deposition on photovoltaic solar cells: the effects of wind velocity and air borne dust concentration on cell performance. SolEnergy1999;66:277–89.

[15] Beattie NS, Moir RS, Chacko C, Buffoni G, Roberts SH, Pearsall NM. Under- standing the effects of sand and dust accumulation on photovoltaic modules. RenewEnergy2012;48:448–52.

[16] Zakzouk AKM, Electrochem M. On the dust-equivalent series resistance of a photovoltaic concentrator. In: Proceedings of the IEEI solid-state and electron devices vol 131;1984.p.17–20.

[17] Guo B, Javed W, Figgis BW, Mirza T. Effect of dust and weather conditions on photovoltaic performance in Doha, Qatar. In: First Workshop on Smart Grid and Renewable Energy (SGRE); 2015. p. 16. http://dx.doi.org/10.1109/SGRE. 2015.7208718.

[18] Hegazy, Adel A, 2001. Effect of dust accumulation on transmittance through glass covers of plate-type collectors. Renewable Energy, Elsevier, vol 11(4), pages 525-540.

[19] Mekhilef S, Saidur R, Kamalisar vestani M. Effect of dust, humidity and air velocity on efficiency of photovoltaic cells. Renew Sustain Energy Rev

[20] Asl-Soleimani E, Farhangi S, Zabihi M S. The effect of tilt angle, air pollution on performance of photovoltaic systems in Tehran. Renew Energy 2001; 24:459– 68.

[21] García M, Marroyo L, Lorenzo E, Pérez M. Soiling and other optical losses in solar-tracking PV plants in navarra. Prog Photovolt: Res Appl2010;19:211–7.

[22] El-Shobokshy MS, Hussein FM .Effect of dust with different physical properties on the performance of photovoltaic cells. SolEnergy1993;51:505–11.

[23] Al-Hasan AY. A new correlation for direct beam solar radiation received by photovoltaic panel with sand dust accumulated on its surface. SolEnergy 1998;63:323–33.

[24] Kohli R, Mittal KL. Developments in surface contamination and cleaning. Volume three, methods for removal of particle contaminants. Amsterdam; Bos- ton: Elsevier;2011.

[25] Appels R, Muthirayan B, Beerten A, Paesen R, Driesen J, Poortmans J. The effect of dust deposition on photovoltaic modules. In: Proceedings of the 38 th IEEE photovoltaic specialists conference (PVSC) ;2012.p.001886–001889.

[26] Appels R, Muthirayan B, Beerten A, Paesen R, Driesen J, Poortmans J. The effect of dust deposition on photovoltaic modules. In: Proceedings of the 38 th IEEE photovoltaic specialists conference (PVSC) ;2012.p.001886–001889.

[27] L. CristaldiL, Faifer M, Rossi M, Catelani M, CianiL ,Dovere E, etal. Economical evaluation of PV system losses due to the dust and pollution. In: Proceedings of the IEEE international instrumentation and measurement technology conference (I2MTC);2012.p.614–618.

[28] Touati F, Al-Hitmi M, Bouchech H. Towards understanding the effects of climatic and environmental factors on solar PV performance in arid desert regions (Qatar) for various PV technologies. In: Proceedings of the first inter- national conference on renewable energies and vehicular technology (reveT); 2012.p.78–83.

[29] Afridi M, Arbab M, Bilal M, Ullah H, Ullah N. Determining the Effect of Soiling and Dirt Particles at various Tilt Angles on Photovoltaic Modules. International Journal of Engineering Works, Kombohwell Publisher Enterprises, 2017, 4 (8) pp.143-14.

[30] J. Cano.Photovoltaic Modules: Effect of Tilt Angle on Soiling. Theses, Arizona State University, August; 2011.

[31] Mike H. Bergin, Chinmay Ghoroi, Deepa Dixit, James J. Schauer, Drew T. Shindell. Large Reductions in Solar Energy Production Due to Dust and Particulate Matter

[32] Dorobantu L, Popescu MO, Popescu C, Craciunesc A. The effect to fsurface impurities on photovoltaic panels. In: Proceedings of the international conference on renewable energies and power quality(icrepq'11). Spain: Las Pal- mas dEGranCanaria;2011.

[33] Maghami MR, Hizam H,Gomes C, Radzi MA, Rezadad M, Hajighorbani S. Power loss due to soiling on solar panel: A review. Renewable and Sustainable Energy Reviews 59, 1307-1306

[34] Bergin M, Ghoroi C, Dixit D, Schauer J, Shindell D. Large reductions in solar energy production due to dust and particulate air pollution. Environmental Science & Technology Letters, June 26, 2017. DOI: 10.1021/acs.estlett.7b00197.